UFMG – FEDERAL UNIVERSITY OF MINAS GERAIS
Post-Graduation Program on Metallurgical and Mining Engineering

Doctoral Thesis

"Prediction and control of geometric distortion and residual stresses in hot rolled and heat treated large rings"

Author: Alisson Duarte da Silva
Advisor: Paulo Roberto Cetlin

March, 2012

UFMG – FEDERAL UNIVERSITY OF MINAS GERAIS
Post-Graduation Program on Metallurgical and Mining Engineering

Alisson Duarte da Silva

PREDICTION AND CONTROL OF GEOMETRIC DISTORTION AND RESIDUAL STRESSES IN HOT ROLLED AND HEAT TREATED LARGE RINGS

Doctoral Thesis presented to the Post-Graduation Program on Metallurgical and Mining Engineering at Federal University of Minas Gerais.

Area of concentration: Metallurgy of Transformation
Advisor: Paulo Roberto Cetlin

Belo Horizonte
School of Engineering, UFMG
2012

This work is dedicated
to my family

ACKNOWLEDGEMENTS:

The author of this work would like to thank all people who helped directly or indirectly towards the completion of this thesis, and in special:

My advisor Dr. Paulo Roberto Cetlin. This research work would not have been possible if not for his trust, efforts and guidance under technical and philosophic aspects.

My co-advisor Dr. Taylan Altan, who has given to me the opportunity of developing this work at ERC/NSM (Engineering Research Center/Net Shape Manufacturing) at The Ohio State University, making possible the cooperative work between UFMG and ERC/NSM.

Tércio A. Pedrosa, Jose L. Gonzalez-Mendes, and Xiaohui Jiang, for all their efforts as part of the group which has worked with me in this project. Sincere thanks are extended to all the students and staff of the Mechanical Forming Laboratory at UFMG and ERC/NSM at The Ohio State University.

SFTC (Scientific Forming Technologies, USA) and Chris Fischer, Research Engineer at SFTC, for establishing the first contact between UFMG and ERC/NSM and for the assistance in the simulations development.

FIA (Forging Industry Association), FIERF (Forging Industry Education and Research Foundation), and Carola Sekreter, Technical Director at FIA, for their trust and financial support.

CAPES (Coordination for the Improvement of Higher Education Personnel), for the Ph.D. scholarship and financial support to the project.

CNPq (Brazilian National Counsel of Technological and Scientific Development), for the "sandwich" Ph.D. scholarship and financial support to the project.

FAPEMIG (Foundation for the Support of Research in the Minas Gerais State), for the financial support to the project.

Sente Software Ltd., UK for providing AISI 4140 material data, based on JMatPro, for the simulation.

My family, which has always been with me during my life journey.

TABLE OF CONTENTS:

LIST OF FIGURES

LIST OF TABLES

ABSTRACT

Seamless rings are produced by hot rolling and heat treatment processes. The heat treatment is used to enhance the material properties of a wide range of mechanical steel components, according to their final application. Quenching is a common step in these heat treatments, involving the fast cooling of previously austenitized parts and leading to a phase transformation from austenite to hard martensite in the material. Quenching commonly causes a geometric distortion in the parts, associated with the thermal contraction and with the change in the mechanical and geometrical properties of the material phases. For the manufacturing of large thin-walled rings, the control of the distortion during the quench process is not possible. The high production rate, the range of rings sizes and all the quench conditions inside the tank represent a very complex system. It is of importance to predict these distortions, so that one can design corrective post-heat treatment shape corrections, leading to a final part with adequate shape and dimensions. This doctoral thesis develops a methodology to predict and correct the ring distortion so-called ovality. This methodology is based on finite element (FE) simulations of the heat treatment (normalizing and quenching) and straightening of an AISI 4140 steel hot rolled ring. The heat treatment simulation is validated using a Navy C-Ring Test. The straightening process uses a compressing machine with flat tools, and an experimental procedure is defined and performed through out simulation.

RESUMO

Anéis sem costura são fabricados através de processos como a laminação a quente e o tratamento térmico. O tratamento térmico é utilizado para aprimorar as propriedades do material, podendo ser conferido a uma grande variedade de componentes mecânicos em aço, conforme a sua aplicação. A têmpera é um estágio bastante comum no tratamento térmico de componentes mecânicos, o qual consiste no resfriamento rápido de peças austenitizadas, provocando a transformação da fase austenita para a martensita. Normalmente, a têmpera causa distorções geométricas, as quais estão associadas com a contração térmica e a modificação das propriedades mecânicas e geométricas. Para o processo de grandes anéis com espessura fina, o controle da distorção durante a têmpera representa uma tarefa complexa e praticamente impossível. A necessidade de uma alta produtividade, a variedade de tamanho dos anéis, além de todas as condições existentes dentro do tanque de têmpera, representam um sistema complexo de processo. Neste caso, torna-se necessário prever estas distorções, visando-se o projeto de sistemas de correção pós-tratamento térmico, buscando-se obter formas e dimensões adequadas. Esta tese de doutorado desenvolve uma metodologia para prever e corrigir a distorção de anéis denominada ovalização. Esta metodologia é baseada em simulação por elementos finitos do tratamento térmico (normalização e têmpera) e do processo de desempeno de um anel laminado a quente de aço AISI 4140. A simulação por tratamento térmico é validada usando-se o Teste do Anel em "C". A etapa de desempeno utiliza um equipamento de compressão, provido por duas ferramentas planas. Um procedimento experimental é definido e numericamente simulado para o processo de desempeno.

1. INTRODUCTION

The global scenario of the manufacturing industry is guided by a high level of market competition. New technologies and innovative ideas are part of the companies' strategies to maintain its products with a good relation between costs and benefits, improve its market share, and attend to the customer's specifications.

Following the same tendency, metal forming industry demands the use of computational technologies applied to Engineering. One typical application is the simulation of manufacturing processes using CAE (Computer Aided Engineering) technology, with the objective of tooling design and manufacturing optimization, saving project time and costs. CAE technology has become essential for metal forming processes, being implemented in the material flow analysis and optimization, and in the die stress analysis. Moreover, the design is developed in shorter periods of time, when compared to the development without computational tools, and experimental tests may be conducted resulting in more assertive process objectives and predictions.

The experimental validation is an essential stage of a metal forming process study. However, this is not a trivial procedure. Its success depends on the correct and methodic conduction of the simulation stage. CAE tools are nothing else than powerful computational tools, and their use should be based on a strong technical background. The model based on the Finite Element Method (FEM) should be correctly set and the results analyzed and criticized, improving the model when necessary. In addition, mechanical machines and tools used for experimental stage are expensive, and are usually defined for new projects, demanding time and investments. The complexity and cost of metal forming facilities increases even more when geometric tolerances are critical issues. Therefore, a complete manufacturing process characterization should consider a financial viability analysis.

Among all the manufacturing processes, the metal forming technology is in a special position. It produces parts with good mechanical properties having a minimum material waste. In this practice, the material to be formed has a relatively simple geometry,

which is plastically deformed through one or more operations towards a relative complex geometry. The near net shape manufacturing, or net shape, drastically reduces the material removal, saving material and energy. Usually, metal forming requires expensive tooling, so the process is economically attractive when a large number of parts has to be produced or the required mechanical properties of the final product can only be obtained through forming process.

Constant increase of material and energy, and tendency to obtain flexible manufacturing systems, requires that metal forming processes de designed with a minimum number of trial and error. For this reason, CAD/CAM (Computer Aided Design/Computer Aided Manufacturing) and also CAE technologies are tools with a large acceptance in the metal forming field. The practical use of these techniques requires a thorough knowledge of the principal variables of a metal forming process and their interactions. Altan *et al.* (1983) include in these variables: the flow behavior of the formed material and the processing conditions; tooling geometry and materials; friction; the mechanics of deformation; the characteristics of the forming equipment; the product geometry, tolerances, surface finishing and mechanical properties, and the effect of the process on the environment.

Seamless rings are an example of parts that are produced using a near net shape metal forming process called ring rolling. Usually, a simple geometry as a billet is heated, upset, backward extruded, and pierced. Then the initial ring is hot rolled to obtain large diameters. This process has been developed by trial and error methodology. However, advanced 3D simulations have been developed in the last years to optimize this process. Despite the advance in computer technology, computation of a complete ring rolling model is still tremendously time consuming. The complexity of the process creates the necessity of special modules in simulation software exclusive for ring rolling practice. But CAE tools have evolved and this process has been better investigated and optimized (Wang *et al.*, 2010).

2D simulations based on the FEM (Finite Element Method) have been considered, for years, the state of art in the beginning of FEM simulation use for engineering problems.

However, the 3D simulation has been widely implemented in the industry for metal forming design. The evolution of computational processing has increased computers efficiency, providing faster systems that can solve equations used in the FEM.

More recently, FEM software packages have been developed for thermomechanical and heat treatment processes emulating capability. The level of the complexity to simulate it increases considerably, when compared to more simple forming simulations. New models and material data are necessary. Grain growth and phase transformation are some examples of processes occurring during simulations. Material phases have to be taken in account, each one with its thermophysical and mechanical properties, and the transformation kinetics has to be established. As a result, FEM equations become more elaborated.

Heat treating is defined as heating and cooling a solid metal or alloy in such a way as to obtain desired conditions or properties (ASM International, 1995). Some of the objectives of heat treating metal and alloy parts include: removing of stresses, refinement of the grains structure, increase hardness, increase thoughness, and change magnetic properties. Heat treatment commonly involves a quenching step, which may cause undesired geometrical distortions in the processed parts. The dimensional accuracy of these parts is affected and leads to production and economical losses. In these cases, the heat treatment process should be optimized, avoiding these distortions, usually caused by fast cooling. FEM simulations can be used to predict the quenching process, predicting defects such as distortions, and be used to improve the process by improving the FE model parameters. However, for certain situations, a mechanical process after heat treatment is necessary due to the impossibility of preventing defects or financial reasons.

Hot rolled rings are heat treated after forming stages. The heat treatment processes for the rings consist of: normalizing, quenching, and tempering. During all the phases, forming and heat treatment, the dimensions of the pieces change dramatically. The rings undergo distortions during heat treatment stage. In particular, situations where there is a lack of symmetry in the cooling conditions, ring distortions include contraction and

rotation of the ring section (Pascon *et al.*, 2004). In many situations, the cooling conditions can be better controlled and distortions may be avoided.

In special, hot rolled ring industry has reported a circumferential distortion in large rings after quenching process. Rings with relatively large diameter and thin thickness may lead to an out-of-roundness shape during fast cooling processes. These rings are quenched in tanks, disposed in stacks with more than one ring each stack. Due to the high production rate necessity, many rings are quenched at the same time, in the same quenching tank. Several parameters influence the quenching process, including: quenchant temperature, polymer concentration, bacteria quantity, and velocity (agitation inside the tank), and rings size and position inside the tank. Due to the described parameter, for the same ring, there is always a non-homogeneous heat transfer between ring and environment along the ring surface.

Forging industry and tank design companies have tried to develop more efficient systems, creating conditions during quenching where the ring may reach a symmetric heat transfer with the environment. For certain products, in special small geometries and/or lower production rate, the tank conditions may be better controlled, resulting in quenched parts without distortion. However, for large geometries inside large tanks, forging industry has concluded that it is impossible or not practical to avoid circumferential distortions. Some of the rings will always reach an out-of-roundness shape.

There is a wide variety of rings. Materials used for the rings include aluminum, titanium, magnesium, steel and nickel based specialty alloys. As an example, steel alloy rings have a minimum market price of 5 thousand dollars, and some inconel rings might cost 60 thousand dollars. The high value-added to these products creates the necessity of correcting the out-of-roundness shape of the rings, in order to satisfy the tolerances to ship to the costumers.

One alternative to correct the ring distortion is to deform the ring after the heat treatment. Some designer companies have created expanders to correct it. The

expanders pull the ring, involving small plastic deformations, reaching a near round shape. However, these are very sophisticated machines, which may cost up to 6 million dollars. In addition, the learning curve for these equipments is long and expensive.

Alternatively, hot rolled ring companies have developed simpler systems in order to correct the out-of-roundness shape of the rings. Compressive machines using flat tools are used to compress the ring, creating small plastic deformation, and correcting the circumference. However, this process is totally based on trial and error methodology, conducted based on operator experiences. Long times are used during this process. Some distortions and/or mistaken procedures can over deform the ring, and the product becomes scrap.

In addition, the rings display residual stresses after quenching process. These residual stresses decrease after tempering stage. However, some residual stresses still remain in the ring. Depending on the residual stresses magnitudes, the ring may distort during subsequent machining process. The mechanical procedure to correct the quench distortion may also decrease the residual stresses in the ring.

Finally, it is necessary to define a methodology to predict circumferential distortion of rings due to heat treatment processes. Once the out-of-roundness ring is obtained, it is possible to develop a procedure to correct the distortion through small plastic deformations.

Understanding and ultimately solving this problem is a challenging task considering the three triggering mechanisms (thermal, metallurgical and mechanical) that affect the ring during heat treatment causing the undesired results. Due to its versatility, accuracy and efficiency, the Finite Element Model technique is a viable and cost effective tool for conducting this study.

2. OBJECTIVES

As introduced in the previous section, distortions of hot rolled and heat treated rings are an important issue for the product quality. This work proposes to define a methodology to predict and correct geometric distortion and residual stresses of hot rolled and heat treated rings. This methodology will be based on FE simulations, using DEFORM-3D^{TM}. An AISI 4140 ring case study will be used for this project investigation. The objective can be divided in 3 main tasks, each one with its specific approaches:

Objective 1: define a methodology to simulate heat treatment distortion using FE simulation. The following approaches should be investigated:

- Conduct experimental oil quenching process using AISI 4140 navy c-ring specimens.
- Investigate AISI 4140 material data for heat treatment simulation, considering its phases and the transformation kinetics between them.
- Simulate oil quenching of AISI 4140 navy c-ring specimens.
- Validate the heat treatment simulation comparing predicted and experimental results for distortion, martensite volume fraction, and hardness.

Objective 2: develop a methodology to obtain circumferential distortion of large rings, investigating predefined heat treatment stages, based on the procedure performed and validated for Objective 1. An AISI 4140 ring should be used as a case study. The stages to be investigated should approach as follows:

- Investigate is the possibility to obtain circumferential distortion during normalizing process due to the proximity between two rings disposed 10 mm distant from each other in the cooling stage.
- Establish a methodology to predict circumferential distortion during quenching of large rings.
- Verify the residual stresses of the distorted ring after quenching process.

Objective 3: propose a methodology to correct circumferential distortion of heat treated rings using compresser machines.

- Propose an experimental methodology to be conducted at the shop floor.
- Perform a distortion correction case study using FE simulation.
- To verify the final residual stresses after compression process.

3. LITERATURE REVIEW

3.1. Metal Forming

3.1.1. Historical Background

Metalworking is probably the earliest technological occupation known to mankind; native metals must have been forged and shaped more than 7,000 years ago (Schey, 1970). The earliest records of metalworking describe the simple hammering of gold and copper in various regions of the Middle East around 8000 B.C. The forming of these metals was crude because the art of refining by smelting was unknown and because the ability to work the material was limited by impurities that remained after the metal had been separated from the ore.

Around 400 B.C. the smelting of the copper was developed, and the metals purifying methodology began to be created. Later, it was observed that hammering metals increased its strength bu plastic deformation steps (strain hardening). Most metalworking was done by hand until the 13^{th} century. At this time, the tilt hammer was developed and used primarily for forging bars and plates. Leonardo da Vinci's notebook includes a sketch of a machine designed in 1480 for the rolling of lead for stained glass windows. In 1495, da Vinci is reported to have rolled flat sheets of precious metal on a hand-operated two-roll mill for coin making purposes (Semiatin, 2005). The 17^{th} century saw the appearance of the slitting mills in which forged flats were split with collared rolls, then rounded by forging and finally drawn into wire. Grooved rolls were also used in France.

Metal forming technology has been developed and played an important role along the history. The past 100 years have seen the development of new types of metalworking equipment and new materials with special properties and applications.

3.1.2. Definition and Classification

Metals exhibit a ductile behavior and respond elastically if stress is kept within a certain region, variously referred to as elastic region, elastic range or elastic domain. Beyond that region, plastic deformation takes place (Pagliettt, 2007). The use and control of the plastic deformation region (and also elastic) in metals is applied to manufacturing processes to obtain a wide variety of metal shapes. This practice can be understood as metal forming.

Metal forming is the group of deformation processes in which a metal billet or blank is shaped by tools or dies. According to Altan (1999), in metal forming, the starting material has a relatively simple geometry; this material is plastically deformed in one or more operations into a product of relative complex configuration. Forming to near net or to near net shape dimensions drastically reduces metal removal requirements, resulting in significant material and energy savings. Metal forming includes processes such as rolling, extrusion, cold and hot forging, bending, and deep drawing.

The design and control of such processes depend on the characteristics of the workpiece material, the conditions at the tool/workpiece interface, the mechanics of plastic deformation (metal flow), the equipment used, and the finished-product requirements. Because of the complexity of many metal forming operations, models of various types, such as analytical, physical, or numerical models, are often relied upon to design such processes (Semiatin, 2005).

Tschaetsch (2005) defined the main terms of metal forming, including: plastic (permanent) deformation, flow stress, deformation resistance, deformability, degree of deformation and principal strain, and strain rate. Unlike elastic deformation, during which, for example, a rod under a tensile load returns to its initial length as long as a defined value (elastic limit of the material) is not exceed, a workpiece which is plastically deformed retains its shape permanently. Flow stress depends on the extend of deformation and on the material that will be formed. A flow stress curve of a material is

the relation between the stress aplied to the material and its plastic deformation. The resistance to be overcome during a deformation is composed of the flow stress and the friction resistances in the tool, which are brought togheter under the term “resistance to flow”. Each material has an ability to be deformed. This ability is called deformability. The deformability is dependent on chemical composition, crystaline structure, and historical heat processes. The measure of the extend of a deformation is the degree of deformation. If the deformation is decomposed in three different directions, the greatest deformation is known as the principal strain. If the deformation is carried out in the time, this results in an average strain rate.

A common way of classifying metal forming processes is to consider cold (below the recrystallization temperature) and hot (above the recrystallization temperature) forming. Most of the materials behave differently under different temperature conditions. However, the general principles governing the forming of metal at various temperatures are basically the same. Therefore, a classification based on initial material temperature does not contribute a great deal to the understanding and improvement of these processes (Altan *et al.*, 1999).

A better way to classify metal forming is dividing in two groups: massive forming and sheet forming processes. For massive forming processes, forging, extrusion, rolling and drawing are some examples. For Sheet forming, brake forming, deep drawing and stretch forming may be mentioned. Table 1 shows the metal forming processes classification under massive forming category, while Table 2 shows the classification under sheet-metal forming category. As an example of a different classification, Tschaetsch (2005) has divided the forming group in: forming by pressure, tensile/compressive forming, forming by tensile forces; forming by bending, and forming by shearing.

Table 3.1 – Classification of massive forming processes (Altan *et al.*, 1983).

Forging	Rolling	Extrusion	Drawing
Closed-die forging with flash	Sheet rolling	Nonlubricated hot extrusion	Drawing
Closed-die forging without flash	Shape rolling	Lubricated direct hot extrusion	Drawing with rolls
Coining	Tube rolling	Hydrostatic extrusion	Ironing tube sinking
Electro-upsetting	Ring rolling		
Forward extrusion forging	Rotary tube piercing		
Backward extrusion forging	piercing		
Hobbing	Gear rolling		
Isothermal forging	Roll forging		
Nosing	Cross rolling		
Open-die forging	Surface rolling		
Orbital forging	Shear forming (flow turning)		
P/M forging	Tube reducing		
Radial forging			
Upsetting			

Table 3.2 – Classification of sheet metal forming processes (Altan *et al.*, 1983).

Bending and straight flanging	**Deep recessing and flanging**
Brake bending	Spinning (and roller flanging)
Roll bending	Deep drawing
	Rubber pad forming
Surface contouring of sheet	Marform process
Contour stretch forming (Stretch forming)	Rubber diaphragm hydroforming
Androforming	**Shallow recessing**
Age forming	Dimpling
Creep forming	Drop hammer forging
Die-quench forming	Electromagnetic forming
Bulging	Explosive forming
Vacuum forming	Joggling
Linear contouring	
Linear stretch forming (Stretch forming)	
Linear roll forming (Roll forming)	

3.2. Heat Treatment of Steel

3.2.1. Definition

Heat treatment of steel, in its broadest sense, refers to any process involving heating and controled cooling of the solid metal by which the properties of the steel are altered (Bullens and Battelle, 1948). It is one of the oldest manufacturing processes, having first been practiced approximatle 5,000 years ago. It continues to be one of the most important fundamental processes in a modern industrial economy. Thermal processing is involved in almost every market sector of the economy, including ground transportation, agriculture, aerospace, the military, oil drilling, fastener production, tools and machinery, manufacturing, and many other industries. In view of its global inportance, research and development is conducted in nearly every advanced and developing economy to identify better materials and more efficient and improved thermal technologies, and to integgrate them into modern production practices (Totten and Howes, 1997).

The main reasons for heat treating are pointed by ASM International (1995) as follows:

- remove stresses, such as those developed in processing a part;
- redefine the grain structure of the steel used in a part;
- add wear resistance to the surface of a part by increasing its hardness, and, at the same time, increase its resistance to impacts by maintaining a soft, ductile core;
- improve the properties of an economical grade of steel, making it possible to replace a more expensive steel and reduce material costs in a given application;
- increase toughness by providing a combination of high tensile strength and good ductility to enhance impact strength;
- improve the cutting properties of tool steels;
- upgrade electrical properties;
- and change or modify magnetic properties.

Steel can be heat treated to produce a great variety of microstructures and properties. The desired results are accomplished by heating in temperatures ranges where a phase

or combination of phases is stable (thus producing changes in the microstructure or distribution of phases), and/ or cooling between temperature ranges in which different phases are stable (thus producing beneficial phase transformation). Krauss (1980) also explains that the iron-carbon equilibrium phase diagram shown in Figure 3.1 is the foundation on which all heat treatment of steel is based. This diagram defines the temperature-composition regions where the various phases in steel are stable, as well as the equilibrium boudaries between phase and fields. The iron-carbon (Fe-C) diagram is a map that can be used to chart the proper sequence of operations for a given heat treatment. In Figure 3.1 it is possible to visualize the carbon steel phases: austenite, cementite and ferrite. Steels with 0.77% carbon are eutectoid. The line A_{cm} is the temperature at which the solution of cementite in austenite is completed during heating

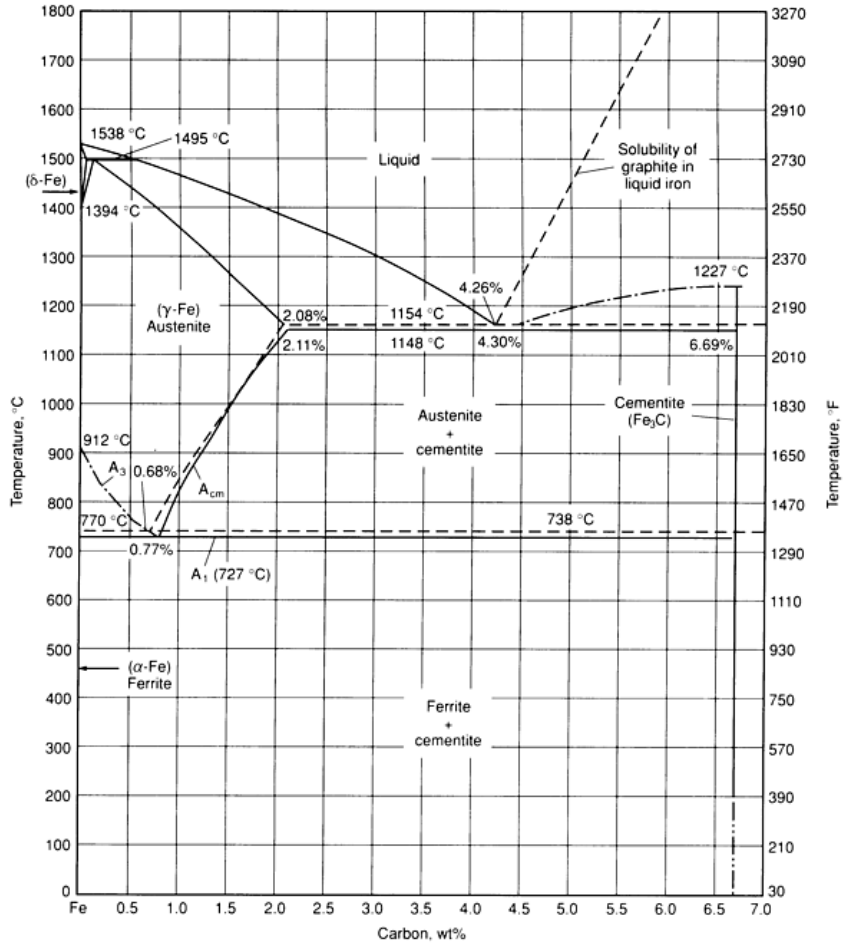

Figure 3.1 – The Fe-C equilibrium diagram up to 6.67 wt% C. Solid lines indicate Fe-Fe_3C diagram; dashed lines indicate iron-graphite diagram (Ericsson, 1991).

for hypereutectoid steels. The line A_{c1} is the temperature at which austenite begins to form during heating, with the c being derived from the French *chauffant.* And line A_{c3} represents the temperature at which transformation of ferrite to austenite is completed during heating. The iron-carbon diagram should be considered only a guide, however, because most steels contain other elements that modify the positions of phase boundaries.

Table 3.3 – Important metallurgical phases and microconstituents (Ericsson, 1991).

Phase (microconstituent)	**Crystal structure of phases**	**Characteristics**
Ferrite (α-iron)	bcc (body-centered cubic)	Relatively soft low-temperature phase; stable equilibrium phase
δ-ferrite (δ-iron)	bcc	Isomorphous with α-iron; high-temperature phase; stable equilibrium phase
Austenite (γ-iron)	fcc (face-centered cubic)	Relatively soft medium-temperature phase; stable equilibrium phase
Cementite (Fe3C) Complex	orthorhombic	Hard metastable phase
Graphite	Hexagonal	Stable equilibrium phase
Pearlite		Metastable microconstituent; lamellar mixture of ferrite and cementite
Martensite	bct (body-centered tetragonal) - supersaturated solution of carbon in ferrite	Hard metastable phase; lath morphology when <0.6 wt% C; plate morphology when >1.0 wt% C and mixture of those in between
Bainite	…	Hard metastable microconstituent; nonlamellar mixture of ferrite and cementite on an extremely fine scale; upper bainite formed at higher temperatures has a feathery appearance; lower bainite formed at lower temperatures has an acicular appearance. The hardness of bainite increases with decreasing temperature of formation

Alloys containing more than 2% carbon are classified as cast irons. A steel that contains, in addition to iron and up to 2% carbon, specially introduced chemical elements not found in an usual carbon steel is called an alloy steel. Chemical elements purposely added into steel are termed alloying elements. The alloy elements must be incorporated into austenite, ferrite and cementite. Incorporation is usual by replacement of iron atoms if the alloy, or impurity, atoms are roughly the same size as iron atoms,

but sometimes the atoms go into interstitial sites if they are significantly smaller than iron. In some cases, if sufficient quantities of alloying elements are present, solubility limits are exceeded and phases other than austenite, ferrite and cementite may form. Table 3.3 shows the most important metallurgical phases and microconstituents, which will be mentioned in the next items of this text.

3.2.2. TTT and CCT Diagrams

According to Krauss (1980), temperature-time-transformation (TTT) diagrams, also known as isothermal transformation (IT) diagrams or S-curves, and continuous cooling transformation (CCT) diagrams have been developed to define the progress of diffusion-controlled phase transformations of austenite to various mixtures of ferrite and cementite. The availability of these diagrams, for a variety of steels, makes possible the selection of steels and the design of heat treatments that will either produce desirable microstructures of ferrite and cementite or avoid diffusion-controlled transformations, and thereby produce martensitic microstructures of maximum hardness.

TTT curves are used to represent the phase transformation of austenitized steel as a function of time when the cooling temperature is held constant. These curves compose the TTT diagram, representing the austenite transformation as function of time. For austenitized steel, the austenite may be transformed, at a constant temperature, in another product. This transformation is time dependent. Figure 3.2 shows a schematic of a TTT curve. The left curve represents the beginning of the transformation product. At a specific temperature, the austenite begins transforming in another product at the time determined by the left curve. The austenite is totally transformed after the time transformation defined by the right curve. The constituted curves are steel composition, grain size and austenitized temperature dependent. Alloying elements change the form and position of the curves.

The application of the TTT diagram consists in predicting the phase transformation occurring in a specific workpiece during heat treatment processes. A common method of hardening steel is heating it until it becomes austenitic, applying a cooling fast enough to avoid any transformation of the austenite before reaching a relatively low

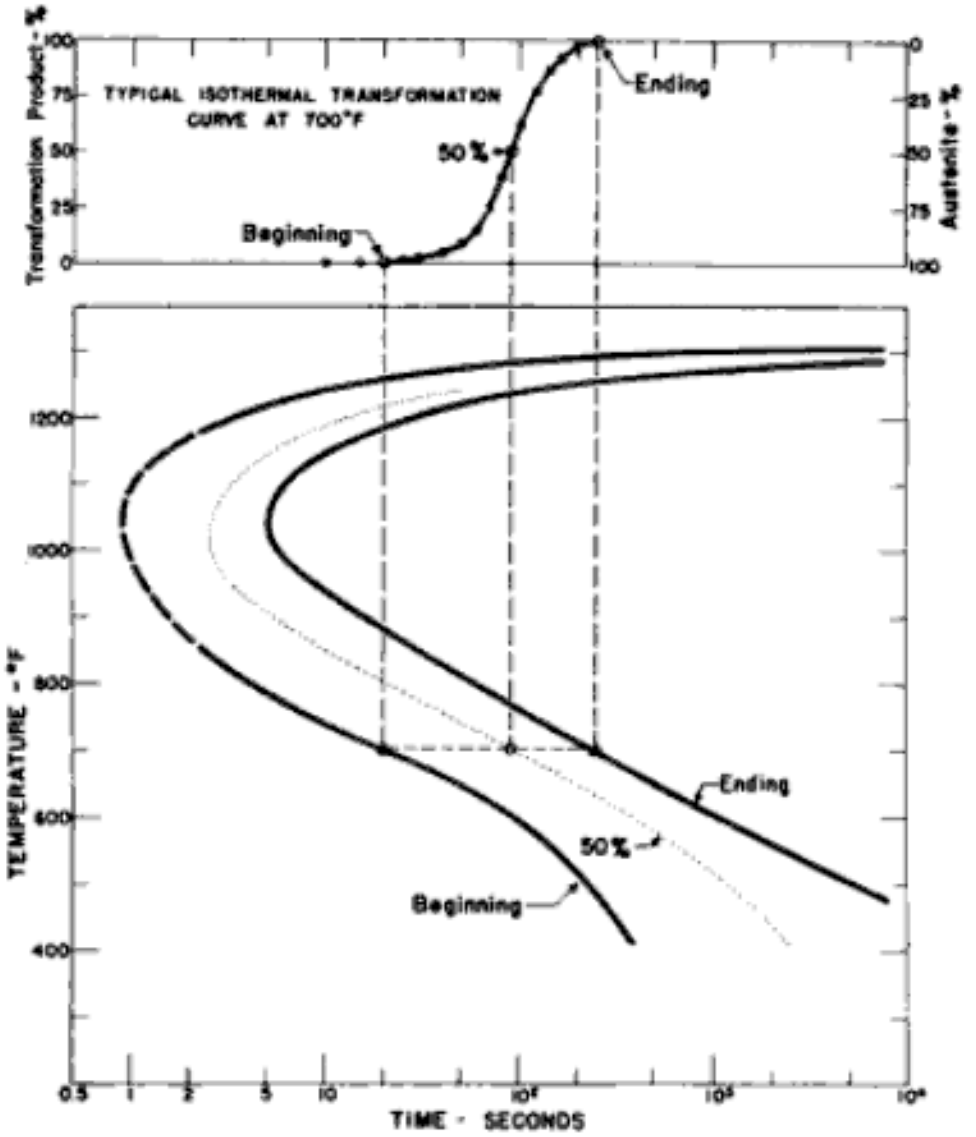

Figure 3.2 – Diagram showing how measurements of isothermal transformation are summarized by the isothermal transformation diagram (Voort, 1991).

temperature. In this case, a hard phase (martensite) is formed, as shown in Figure 3.3 (a). Quenching is usually followed by a tempering process. Figure 3.3 (b) shows another application, in which the cooling rate is slower than the quenching process. The TTT diagram in conjunct with the cooling curve may indicate the temperature range when slow cooling may be safely discontinued, and also estimate cooling rate necessary to develop harder or softer microstructures.

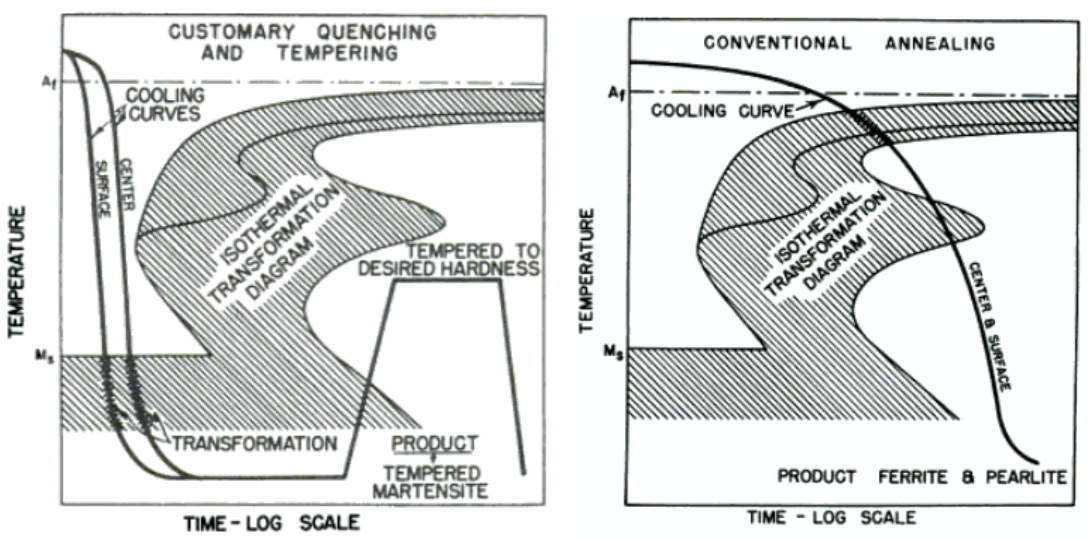

(a) (b)

Figure 3.3 – Schematic chart illustrating relationship of (a) quench and temper type of hardening treatment and (b) conventional annealing cycle to a typical TTT diagram (Voort, 1991).

The TTT diagram is useful in planning heat treatments and in understanding why steel responds as it does to a particular heat treatment, but it cannot be used directly to predict accurately the course of transformation as it occurs during continuous cooling. It is possible, however, to derive from the TTT diagram another time-temperature-transformation diagram which while not highly accurate, is of considerable aid in bridging the gap between isothermal and continuous cooling transformation. This diagram will be referred to as the CCT diagram (Voort, 1991). A comparison between TTT and CCT curves can be visualized in the Figure 3.4. The CCT diagram has been derived for the AISI 4140 steel and superimposed on the TTT diagram. The cooling rates plotted are based upon measurement of temperature change at indicated locations in an end-quenched bar.

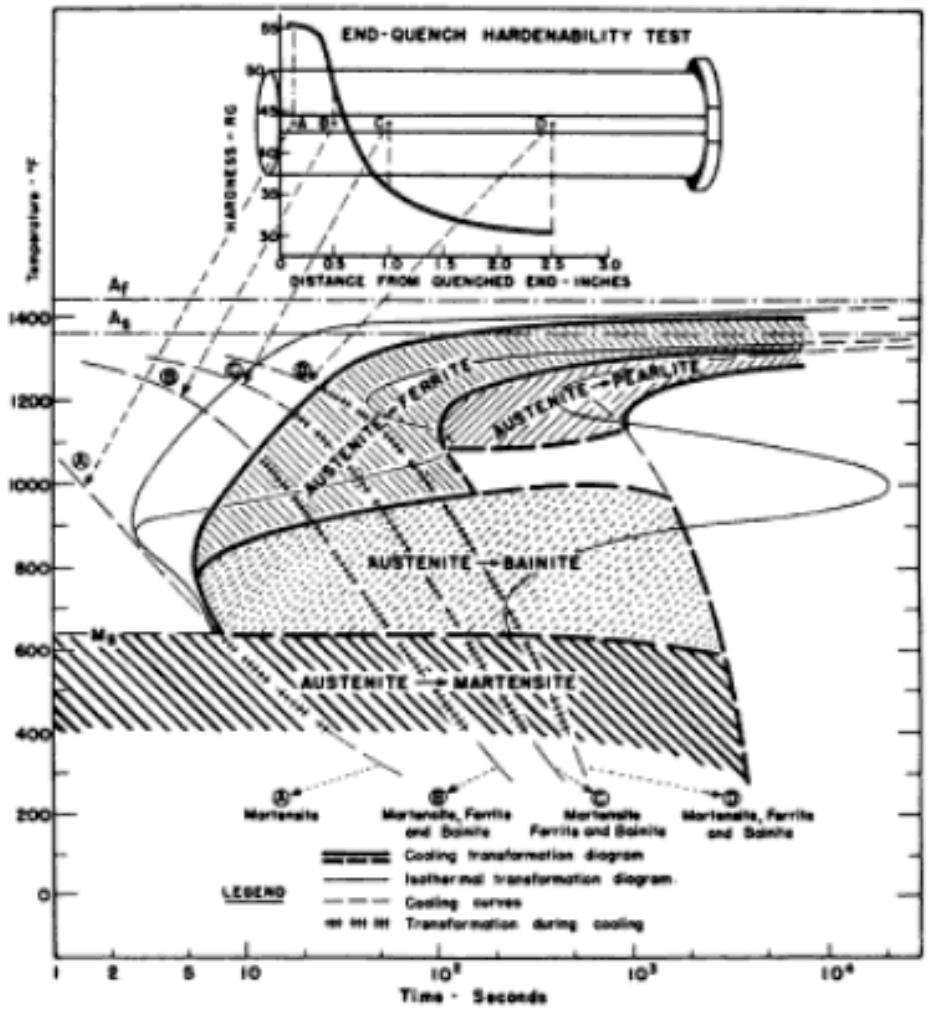

Figure 3.4 – Correlation of CCT and TTT diagrams with end-quench hardenability test data for 4140 steel (Voort, 1991).

3.2.3. Normalizing

Normalizing is a heat treatment which, similarly to full annealing, produces a uniform microstructure of ferrite and pearlite. Reasons for normalizing are diverse: for example, to increase or decrease strength and hardness, depending on the thermal and mechanical history of the product. In normalizing, heating is followed by air cooling, in contrast to the slower furnace cooling of full annealing. Normalizing of steel is often considered from both thermal and microstructural standpoints. In the thermal sense, normalizing is an austenitizing heating cycle, followed by cooling in still or agitated air. In terms of

microstructure, areas that contain about 0.8% carbon are pearlitic. Those low in carbon are ferritic.

The somewhat higher austenitizing temperatures used for normalizing, as compared to those used for annealing hypoeutectoid steels, in effect produce greater uniformity in austenitic structure and composition similar to a homogenizing treatment, although at a much lower temperature and for shorter times than those used for homogenizing. Another of the major objectives of normalizing is to refine the grain size that frequently becomes very coarse during hot working at high temperatures or that is present in as-solidified steel castings. As such hot worked or cast products are heated through the A_{c1} and A_{c3} temperatures, new austenite grains are nucleated and, if the austenitizing temperature is limited to the range in the Figure 3.5, a uniform fine-grained austenite is produced. Exceeding the indicated temperature range might result in excessive austenitic grain size. Normalizing, then, produces a uniform, fine-grained austenite grains structure that in hypoeutectoid steels transforms to ferrite-pearlite microstructures on air cooling. The resulting microstructure may have good uniformity and desirable mechanical properties for a given application or may be reaustenitized for final hardening by quenching to martensite (Krauss, 1980). Figure 3.6 gives a typical temperature profile during normalizing, also comparing to annealing.

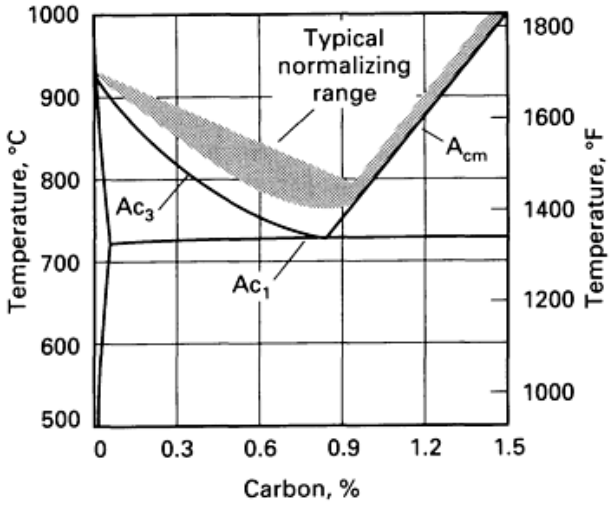

Figure 3.5 – Partial iron-iron carbide phase diagram showing typical normalizing range for plain carbon steels (Ericsson, 1991).

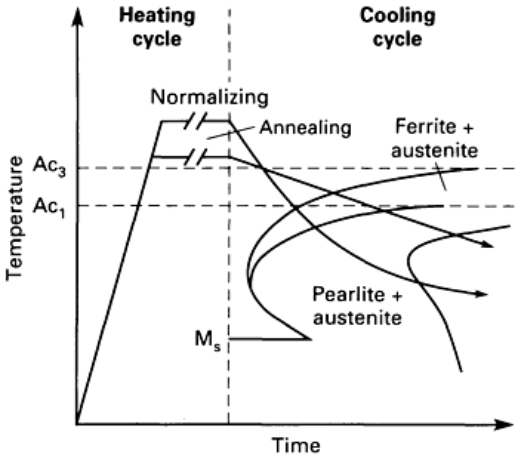

Figure 3.6 – Comparison of time-temperature cycles for normalizing and full annealing. The slower cooling of annealing results in higher temperature transformation to ferrite and pearlite and coarser microstructures than does normalizing (Kraus, 1980).

After hot worked, the steel is relatively coarse grain structure and perlite is widely dispersed. Then, during autenitization prior to quenching in a quench hardening treatment, homogeneous austenite may not be obtained during the normal (recommended) austenitizing cycle. Heating to higher temperatures and/or for longer times to obtain homogeneous austenite may lead to unacceptable large austenite grains size. Normalizing gives a general refinement of structure and facilitates the formation of homogeneous autenite during austenitizing, without much grain coarsening, as examplified in Figure 3.7.

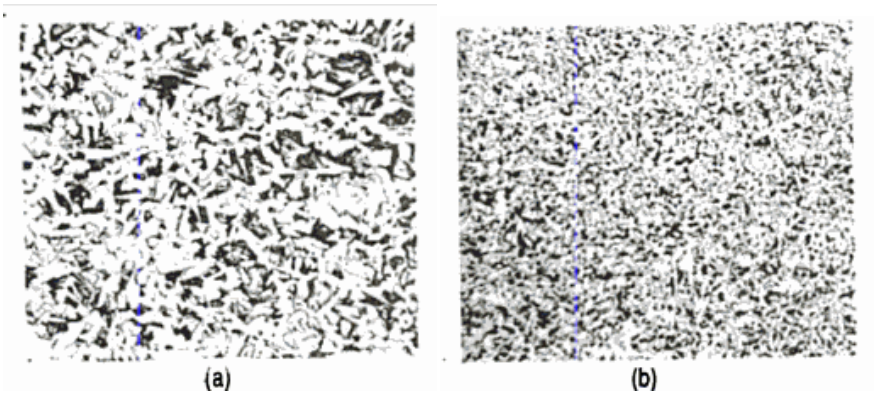

Figure 3.7 – Effect of normalizing on the grain structure in steels; (a) structure of as-hot rolled steel, and (b) the same steel after normalizing (Sharma, 1996).

3.2.4. Quenching

This chapter proposes to give only an introduction about quenching process. The main quenching aspects covering heat exchange between workpiece and quench bath are discussed later (Itens 3.5 and 3.6).

The material properties of steels are very important according to the component application. The outstanding importance of steels in engineering is associated with their ability to change its mechanical properties over a wide range when subjected to controlled heat treatment. Quenching is a common method of hardening steel. This process is based on a diffusionless process caused by a fast cooling rate. A quenching cycle is illustrated schematically in Figure 3.8 (a). It is possible to accelerate cooling from the solution-treating temperature and control the transformation of austenite to bainite and martensite to have higher strength and hardness than obtained with annealing and normalizing.

In order to demonstrate how cooling rate affects the phase transformations during quenching, Figure 3.8 compares the phase transformation for an AISI 4140 during fast (20°C/s) and slow (5°C/s) cooling rates. For a specific part, a significant amount of martensite is formed during cooling at 20°C/s, but much less at 5°C/s. Cooling at 5°C/s results in about 4% and 6% ferrite formed before the start of bainite (Bs) and martensite (Ms) formation, respectively.

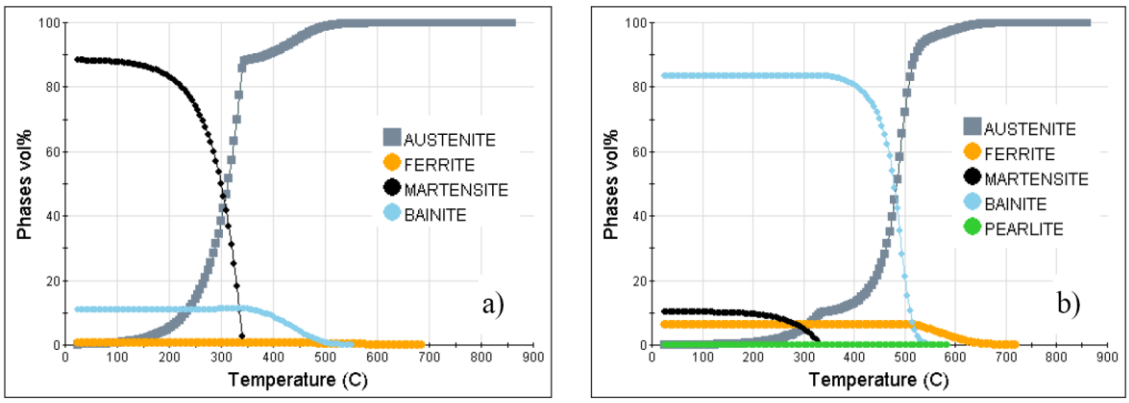

Figure 3.8 - Microstructure evolution in a 4140 steel during cooling at (a) 20°C/s and (b) 5°C/s (Guo *et al.*, 2009).

The TTT diagram is defined for diffusion-controlled transformations. Bainite is one of the products obtained during quenching process. However, Voort (1991) observes that a horizontal line, labeled M_S, appears on each TTT diagram. This line indicates the temperature at which martensite (diffusionless transformation) starts to form on quenching from the austenitizing temperature. Upon further cooling below this temperature, more and more martensite will form. The percentage o austenite transformed to martensite as cooling progresses is commonly defined as a function of temperature. The temperatures may be indicated as M_S, M_{50} and M_{90}, representing the temperatures in which the martensite begins to form, the austenite is half transformed and the austenite is 90% transformed, respectively.

According to Totten and Howes (1997), the most common quenchants in hardening practice are liquids including water, water that contains salt, aqueous polymer solutions, and hardening oils. Inert gases, molten salt, molten metal, and fluidized beds are also used. Quenching techniques used for liquid media are immersion quenching and spray quenching. Immersion quenching, where the part is submerged into an unagitated or agitated quenchant, is the most widely used. The part may be quenched directly from the austenitizing temperature to room temperature (direct quenching) or to a temperature above the M_S temperature, where it is held for a specified period of time, followed by cooling in a second medium at a slower cooling rate (time quenching or interrupted quenching). The quenching intensity can be changed by varying the type of quenchant, its concentration and temperature, and the rate of agitation. The heat transfer is mainly determined by the impingement density and its local distribution.

Quenching is proposed to obtain the hardest microstructure that can be produced in any carbon steel: martensite. However, according to the process conditions and workpiece dimensions, bainite is also obtained. Two major types of martensite form in iron-base alloys as a result of the shear-type, diffusionless martensitic transformation of high-temperature stable solid solution austenite: lath (lower %C) and plate (higher %C) martensite (Figure 3.9).

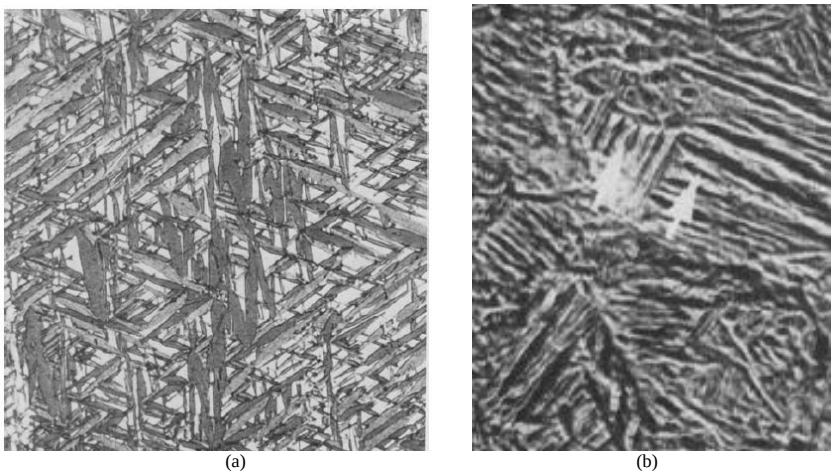

(a) (b)

Figure 3.9 – Typical (a) plate and (b) lath martensite (Krauss and Marder, 1971).

3.2.5. Hardenability

Martensite is the hardest microstructure that can be produced in any carbon steel. To obtain martensite through the transformation of austenite, mixtures of ferrite and cementite should be avoided. Thus, the maximum hardness that can be produced in any given steel is that associated with a fully martensitic microstructure. Therefore, the quenching process is used to obtain martensite, and also bainite, to increase the material hardness.

Qualitatively, Sharma (1996) defines hardenability as a property of steel which corresponds to its susceptibility to hardening upon quenching. The concept of hardenability is different of intensity of hardening. Hardness of quenched (martensitic) steels is essentially a function of their carbon content and generally refers to the hardness of 100% martensite structure. Hardenability, on the other hand, deals with the depth of hardening upon quenching finite sized samples. As an example, steel quenched to 100% martensite may have lower hardness but higher hardenability as compared to steel having higher hardness on quenching to 100% martensite.

An important approach to the evaluation of hardenability is the use of the end-quench test developed by Jominy and Boegehold (Jominy and Boegehold, 1938). The test is now commonly referred as the Jominy test, and has the great advantage of characterizing the hardenability of a given steel from a single specimen rather than from

a series of round bars. The specimen is cooled at one end by a colum of water, thus the entire specimen experiences a range of cooling rates between those associated with water and air cooling. After quenching, parallel flats ground on opposite sides of the specimen, and hardness readings are taken along the bar starting from the quenched end, and plotted as shown in Figure 3.10 (Krauss 1980).

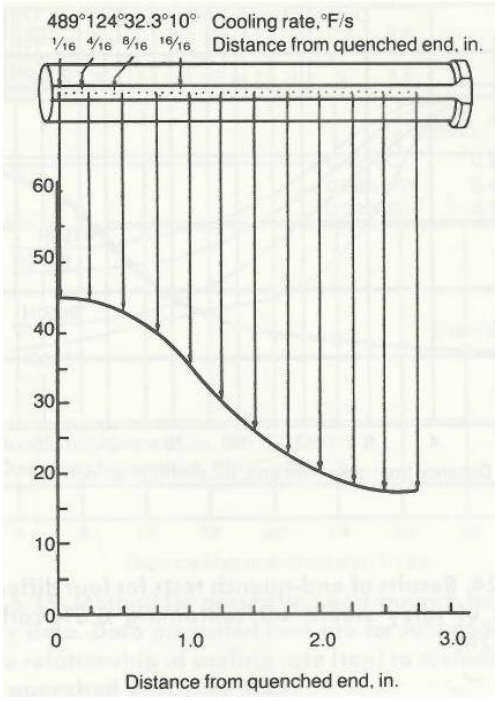

Figure 3.10 – Method of plotting hardness data from an end-quenched Jominy specimen (Melloy, 1977; in Krauss, 1980).

As the cooling rate changes along the Jominy bar, the transformed phases also change along the bar. Therefore, the hardness is different for each point of the bar. The hardness can be readily calculated when the microstructure at room temperature is known. Figure 3.11 exemplifies the phases volume fraction along the bar for 4140 and 5140 alloys.

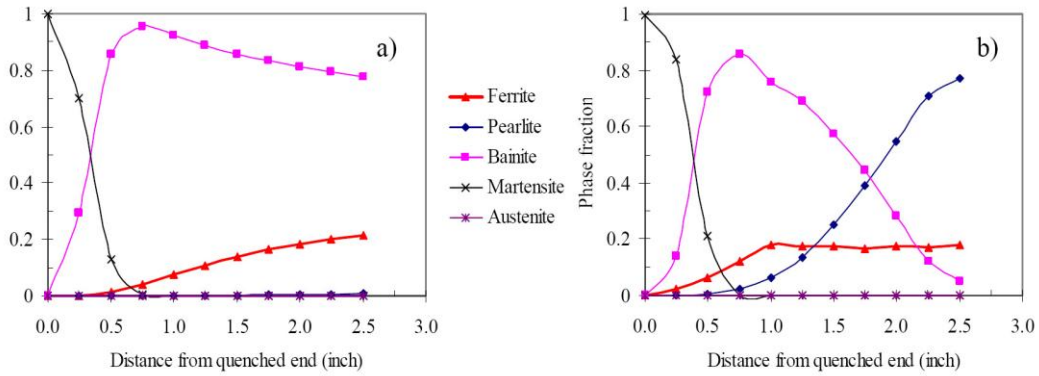

Figure 3.11 - Microstructure change along the Jominy quench bar for (a) 4140, and (b) 5140 alloys (Guo *et al.*, 2009).

The material hardness is cooling rate dependent. The hardenability is different for each steel composition. For AISI 4140 steel, Figure 3.12 relates cooling rate and hardenability superposed on TTT and CCT diagrams. It can be observed that martensite and bainite are the hardest phases compared to ferrite and perlite.

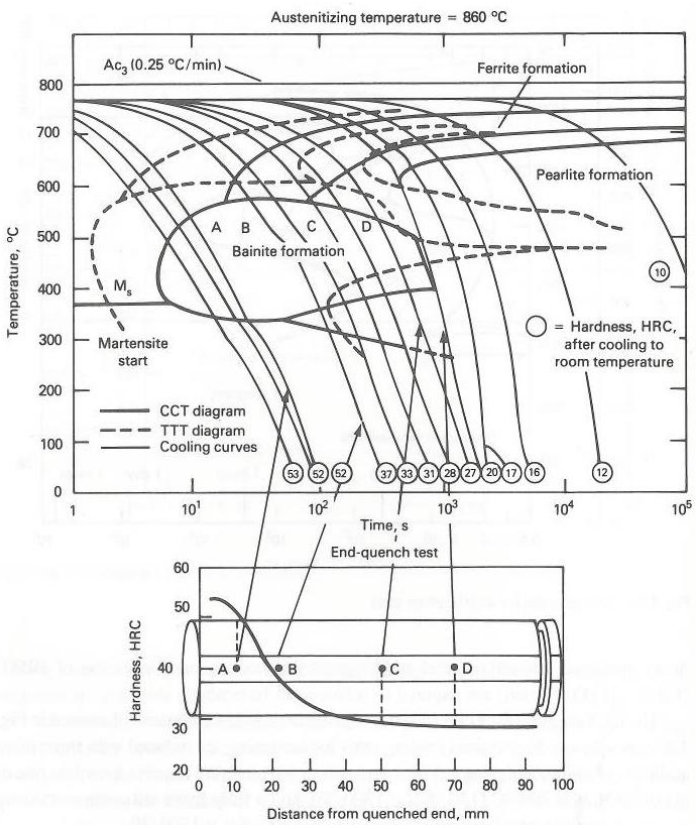

Figure 3.12 – Experimentally determined CCT diagram (solid lines) for AISI 4140. TTT diagram (dashed lines) is also shown (Totten *et al.*, 1993).

The effectiveness of a given quenching medium is ranked by a parameter referred to as its "severity of quench". This measure of cooling or quenching power is determined experimentally by quenching a series of round bars of given steel (Krauss, 1980). Figure 3.13 shows schematically the results of oil and water quenching bars of SAE 3140 steel. The cross-hatched areas represent the unhardened areas of the various bars, assuming that less than 50% martensite represents an unhardened microstructure. The larger the bar diameter, the greater the unhardened diameter. Oil-quenched bars also produce larger nothardened diameters when compared to water-quenched bars.

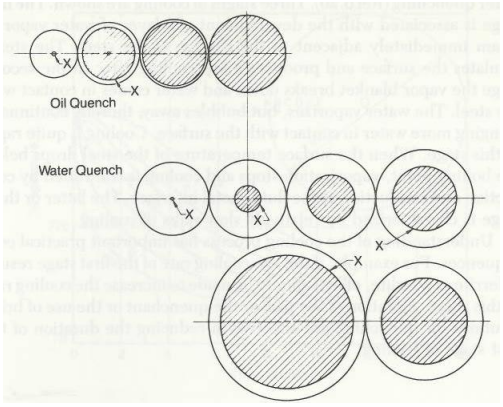

Figure 3.13 – Schematic representation of extend of hardening in oil-quenched and water-quenched bars of SAE 3140 steel of various diameters. The cross-hatched areas represent the unhardened core (Grossmann and Bain, 1964).

3.3. Stress

3.3.1. Principal Stress

Hosford and Caddell (2007) define the stress as the intensity of force, *F*, in a specific point:

$$\sigma = \frac{\partial F}{\partial A}\,, \quad com\ \partial A \to 0 \tag{3.1}$$

where A is the area that undergoes *F*.

When the stress is constant over a given area, the following relation can be written:

$$\sigma = \frac{F}{A}\,. \tag{3.2}$$

Figure 3.14 (a) shows a bidimensional perspective of the beginning of a compressive process. The cylindrical workpiece is divided in small elements, and the stresses in each one can be analyzed as shown in Figure 3.14 (a) and (b). The stress is divided in 9 components. The normal component is referred to the one in which the force is applied on the normal direction to the plane. The normal stress may be tensile or compressive. The shear components are the stresses parallel to the plane.

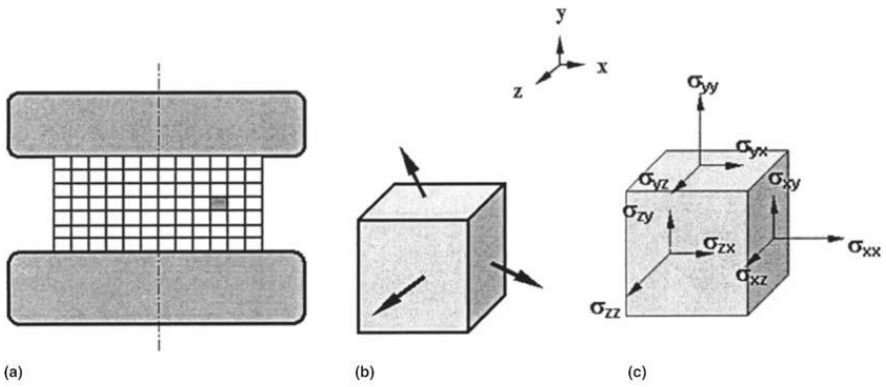

Figure 3.14 – Stress acting on an element. (a) Cylinder upsetting process. (b) Forces acting on an element. (c) Stress components acting on an element (Altan *et al.*, 2005).

Stress components are defined with two subscripts. The first indicates the normal direction to the plane, and the second indicates the force direction. The normal stresses are compressive when negative, and tensile when positive. This collection of stresses is referred to as the stress tensor:

$$\sigma_{ij} = \begin{bmatrix} \sigma_{xx} & \sigma_{yx} & \sigma_{zx} \\ \sigma_{xy} & \sigma_{yy} & \sigma_{zy} \\ \sigma_{xz} & \sigma_{yz} & \sigma_{zz} \end{bmatrix}. \tag{3.3}$$

The stresses expressed along one set of axes may be expressed along any other set of axes. In Figure 3.15 the force F'_y on y' direction can be calculated as $F'_y = F_y \cos\theta$, and the area normal to y' will be $A_{y'} = A_y/\cos\theta$. So,

$$\sigma_{y'} = \frac{F_{y'}}{A_{y'}} = \frac{F_y \cos\theta}{\frac{A_y}{\cos\theta}} = \sigma_y \cos^2\theta\ . \tag{3.4}$$

In the same way,

$$\tau_{y'x'} = \frac{F_{x'}}{A_{y'}} = \frac{F_y \operatorname{sen}\theta}{\frac{A_y}{\cos\theta}} = \sigma_y \cos\theta \operatorname{sen}\theta \ . \tag{3.5}$$

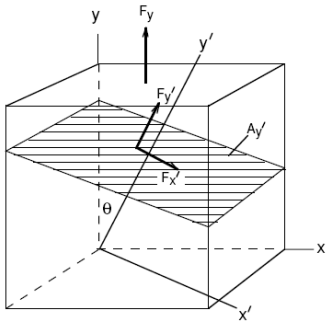

Figure 3.15 – The stresses acting on a plane, A', under a normal stress, σ_y (Hosford and Caddell, 2007).

It is possible to define a set of axes in which the shear stresses become zero. In this case, the normal stresses σ_1, σ_2 e σ_3 will be called principal stresses. The principal stress magnitudes, σ_P, are calculated:

$$\sigma_P{}^3 - I_1\sigma_P{}^2 - I_2\sigma_P - I_3 = 0 \tag{3.6}$$

where I_1, I_2 e I_3 are called the *invariants* of the stress tensor:

$$\begin{aligned} I_1 &= \sigma_{xx} + \sigma_{yy} + \sigma_{zz}, \\ I_2 &= \sigma_{yz}{}^2 + \sigma_{zx}{}^2 + \sigma_{xy}{}^2 - \sigma_{yy}\sigma_{zz} - \sigma_{zz}\sigma_{xx} - \sigma_{xx}\sigma_{yy} \quad \text{e} \\ I_3 &= \sigma_{xx}\sigma_{yy}\sigma_{zz} + 2\sigma_{yz}\sigma_{zx}\sigma_{xy} - \sigma_{xx}\sigma_{yz}{}^2 - \sigma_{yy}\sigma_{zx}{}^2 - \sigma_{zz}\sigma_{xy}{}^2 \ . \end{aligned} \tag{3.7}$$

The first invariant $I_1 = -p/3$ where p is the pressure. I_1, I_2 e I_3 are not dependent on the orientation of the axes. Expressing them as a function of principal stresses, they are:

$$\begin{aligned} I_1 &= \sigma_1 + \sigma_2 + \sigma_3, \\ I_2 &= -\sigma_2\sigma_3 - \sigma_3\sigma_1 - \sigma_1\sigma_2 \quad \text{e} \\ I_3 &= \sigma_1\sigma_2\sigma_3 \ . \end{aligned} \tag{3.8}$$

3.3.2. Effective Stress

The development of mathematic relations able to predict conditions to reach the plastic strain (yield strength) of a material, when it undergoes any combination of stresses, is very important for plasticity studies. Under uniaxial tensile stresses, as in a tension test,

the yielding starts when the yield strength, σ_0, is reached. For each situation with a particular stress combination, the yielding is related for a particular combination of principal stresses.

The effective stress, $\bar{\sigma}$, is a very practical and useful definition. It is given by a function of the principal stresses, and can also be related, for example, to a yielding criterion. A yielding criterion is a postulated state of stress that will cause yielding, indicating that it will occur in case the effective stress reaches a critical value.

During plastic deformation, the effective stress concept is still valid, and is used as a useful parameter in order to define the behavior in a specific point of a system. Two main criterias are used: Tresca and von Mises ones. Since this work is based on a CAE tool, which approaches effective stress based on von Mises criterion, the here described theory is based von Mises criterion. Tresca criterion is simpler than von Mises criterion, and does not consider the intermediary stress. However, Tresca criterion is more used for engineering projects, while von Mises is used for theoric works, since it is more precise.

Von Mises criterion postulates that yielding will occur when the following mathematical expression reaches a critical value:

$$\left[\frac{(\sigma_2-\sigma_3)^2+(\sigma_3-\sigma_1)^2+(\sigma_1-\sigma_2)^2}{3}\right] = C_1 \,, \tag{3.9}$$

or

$$(\sigma_2-\sigma_3)^2+(\sigma_3-\sigma_1)^2+(\sigma_1-\sigma_2)^2 = C_2 \,. \tag{3.10}$$

The critical value C_2 may be found considering a uniaxial tensile test in the 1-direction. Substituting $\sigma_1 = Y$ e $\sigma_2 = \sigma_3 = 0$ during yielding, the de von Mises criterion can be written as:

$$(\sigma_2-\sigma_3)^2+(\sigma_3-\sigma_1)^2+(\sigma_1-\sigma_2)^2 = 2Y^2 = 6k^6 \,. \tag{3.11}$$

A general equation can be expressed as follows:

$$\left(\sigma_y-\sigma_z\right)^2+(\sigma_z-\sigma_x)^2+\left(\sigma_x-\sigma_y\right)^2+6\left(\tau_{yz}+\tau_{zx}+\tau_{xy}\right) = 2Y^2 = 6k^6 \,. \tag{3.12}$$

Figure 3.16 represents a graph with possible combination for yielding, assuming that $\sigma_2 = 0$. The tridimensional Tresca and von Mises criterions can be visualized in Figure 3.17. The Tresca criterion is a regular hexagonal prism and the von Mises criterion is a cylinder. Both criterions are centered on a line $\sigma_1 = \sigma_2 = \sigma_3$.

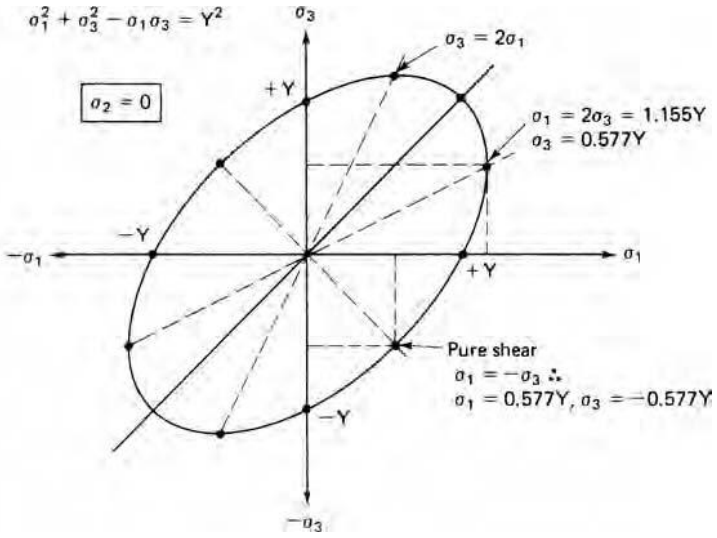

Figure 3.16 - Tresca and von Mises loci showing certain loading paths (Hosford and Caddell, 2007).

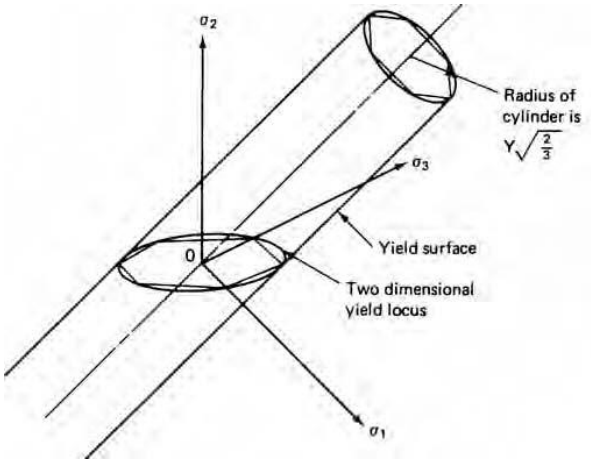

Figure 3.17 - Three-dimensional plots of the Tresca and von Mises yield criterion (Hosford and Caddell, 2007).

Finally, according to Von Mises criterion, the effective stress is:

$$\bar{\sigma} = \frac{1}{\sqrt{2}}[(\sigma_2 - \sigma_3)^2 + (\sigma_3 - \sigma_1)^2 + (\sigma_1 - \sigma_2)^2]^{\frac{1}{2}}. \quad (3.13)$$

3.3.3. Residual Stress

Residual stresses are present in parts after any process that strains the material heterogeneously. A number of thermal and mechanical processes produce residual stresses that might be detrimental to the performance of fabricated steel parts or assemblies. Heavy metalworking such as forging, rolling, and extrusion causes stresses that remain in the metal if the work is performed below the hot-working temperature. Heat treatment processes are also sources of residual stresses.

Residual stresses can be defined as resulting stresses in equilibrium in components that are not undergoing external stresses. They are the result of nonhomogeneous elastic e/or plastic deformation, due to plastic work or phase transformations with volume changing, affecting the state of strain along the workpiece. As an example, Dieter (1988) considers a metal specimen where the surface has been deformed in tension by bending so that part of it has undergone plastic deformation. When the external force is removed, the regions which have been plastically deformed prevent the adjacent elastic regions from undergoing completely elastic recovery to the unstrained condition. Thus, the elastic deformed regions are left in residual tension, and the regions which were plastically deformed must be in a state of residual compression to balance the stresses over the cross section of the specimen. Figure 3.18 gives possible situations in which applied and residual stresses are superposed.

Another source of residual stresses is the cooling of heavy sections after austenitizing. According to Krauss (1980), even during air cooling, the surface of a heavy section may transform to ferrite and cementite well before the center. When the center eventually transforms, the volume expansion associated with the ferrite formation is restrained by the cooler, already transformed surface. As a result the center is compressed and the surface put in tension. Quenching to form martensite produces a similar but even more severe residual stress problem, even in smaller sections, and is one reason why hardenable steels are alloyed to permit martensite formation at lower cooling rates.

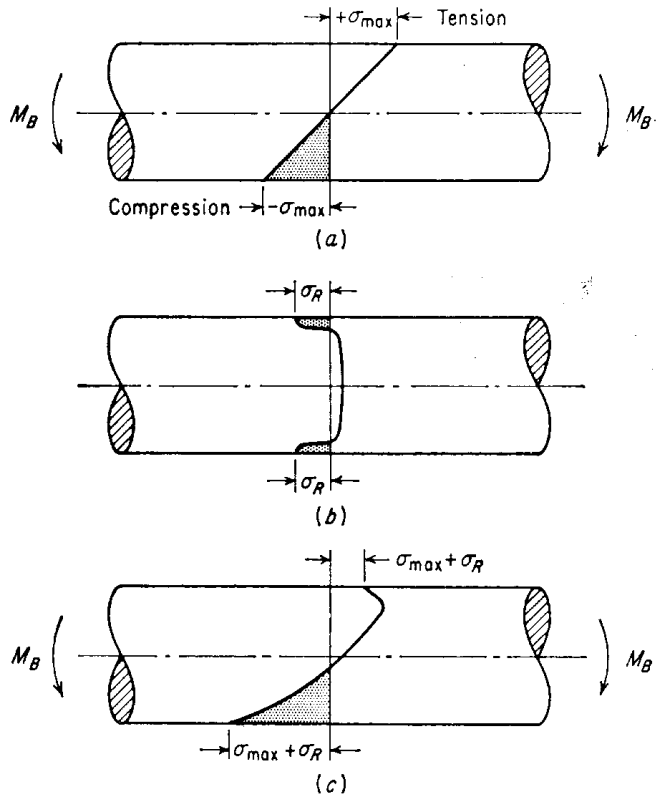

Figure 3.18 – Superposition of applied and residual stresses. (a) Elastic stress distribution with no residual stress; (b) residual stress distribution produced by shot peening; and (c) the algebraic summation of external bending stresses and residual stresses (Dieter, 1988).

Ebert (1978) has studied the manner in which residual stresses are generated on normal cooling down of metallic bodies from elevated temperatures, as shown schematically in Figure 3.19. In this figure, the normal temperature-time cooling curves for the surface and the center of a metallic cylinder are shown in the upper left corner. The cooling rate of the surface of the bar is much greater than that of the center. The manner in which this difference in cooling rates affects the generation of residual stresses is shown in the balance of the figure.

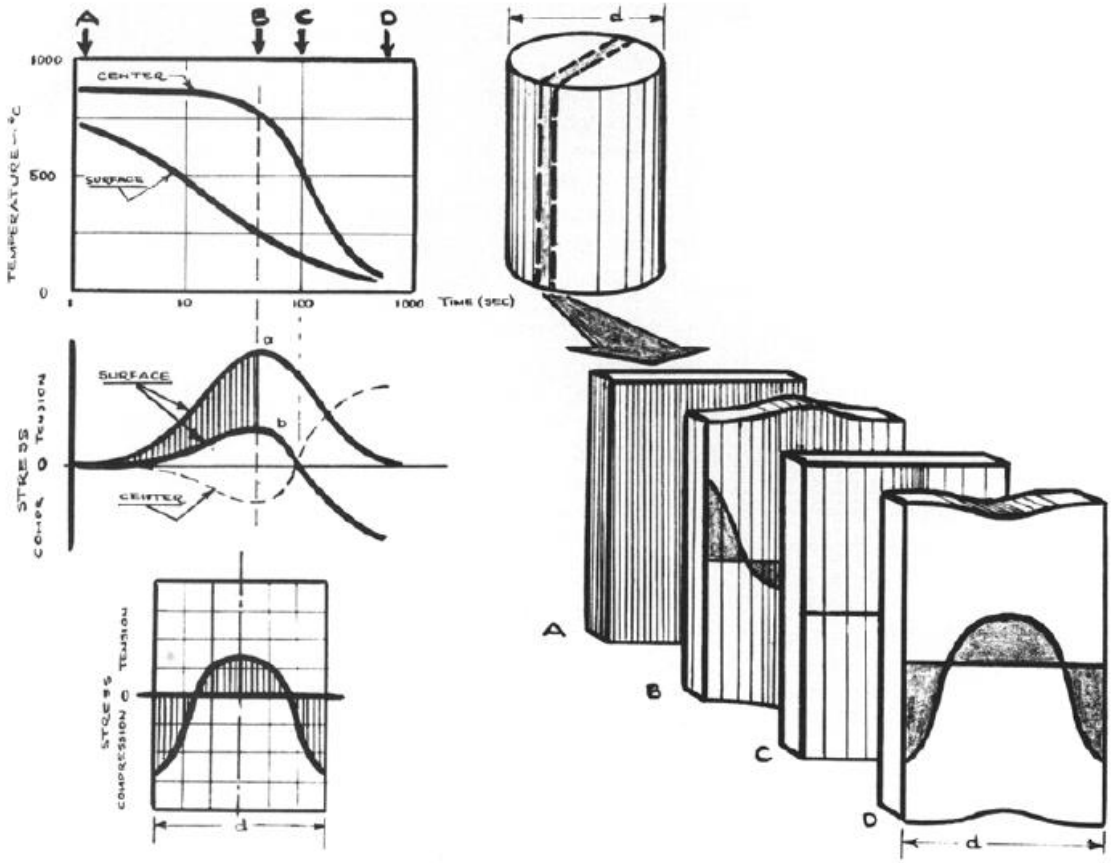

Figure 3.19 - Schematic illustration showing the development of residual stresses on cool-down of a metallic material which undergoes no allotropic transformation on cooling. Only longitudinal stresses are shown (Ebert, 1978).

Totten and Howes (1997) classified the residual stresses according to the area within which they are constant in magnitude and direction into three categories (Figure 3.20). Residual stresses of the first kind are those homogeneous across large areas of the material, i.e., across several grains. Residual stresses of the second kind are those homogeneous across microscopically small areas (one grain or subgrain region) and are in equilibrium across a sufficient number of grains. Residual stresses of the third kind are those inhomogeneous across microscopically small areas (within several atomic distances of single grains) and are in equilibrium across subgrain regions. Residual stresses of the first kind are called macroresidual stresses, and those of the second and third kinds are called microresidual stresses. In practice, only macroresidual stresses of the first kind are considered, and they are characterized by the technological processes

by which they originate. The main groups of residual stresses are: casting, forming, working-out, heat treatment, joining and coating residual stresses.

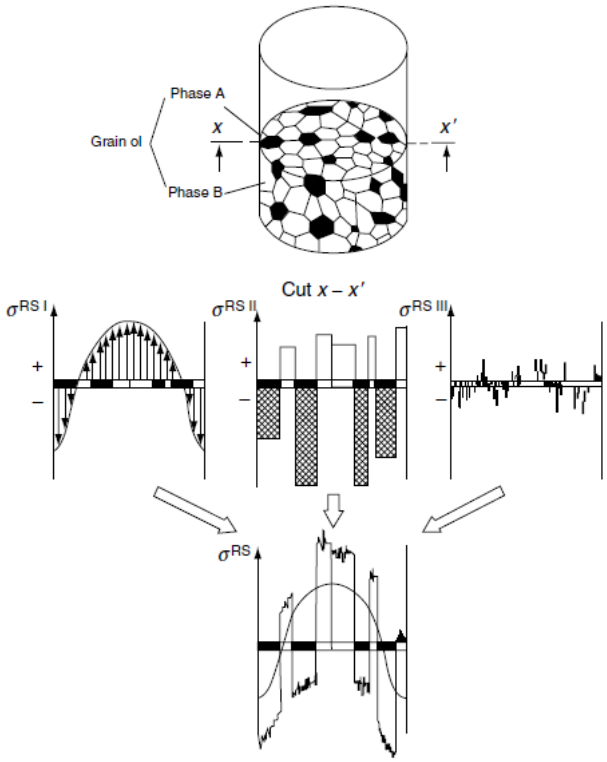

Figure 3.20 – Schematic of all three kinds of residual stresses in a two-phase material after quenching and their superposition (Liscic *et al.*, 1992).

Compressive residual stresses are desirable in a finished component to enable it to resist applied stress systems. However some stresses originated during manufacturing will be relieved during heating as the stress system readjusts. Residual stresses due to heat treatment processes may distort and crack components, making them not satisfactory for service. In addition, residual stresses from heat treatment may distort parts during subsequent manufacturing such as machining. The residual stresses may also result in failure in service below design stresses. The maximum value of the residual stress which can be produced is equal to the elastic limit of the material.

Some of techniques to measure residual stresses are: x-ray diffraction, hole-drilling and bending and deflection methods (Totten and Howes, 1997). Advanced computational tools can also predict residual stresses resulting from a specific process. Koç *et al.*

(2006) used numerical techniques to predict residual stresses after quenching of a forged aluminum block, and the predictions were compared with experimental measurements. Looking for reducing residual stresses, they performed two different methods of cold working (compression and stretching) which are commonly used to reduce the residual stresses. The comparison of results showed that both compression and stretching processes reduced the residual stresses more than 90% (Figure 3.21).

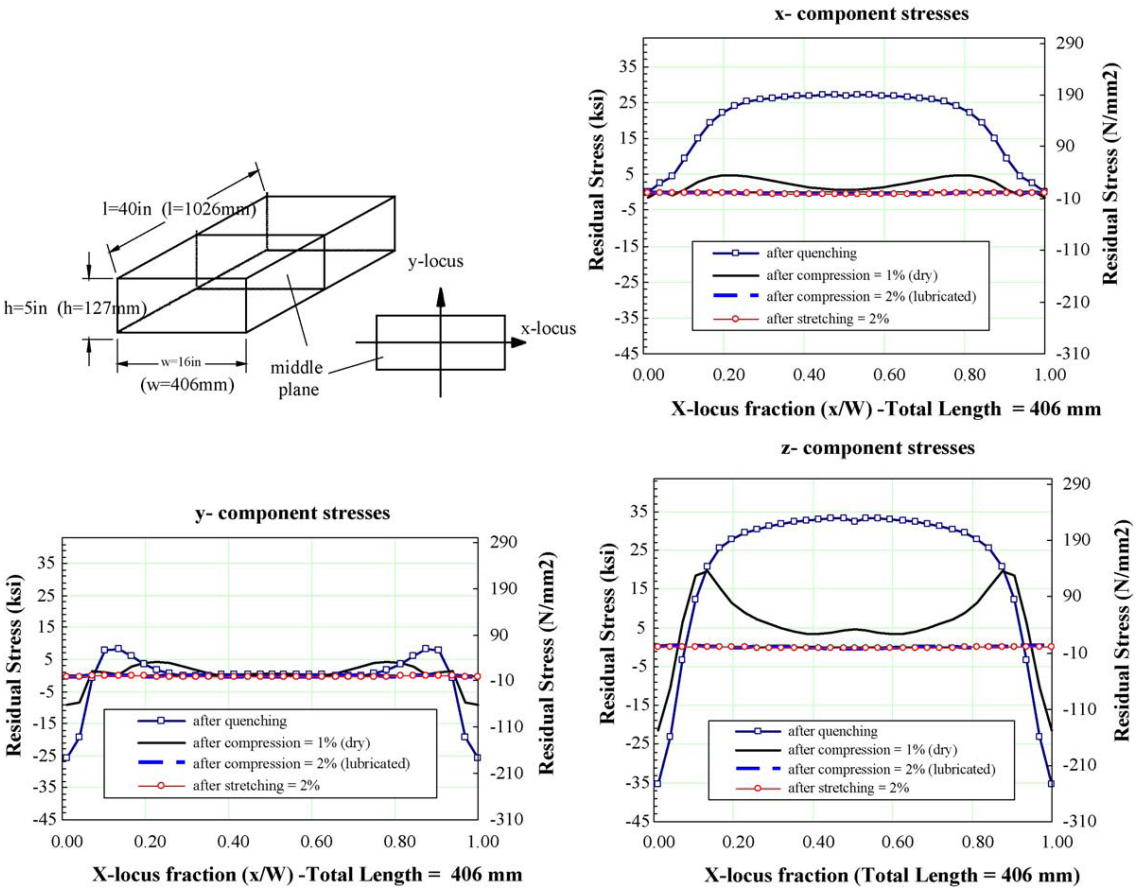

Figure 3.21 – *x*-, *y*- and *z*-component residual stress of an aluminum block along *x*-locus after quenching, compression, and stretching (Koç *et al.*, 2006).

3.4. Strain

3.4.1. Definition

Strain, ε, describes the amount of deformation in a body. When a body is deformed, points in that body are displaced. Figure 3.22 shows a line in a material that has been

deformed. The line has been translated, rotated, and deformed. The deformation is characterized by the engineering or nominal strain, e:

$$e = \frac{(l - l_0)}{l_0} = \frac{\Delta l}{l_0} \qquad 3.14$$

However, an alternative definition is called true or logarithmic strain, which is a nonlinear strain measure that is dependent upon the final length of the model:

$$\varepsilon = \frac{dl}{l} \quad \therefore \quad \varepsilon = \ln\frac{l}{l_0} = \ln(1 + e) \qquad 3.15$$

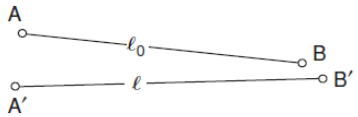

Figure 3.22 - Deformation, translation, and rotation of a line in a material (Hosford and Caddell, 2007).

Strains may be caused by mechanical work, heat and heat treatment processes, including all boundary conditions of each specific system. For deformation, the total incremental strain is assumed to consist of several components:

$$\dot{\varepsilon}_{ij}^{Total} = \dot{\varepsilon}_{ij}^{e} + \dot{\varepsilon}_{ij}^{p} + \dot{\varepsilon}_{ij}^{th} + \dot{\varepsilon}_{ij}^{tr} + \dot{\varepsilon}_{ij}^{tp} \qquad 3.16$$

where e, p, th, tr, and tp represent the entities for elastic, plastic, thermal, phase transformation and transformation plasticity, respectively. The phase transformation occurs from phase i to phase j.

3.4.2. Elastic, Plastic and Thermal Strain

Elastic strain is the amount of nonpermanent deformation in a body. The recovery of the original dimensions of a deformed body when the load is removed is known as elastic behavior. As a result from the changes in strain produced by elastic recovery, a dimensional change of the formed part occurs after the pressure of the forming tools is released. This dimensional change is called springback. The elastic recovery, and therefore the springback, will be greater the higher the yield stress, the lower the elastic modulus, and the greater the plastic strain.

For elastic behavior, Hooke's laws can be expressed as:

$$\varepsilon_x = \frac{1}{E} = \left[\sigma_x - \nu\left(\sigma_y - \sigma_z\right)\right],$$
$$\varepsilon_y = \frac{1}{E} = \left[\sigma_y - \nu(\sigma_z - \sigma_x)\right], \quad 3.17$$
$$\varepsilon_z = \frac{1}{E} = \left[\sigma_z - \nu\left(\sigma_x - \sigma_y\right)\right],$$

and,

$$\gamma_{yz} = \frac{1}{G}\tau_{yz},$$
$$\gamma_{yz} = \frac{1}{G}\tau_{yz}, \quad 3.18$$
$$\gamma_{yz} = \frac{1}{G}\tau_{yz},$$

where E is Young's modulus, ν is Poisson's ratio, γ is shear strain, τ is shear stress, and G is the shear modulus. For an isotropic material, E, ν, and G are interrelated by:

$$\mathrm{E} = 2\mathrm{G}(1 + \nu), \text{ or} \quad 3.19$$

$$G = \frac{E}{2(1+\nu)}. \quad 3.20$$

In manufacturing processes such as metal forming, permanent deformations are desired. Plastic strain is the term used for permanent strain. According to yielding criterion (i.e. von Mises), a postulated state of stress will cause yielding, and therefore plastic strain, indicating that yielding will occur in case the effective stress reaches a critical value. The incremental plastic work per volume is the effective strain, $\bar{\varepsilon}$, defined below:

$$dw = \sigma_1 d\varepsilon_1 + \sigma_2 d\varepsilon_2 + \sigma_3 d\varepsilon_3 = \bar{\sigma} d\bar{\varepsilon} \quad 3.21$$

The von Mises strain may be expressed as:

$$d\bar{\varepsilon} = \frac{\sqrt{[(d\varepsilon_2 - d\varepsilon_3)^2 + (d\varepsilon_3 - d\varepsilon_1)^2 + (d\varepsilon_1 - d\varepsilon_2)^2]}}{3} \quad 3.22$$

For proportional straining with a constant ratio of $d\varepsilon_1 : d\varepsilon_2 : d\varepsilon_3$, the total effective strain is:

$$\bar{\varepsilon} = \sqrt{\left(\frac{2}{3}\right)(\varepsilon_1^2 + \varepsilon_2^2 + \varepsilon_3^2)} \quad 3.23$$

A considerable part of the energy applied in manufacturing processes is converted in heat. The reasons for the generated heat may include: mechanical work generates heat during material deformation; friction between workpiece and tools generates heat; and

heat and cooling processes change the workpiece temperature. This temperature changing expands or shrinks the part. Therefore, thermal strain occurs when coefficient of thermal expansion is specified and a temperature change is applied:

$$\varepsilon^{th} = \alpha(T - T_0) = \alpha\Delta T, \quad 3.24$$

where α is the thermal expansion coefficient, and T_0 is the reference temperature.

Depending on the system boundary conditions, the material dilatation can elastically and plastically deform the material. In addition, plastic flow, especially at elevated temperature, can be considered a thermally activated process (Dieter, 1988).

3.4.3. Phase Transformation and Transformation Plasticity Strain

Phase transformation occurs during heating and cooling processes of steels. As an example, for steel alloys, austenite is the parent phase that can transform into martensite following fast cooling. Martensite transformation is diffusionless, having the same composition as does its parent austenite. Krauss (1980) explains that since diffusion is suppressed, usually by rapid cooling, the carbon atoms do not partition themselves between cementite and ferrite but instead are trapped in the octahedral sites of a body-centered cubic structure, thus producing a new phase, martensite. The solubility of carbon in a bbc structure is greatly exceeded when martensite forms; hence martensite assumes a body-centered tetragonal (bct) unit cell in which the *c* parameter of the unit cell is greater than the other two *a* parameters (Figure 3.23). With higher carbon concentration of the martensite, more interstitial sites are filled, and the tetragonality increases. Thermal expansion and quench contraction curves for an AISI 4340 steel are illustrated in Figure 3.24.

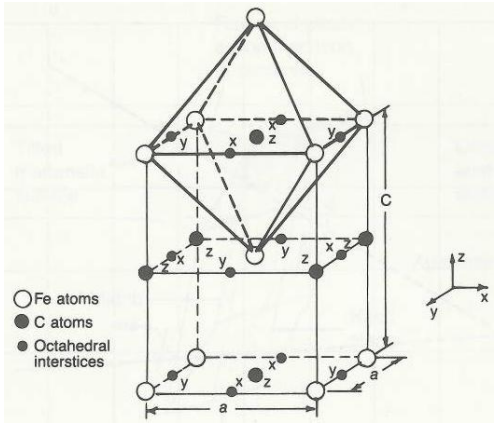

Figure 3.23 – Body-centered tetragonal crystal structure of martensite in Fe-C alloys. Carbon atoms are trapped in one set (z) of interstitial octahedral sites. The x and y sites are unoccupied (Cohen, 1962; in Krauss, 1980).

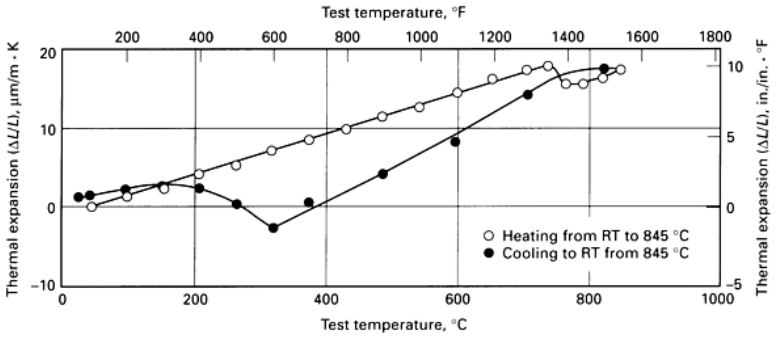

Figure 3.24 – Thermal expansion and contraction curves for 4340 steel (Bates *et al.*, 1991).

Phase transformation strain is a consequence of the structure change during the transformation. As a result of phase transformation, the material may change its volume. The volume change due to transformation is induced by a change in the lattice structure of the metal. This amount of strain is in the form of:

$$\dot{\varepsilon}_{ij}^{tr} = \sum \beta_{ij} \dot{\xi}_{ij} \delta_{ij}, \qquad 3.25$$

where β_{ij} is the fractional length change due to transformation, $\dot{\xi}_{ij}$ is the transformation volume fraction rate, and δ_{ij} is the Kronecker delta.

Phase transformations are accompanied by sharp reductions in plastic-strain resistance, which has been classified as transformation plasticity (Volkov *et al.*, 1984). The change of the dimensions of a part due to transformation plasticity occurs in combination with

the dimensional changes due to transformation induced volume change. For FE simulation, the equation for transformation plasticity can be considered as:

$$\dot{\varepsilon}_{ij}^{tp} = \frac{3}{2} K_{ij} h(\xi_j) \dot{\xi}_j s_{ij}, \quad 3.26$$

where K_{ij} is the transformation plasticity coefficient, $h(\xi_j) = 2(1 - \xi_j)$, $\dot{\xi}_j$ is the volume fraction rate, and s_{ij} is the deviatoric stress tensor. A general range for K_{ij} for steel is (SFTC, 2010):

- austenite phase to ferrite, pearlite or bainite phase: between 4 and 13 ($x10^{-5}$/MPa);
- austenite to martensite: between 5 and 21 ($x10^{-5}$/MPa);
- and ferrite or pearlite to austenite: between 6 and 21 ($x10^{-5}$/MPa).

3.5. Stress-Strain Curves

3.5.1. The Tension Test

Tension tests are used to measure the effect of strain on strength. Sometimes other tests, such as torsion, compression, and bulge testing are used, but the tension test is simpler and most commonly used. Moosbrugger (2002) explains that the simplest loading to visualize is an one-dimensional tensile test, in which a uniform slender test specimen is streched along its long central axis. The stress-strain curve is a representation of the performance of the specimen as the applied load is increased monotonically usually to fracture. Stress-strain curves are usually represented as:

- “Engineering” stress-strain curves, in which the original dimensions of the specimen are used in most calculations;
- “True” stress-strain curves, where the instantaneous dimensions of the specimen at each point during the test are used in the calculations. This results in the true curves being above the engineering curves, notably in the higher strain portion of the curves.

According to Hosford and Caddell (2007), initially the deformation is elastic and the tensile force is proportional to the elongation. Elastic deformation is recoverable. It disappears when the tensile force is removed. At higher forces the deformation is

plastic, or nonrecoverable. In a ductile material, the force reaches a maximum and then decreases until fracture. Figure 3.25 shows a typical engineering stress-strain curve obtained through a FE simulation. The engineering stress-strain curve is compared to the true stress-strain curve, obtained from the effective stresses and strains up to necking start, in Figure 3.26 for the plastic behavior.

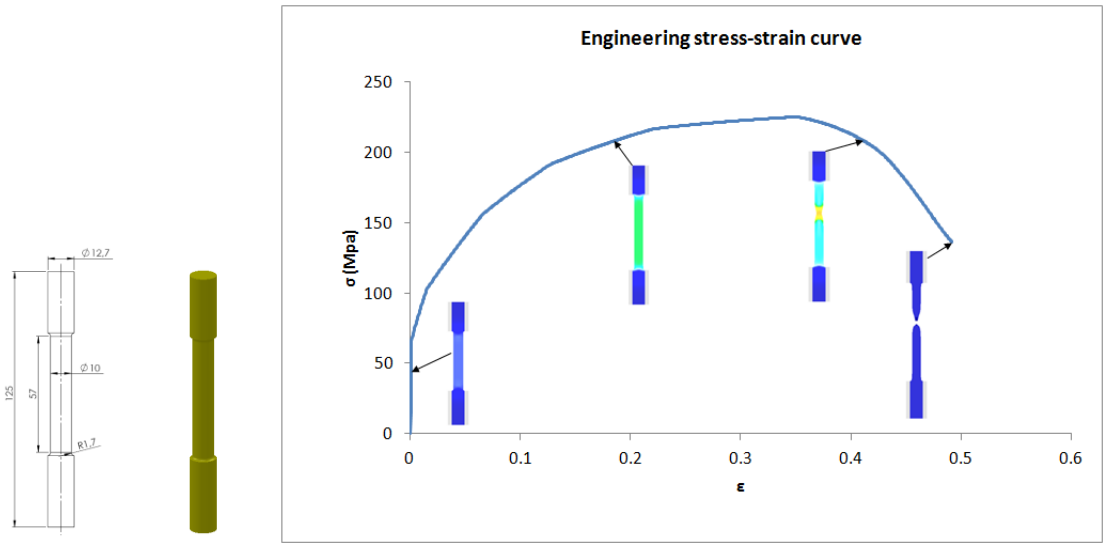

Figure 3.25 – Simulated tension test: (a) axisymmetric specimen (dimensions in mm) and (b) tension test for cooper (da Silva *et al.*, 2010).

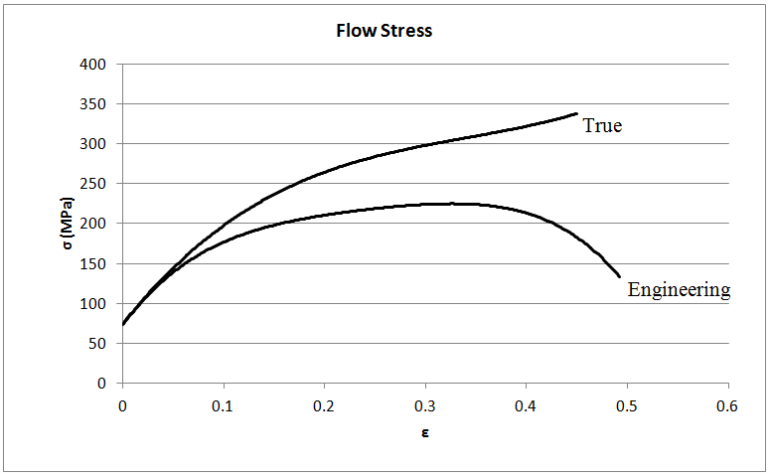

Figure 3.26 – Simulated tension test for cooper (da Silva *et al.*, 2010).

The engineering stress, σ_e, is calculated based on the initial cross section area, A_0, of the specimen, following the relation

$$\sigma_e = \frac{F}{A_0} \ , \qquad 3.27$$

and the engineering strain, e, is calculated as

$$e = \frac{\Delta l}{l_0} \ , \qquad 3.28$$

where, l_0 is the original gauge length, and Δl is the elongation of l_0 during the test.

Several basic mechanical material properties are shown in Figure 3.27, and described by Server *et al.* (2011) as follows:

- Yield Strength (Y): indicates the start of plastic deformation. Y is determined approximately by drawing a parallel line to the linear elastic region of engineering stress-strain curve from 0.2% engineering strain. The intersection of this parallel line with the engineering stress-strain curve gives the value of Y.
- Ultimate Tensile Strength (UTS) is the maximum engineering stress in a tensile test and is connected to the end of uniform elongation and start of localized necking.
- Elastic Modulus (E) (also known as Young's Modulus) is the slope of the elastic part of an engineering stress-strain curve.
- e_0 is the elongation at yield strength (Y).
- Uniform elongation (e_u) is the elongation at the maximum load.
- Total elongation (e_t) (also known as elongation at break) is the total elongation of the original gage length of a tensile specimen at fracture. This includes both uniform (e_u) and post-uniform elongations.
- Area Reduction (A_r) is the percentage of reduction in the area, and calculated by cross section area at fracture (A_f) and initial cross section area (A_0):

$$A_r = \frac{A_0 - A_f}{A_0} x100\% \ . \qquad 3.29$$

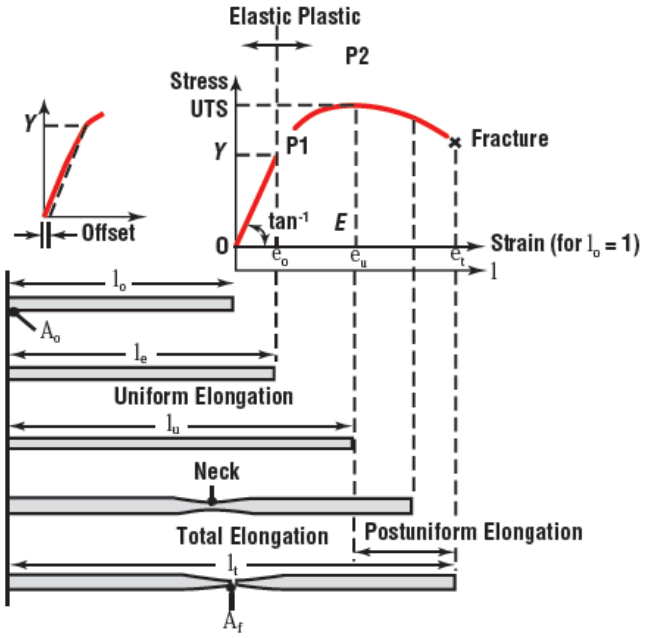

Figure 3.27 – A tensile-test sequence showing different stages in the elongation of the specimen (Kalpakjian and Schimd, 2006).

The true stress is based upon the instantaneous cross sectional area, A_i,

$$\sigma = \frac{F}{A_i} = \sigma_e \frac{A_0}{A_i} = \sigma_e \frac{l_i}{l_0} = \sigma_e(1+e), \tag{3.30}$$

where, $l_i = \Delta l + l_0$. Before necking, the true strain can be calculated as:

$$d\varepsilon = \frac{dl}{l} \quad \therefore \quad \varepsilon = ln\frac{l}{l_0} = ln(1+e). \tag{3.31}$$

After necking, the true strain must be based on the area:

$$d\varepsilon = \frac{-dA}{A} \quad \therefore \quad \varepsilon = ln\frac{A_0}{A}. \tag{3.32}$$

3.5.2. Determining the True Stress-Strain Curve with Yield and Ultimate Tensile Strengths

In some situations, a few material properties are known. For some applications, such as simulation proposes, it is necessary to obtain the behavior of the material based on the true stress-true strain curve, shown in Figure 3.26 for the plastic region (flow stress curve). Elastic region is linear and can be defined according to the Hooke's Law:

$$\sigma = E\varepsilon\,. \tag{3.33}$$

The flow stress curve can be approximated by the power-law expression, also called the Hollomon equation,

$$\sigma = K\varepsilon^n \,, \tag{3.34}$$

where, K is the strength coefficient and n is the strain hardening exponent.

Hosford and Caddell (2007) demonstrated that at UTS, $\varepsilon = n$. Since $F = \sigma A$, when $dF = 0$, $\sigma dA + Ad\sigma = 0$. So, $\sigma/d\sigma = -dA/A = d\varepsilon$, and the maximum load corresponds to $d\sigma/d\varepsilon = 0$. Considering the power law and solving this equation, the true stress at the maximum load can be expressed as

$$\sigma_u = K{\varepsilon_u}^n = Kn^n. \tag{3.35}$$

As it can be analyzed in Figure 3.27, points P1 and P2 represent Y and UTS, respectively. Since Y and UTS are known, a system of two equations, power law, is solved. Equation 3.34 is applied for Y, and Equation 3.35 is applied for UTS. The strain at P1 changes depending on material and it is larger than 0.2% engineering strain. For steel, it may be assumed it is 0.6% (Server *et al.*, 2011). In case the Young's Modulus, E, is known, the strain at P1 can be defined, and the curve more precise. For this method, it is assumed that the effect of the strain rate is neglected and the strain hardening exponent, n, does not change with strain.

3.6. Interface Conditions between Workpiece and Environment

3.6.1. Heat Transfer during Air Cooling

Processes such as normalizing are usually used to eliminate some microstructural irregularities and to refine the grain structure of hot worked steels, and for general refinement of structure prior to quenching hardening treatment. The austenitized part during normaling process is air cooled. The mechaninsm of heat transfer between steel components and enviroment are convection and radiation.

Incropera *et al.* (2007) define that the convection heat transfer mode comprises two mechanisms: the energy transfer due to ramdom molecular motion (diffusion), and

transferred by the bulk, or microscopic, motion of the fluid. It is costumary to use the term convection when referring to this cumulative transport and the term advection when referring to transport due to bulk fluid motion. Convection heat transfer may be classified as forced or free (natural) convection (Figure 3.28). Boiling and Condensation are also heat transfer processes. Regardless of the particular nature of the convection heat transfer process, the appropriate rate equation is of the form:

$$q_c" = h_c(T_s - T_\infty), \tag{3.36}$$

where $q_c"$ is the convective heat flux, h_c is the convection heat transfer coefficient, and T_s and T_∞ are surface and fluid temperature, respectively.

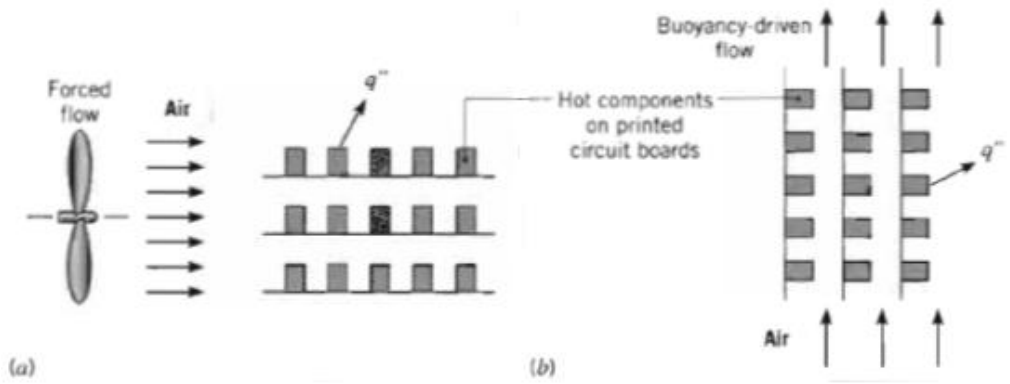

Figure 3.28 – Convection heat transfer processes; (a) forced convection and (b) natural convection (Incropera *et al.*, 2007).

Thermal radiation is energy emitted by matter that is at a nonzero temperature. The energy of the radiation field is transported by electromagnetic waves. There is an upper limit for the emissive power, which is described by the Stefan-Boltzmann law:

$$q_{r;b}" = \varphi T_s^4, \tag{3.37}$$

where φ is the Stefan-Boltzmann constant ($\varphi = 5.67 \times 10^{-8}\ W/m^2 \cdot K$). The heat flux emitted by a real surface is given by:

$$q_r" = \epsilon \varphi T_s^4, \tag{3.38}$$

where and ϵ is a radiative property of the surface termed emissivity. With values in the range $0 \leq \epsilon \leq 1$, this property provides a measure of how efficiently a surface emits energy relative to a blackbody. It depends strongly on the surface material and finish (Incropera *et al.*, 2007).

Bamberger and Prinz (1986) have investigated the heat transfer coefficients for various cooling methods. For air cooling, Figure 3.29 shows the coefficients of heat transfer by means of convection and radiation.

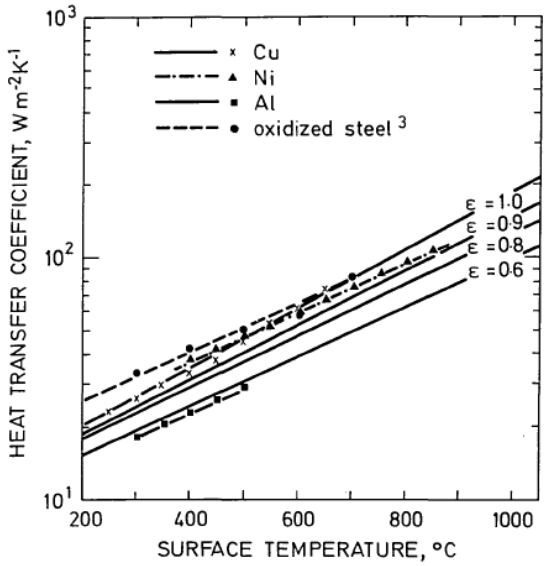

Figure 3.29 – Heat transfer coefficients for air cooling as function of surface temperature (Bamberger and Prinz, 1986).

3.6.2. Radiation Exchange between Surfaces

During heating and cooling processes, components being heat treated may be disposed close to other components. In this case, the temperature profile of each part may change due to the proximity of other parts in the same process. Since a body radiates energy to environment, other bodies may be part of the environment, and part of the system as a consequence.

Therefore, radiation may also be incident on a surface from its surroundings. The radiation may be originated from other body surfaces and/or other sources. Figure 3.30 shows an example of two rings disposed next to the other. In case the parts are normalized, each one will transfer heat to the environment through convection and radiation, but also receive heat from the other through radiation.

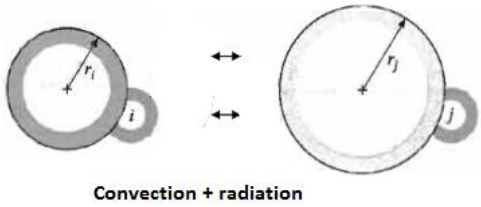

Figure 3.30 – Two rings exchanging heat with the environment (modified from Incropera *et al.*, 2007).

The heat flux to the environment for one ring in the system shown in Figure 3.30 may be defined as:

$$q" = q_c" + q_r". \tag{3.39}$$

So, considering equations 3.27 and 3.29:

$$q" = h_c(T_s - T_\infty) + (\epsilon\varphi T_s^4 - \alpha\varphi T_{sur}^4) = h_c(T_s - T_\infty) + \epsilon\varphi(T_s^4 - T_{sur}^4), \tag{3.40}$$

where the absorptivity $\alpha = \epsilon$ (surface is assumed to be one), and T_{sur} is the surface temperature of the surrounding bodies.

To compute radiation exchange between any two surfaces, a view factor F_{ij} between two bodies i and j (as in Figure 3.30 as an example) should be considered. Incropera *et al. (*2007) defines the view factor as the radiation leaving surface i that is intercepted by surface j. The view factor is influenced by the bodies' dimensions and position in the system. According to Incropera *et al.* (2007), for the bidimensional system in Figure 3.27, the view factor is:

$$F_{ij} = \frac{1}{2\pi}\Big\{\pi + [C^2 - (R+1)^2]^{1/2} - [C^2 - (R-1)^2]^{1/2} + (R-1)\cos^{-1}\left[\left(\frac{R}{C}\right) - \right.$$
$$\left. - \left(\frac{1}{C}\right)\right] - (R+1)\cos^{-1}\left[\left(\frac{R}{C}\right) + \left(\frac{1}{C}\right)\right]\Big\}, \tag{3.41}$$

where $R = r_j/r_i$, $S = s/r_i$ (s is the distance between the rings), and $C = 1 + R + S$. The heat flux is dependent on the view factor, represented by the relation:

$$F_{ij} = \frac{q_{i\to j}"}{J_i}, \tag{3.42}$$

where the total radiosity J_i represents the rate at which radiation leaves a unit are of the surface.

3.6.3. Heat Transfer during Quenching Process

For most of the steels, high cooling rates must be applied to austenitized due to the necessity of quenching and hardening. The higher the cooling rate, the higher is the possibility of obtaining a martensitic structure. However, high cooling rates may cause residual stresses, deformation and cracking. Figure 3.8 showed the microstructure evolution of AISI 4140 during two different cooling rates. The austenite phase is transformed into different phases: ferrite, martensite, bainite, and pearlite. For a high cooling rate (20°C/s), most of austenite is transformed in martensite, while for lower cooling rates, the percentage of formed martensite is lower. Successful hardening usually means achieving the required microstructure, hardness, strength, or toughness while minimizing residual stress, distortion, and the possibility of cracking.

The most common quenchant media are either liquids or gases. The liquid quenchants commonly used include: oil that may contain a variety of additives; water; aqueous polymer solutions; and water that may contain salt or caustic additives. According to Bates *et al.* (1991), the examination of quenching performance by cooling curve analysis is perhaps the most informative method of characterizing a quenchant media. Cooling curves are obtained by quenching a test piece containing one or more thermocouples into a test sample of the quenching fluid, in a laboratory quenching bath, or in the production bath itself.

Three stages of heat removal have been defined by Tensi *et al.* (1994) during quenching in liquid media: the film boiling or vapour blanket stage (stage A); the nucleate boiling stage (stage B); and the convection stage (stage C). The three stages are correlated to a typical cooling temperature curve as shown in Figure 3.31. During stage A, the vapor blanket develops and is maintained while the supply of heat from the interior of the part to the surface exceeds the amount of heat needed to evaporate the quenchant and maintain the vapor phase. In stage B heat is rapidly removed from the surface as liquid quenchant contacts the metal surface and is vaporized. And during stage C boiling stops and cooling takes place by conduction and convection into the quenchant. In addition, during immersion cooling in several fluids, e.g. in water, oil and certain polymer

solutions, the three periods of heat transfer with their strongly varying heat transfer coefficients, can be simultaneously present on the surface. Figure 3.32 shows a real quenching process of a cylinder. After 10 seconds, a boiling vapor film around component starts at the corner of front and moves along the component (stage B), and stage C occurs after 60 seconds. Tiryakioglu (1996) also considers a 4th stage: the initial liquid contact stage, that lasts for a very short time and may not be measured by regular thermocouples. Figure 3.33 shows a schematic of the 4 stages.

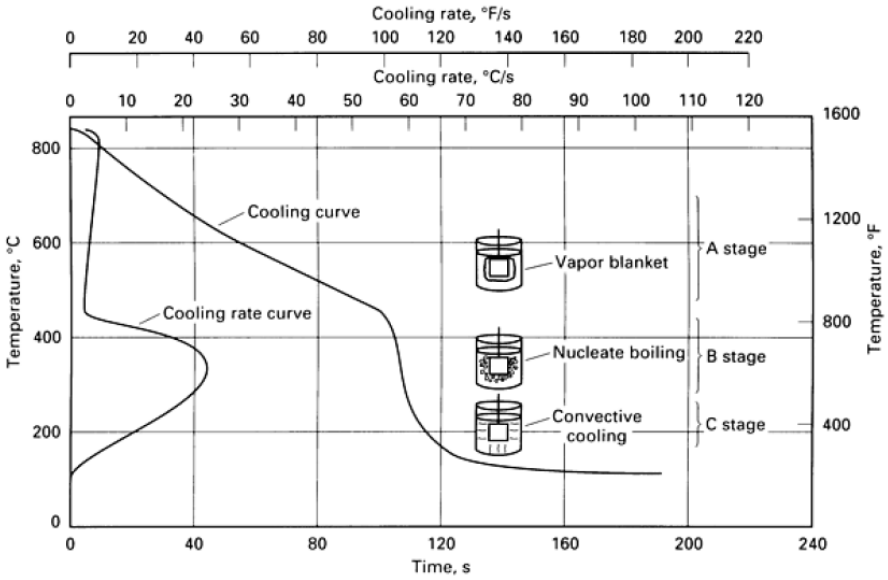

Figure 3.31 - Cooling curve and cooling rate curve at the center of a 25 mm diameter stainless probe quenched with 95 °C water flowing at 15 m/min (Bates *et al.*, 1991).

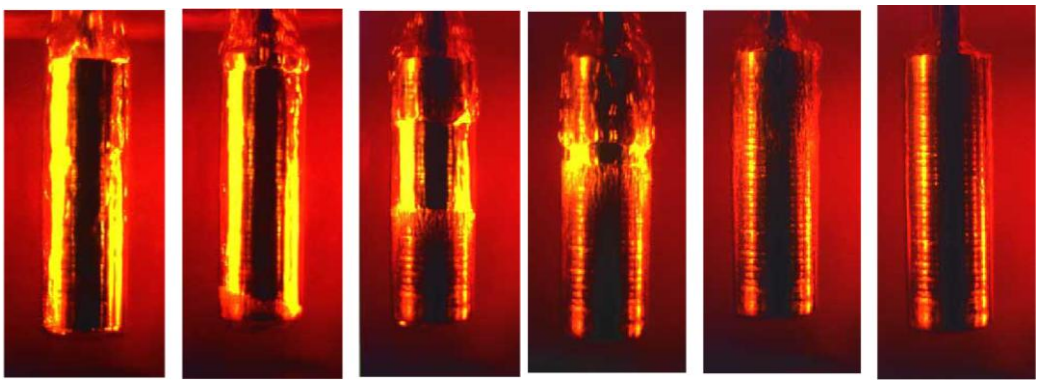

Figure 3.32 – Series of photographs illustrating the various stages in the quenching process using normal speed quenching oil (Houghton, 2011).

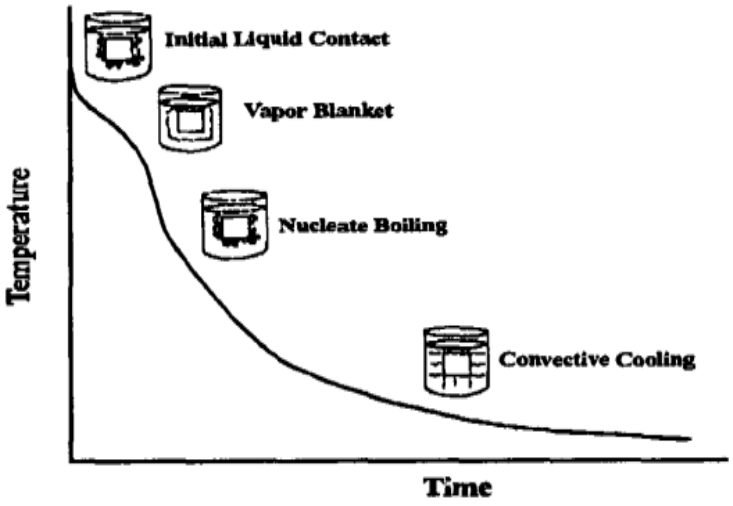

Figure 3.33 – Different cooling mechanisms during quenching (Tiryakioglu, 1996).

Totten (2007) explains that the velocity of the spreading wetting front and the time interval of the simultaneous presence of film boiling and nucleate boiling, and therefore the heat transfer coefficient, can be strongly influenced by changing the physical properties of the quenchant and the sample. The items varied are:

- type of quenchant as described by its boiling temperature, viscosity, thermal capacity and surface tension;
- additives to the quenchant, and their concentration;
- temperature and agitation rate of the quenchant;
- thermal characteristics of the body and its transformation behavior;
- surface roughness of the body and surface layers;
- and geometry and initial temperature distribution of the sample.

The heat transfer coefficient, HTC, between the body surface and the surrounding medium is strongly dependent on the surface temperature, and may be mathematically described as:

$$HTC = \frac{Q}{A(T_S - T_\infty)}, \qquad 3.43$$

where A is the surface area changing energy, and Q is the heat transfer rate.

The determination of the heat transfer coefficient is based on Fourier's law of heat transfer, which states that heat flow across the surface of a body is proportional to the temperature gradient at the surface:

$$Q = -\lambda A \frac{\partial T}{\partial x}, \tag{3.44}$$

where λ is the thermal conductivity, and x is a local coordinate. Heat transfer in a solid where temperature changes with time and no heat sources are present within the body is:

$$\frac{\partial T}{\partial t} = a\left(\frac{\partial^2 T}{\partial x^2} + \frac{\partial^2 T}{\partial y^2} + \frac{\partial^2 T}{\partial z^2}\right), \tag{3.45}$$

where t is the time, and $a = \lambda/\rho C_p$ is the thermal diffusivity dependent on density, ρ, and specific heat capacity, C_p.

The temperature dependence of the heat transfer coefficient, h, during quenching of an austenitic steel in water and oil is shown in Figure 3.34. It can be observed that water provides a higher heat transfer when compared to oil. Another example of heat transfer variation is shown in Figure 3.35. Due to the body shape (a cylinder), the heat transfer varies around its surface, and also varies when the quenchant is agitated.

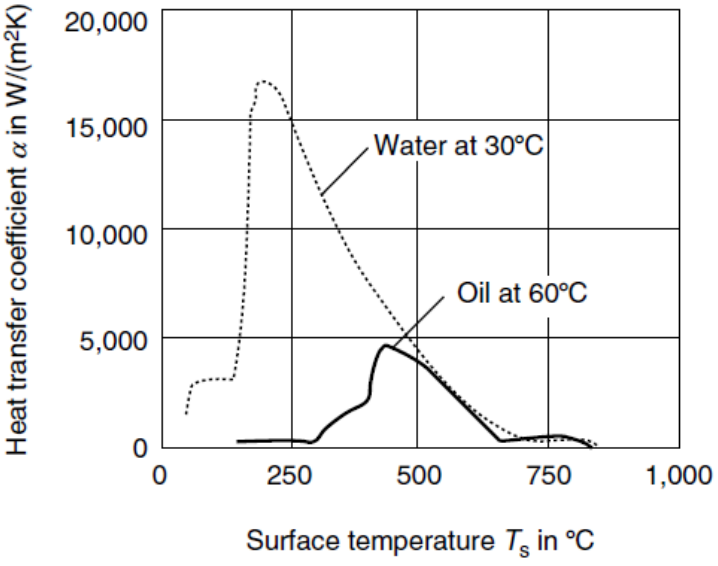

Figure 3.34 – Heat transfer coefficient versus surface temperature of an austenitic steel cylinder (25-mm diameter x 100mm) quenched into water at 30°C and into a fast oil at 60°C flowing at 0.3 m/s (Totten, 2007).

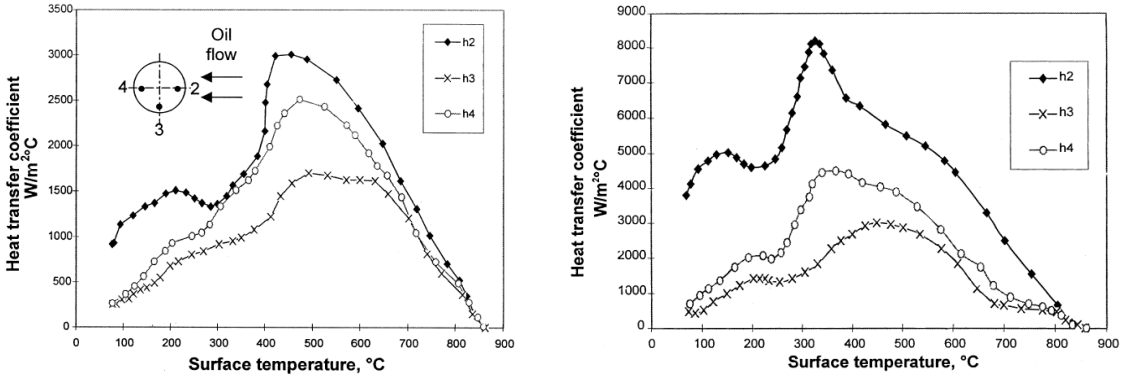

Figure 3.35 – Variation in the heat transfer coefficient around the bar for transverse flow with (a) no agitation and (b) agitation (Sedighi and McMahom, 2000).

3.6.4. Heat Transfer Coefficient Calculation

The heat transfer coefficient, HTC, between a body surface and the surrounding medium is usually described as a function of the surface temperature. The HTC can be defined for an incremental surface area through the measuring of the heat flux to the cooling agent, considering all the process conditions described in the previous items. However, it is common to define a single heat transfer behavior for the surface of the body, or use different behaviors for different surface orientation in the part.

A mathematical method for the determination of HTC can be applied based on temperatures measured within workpieces during the cooling process. Bamberger and Prinz (1986) explain that direct measurement of the heat flux to the cooling agent can be done only under thermal equilibrium, where the heat flux outwards is compensated by a known heat flux into the specimen so that its temperature remains constant. However, in quenching process the heat flux for cooling increases rapidly as the surface temperature decreases in the range of lower surface temperatures (below 900°C), which makes it to be impossible to obtain thermal equilibrium during cooling in this temperature range. As a common practice, the determination of the HTC is based on the solution of the transient heat conduction equation, taking into account a temperature measured at the centre of a small specimen or few millimeters below its surface. So, the HTC is calculated based on equations already described in the previous item. Figure 3.36 shows

a metal component with thermocouples that are installed for temperature data acquisition during heat treatment process.

Figure 3.36 – (a) Surface thermocouples used on an instrumented high-pressure turbine disk to establish HTC (Schirra and Goetisshius, 1992; in Wallis, 2010).

According to Wallis (2010), in industry, the calculation of HTC has generally been obtained either by trial and error or by inverse engineering techniques. In either case, the surface of a part will be divided into zones, and normally, each zone will have a thermocouple associated with it that is beneath the surface and somewhere midzone. A computer model can be used to predict the temperatures during the process and compare to the experimental data. The heat transfer coefficients are modified and the procedure is repeated until the experimental and model results have converged (Figure 3.37). An alternate method is to use inverse engineering techniques, where, as with the iterative method, the part is divided into surface areas. However, in the inverse case, the measured temperature data are input into a nonlinear finite-difference or finite-element computer code. Figure 3.38 shows the correlation between cooling curves and determined HTC. For a ring shape, Figure 3.39 shows typical locations for temperature measuring and the HTC for oil quenching.

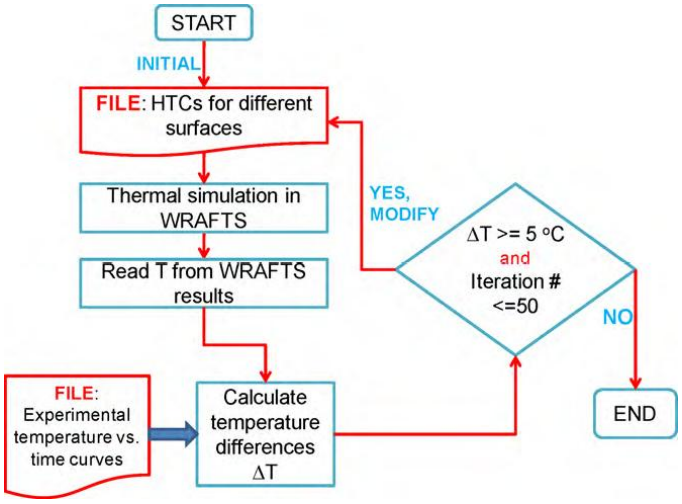

Figure 3.37 – A flow chart for iterative determination of HTC (Xiao *et al.*, 2010).

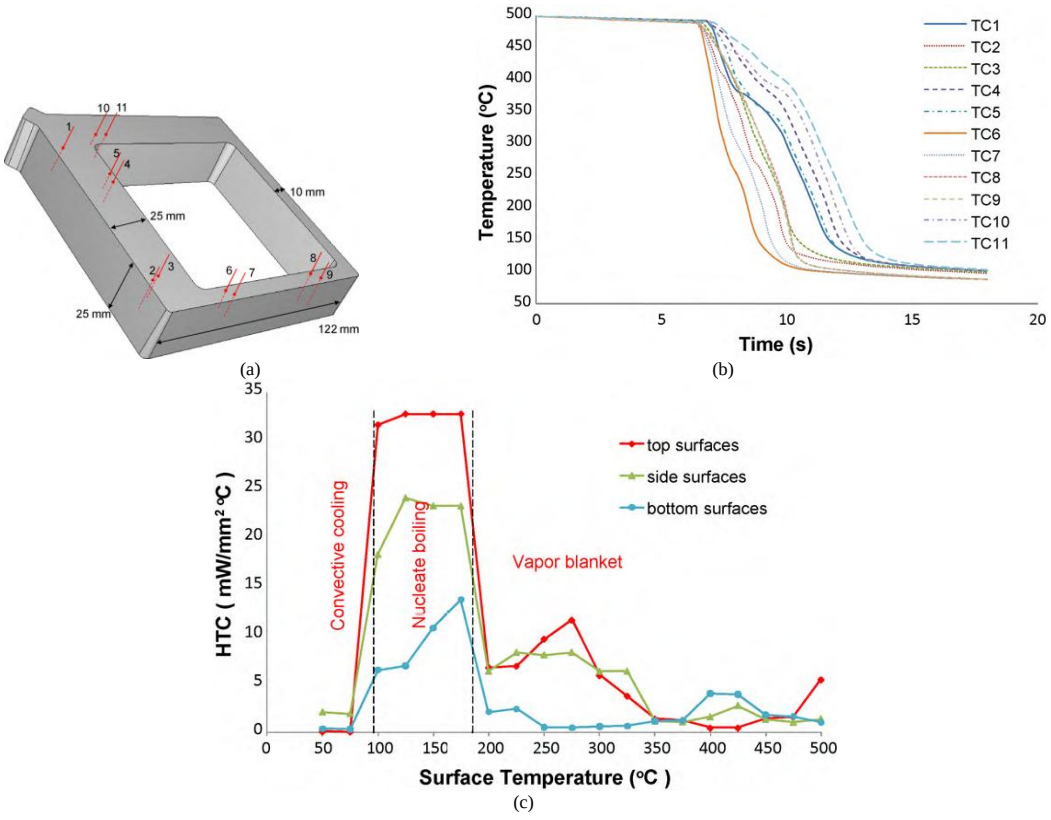

Figure 3.38 – Case study of the determination of heat transfer coefficient during quenching of an aluminum casting part: (a) thermocouples locations; (b) measuring cooling curves; and (c) interactively determined HTC (Xiao *et al.*, 2010).

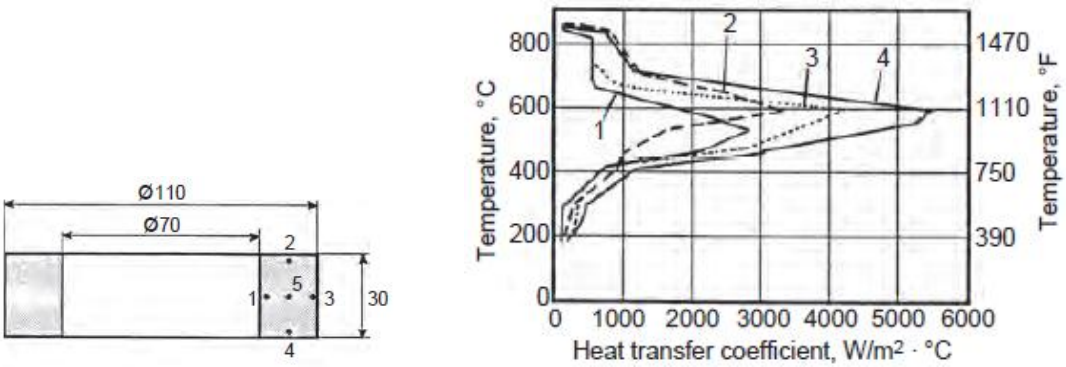

(a) (b)

Figure 3.39 – Heat transfer coefficients around a ring cooled in oil (Segerberg and Bodin, 1992; in Wallis, 2010).

3.7. Heat Treatment Distortion

3.7.1. Mechanisms of Distortion

Distortion is a geometric change cause by deformation occurring during manufacturing processes. A schematic plot of distortion is shown in Figure 3.40. Heat treatment distortions are associated with deformations caused by temperature changes. The basic mechanisms that change shape and size of a steel part during heat treating are attributed by Totten (2007) to three fundamental causes:

- residual stresses that cause shape change when they exceed the material yield strength. This will occur on heating when the strength properties decline;
- stresses caused by differential expansion due to thermal gradients. These stresses will increase with the thermal gradient and will cause plastic deformation as the yield strength is exceeded;
- and volume changes due to transformational phase change. These volume changes will be contained as residual stress systems until the yield strength is exceeded.

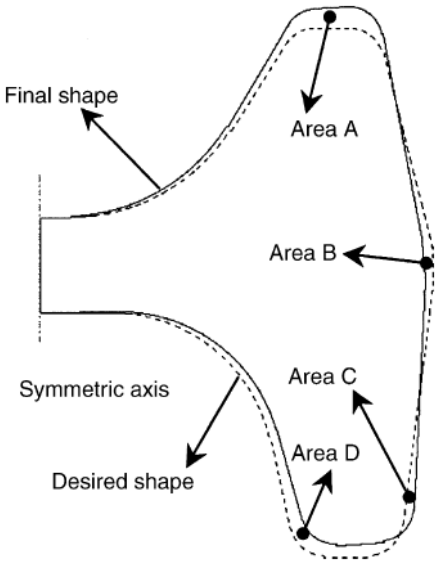

Figure 3.40 – Definition of distortion (Li *et al.*, 2006).

The distortions may occur in five different stages: prior to heat treatment; during heat-up for heat treatment; at treatment temperature, i.e., carburizing, nitriding, etc; during quenching and cooling; and during postquenching processing. Manufacturing and design factors prior to heat treatment that affect distortion include: material properties, homogeneity of properties across the cross section of the material; residual stress system magnitude and distribution; and part geometry. Distortion during component heating occurs due to different reasons, such as: shape change due to relief of residual stress; shape change due to thermal stresses causing plastic flow; and volume change due to phase change on heating. Distortions during high-temperature processing are due to: volume expansion during diffusion treatments; and creep. During quenching process, the distortion causes are: cooling characteristics in quenching – quenchant selection and agitation; quenching uniformity; parts shape and size – component design; surface condition of parts; and steel grade selection. Finally, distortions can be treated during post quenching process, such as: straightening; tempering; stabilization with tempering and subzero treatment; metal removal by grinding; etc (Totten, 2007).

During quenching processes, the distortion mechanism can be described based on Figure 3.41. Totten and Howes (1997) explain the coupling effects among the three different characteristic of quenching – cooling rate, metallic structure, and internal stresses. The cooling rate influences the phase transformation of the metallic structure,

whereas the latent heat due to structural changes affects the cooling rate. All phase transformations of austenite during quenching are accompanied by volume expansion. In addition, steels contract with decreasing temperature. As a consequence, locally and temporally different changes of structure and temperature cause nonuniform volumetric changes in the quenched part that can result in transformational and thermal stresses. These stresses accelerate or hinder the phase transformation and influence the volume expansion. While the phase transformation brings out a defined metallic structure, the volumetric dilatation and thermal and transformational stresses result in deformation and residual stresses. At room temperature, both characteristics influence the material properties.

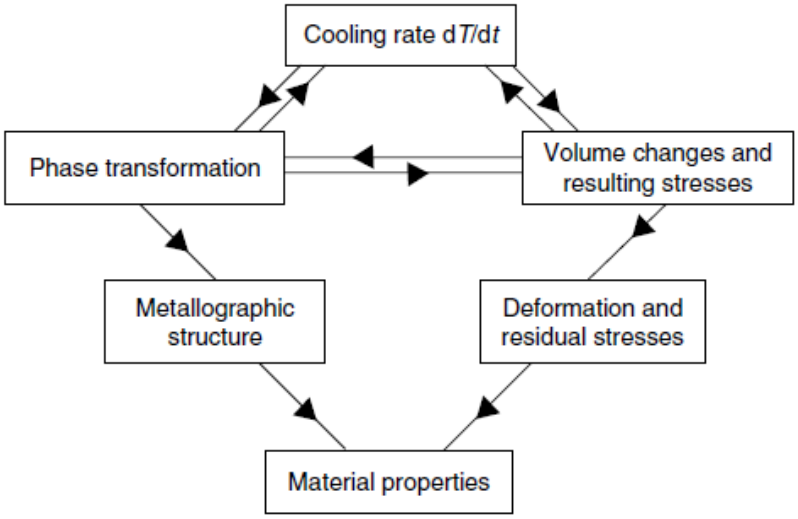

Figure 3.41 – Coupling effects among quenching characteristics (Totten and Howes, 1997).

When a steel part is cooled from the austenite phase field, the surface cools most rapidly and austenite transformation with the attendant volume expansion occurs there first. The outer surface is, therefore, into tension and the core is into compression, causing internal plastic flow. When the center cools and tries to expand due to the martensite formation, the hard surface is put into tension and the core into compression. For subcritical heat treated parts, the core contracts. In this case, the surface is put into compression and the core into tension.

In order to minimize quench distortion, the component design can be more effective considering symmetry and balance of cross-sectional area, and avoiding sharp corners and edges. For the steel grade selection, the compositional tolerances should be checked, low-carbon steels that have lower susceptibility for distortion, and, if possible, to combine high-alloy steel and a very slow cooling. For the selection of quenchant, it is not desirable to use quenchants with excessively high heat-removal rates. It is necessary to optimize the cooling rate and the obtained microstructure, which makes the selection of quenchant and agitation a difficult task.

Some possibilities of correcting quench distortion have been described above. However, we will consider the straightening in special, due to the objectives of this work. Straightening is the procedure conducted on distorted components by flexing or selective peening processes. This procedure is usually performed after tempering and may also be applied under hot condition, avoiding risks of cracking. The straightening also reduces residual stresses, as exemplified in Figure 3.21.

3.7.2. Quench Distortion

The mechanisms for quenching distortion were defined in the previous item. Thermal, metallurgical and mechanical properties influence on the final distortion and residual stresses during metal quenching processes, as shown in Figure 3.42. The Finite Element Method (FEM) is a powerful tool employed to help to understand the sensitivity of material properties on distortion and residual stress. The coupling effects such as phase transformation enthalpy, transformation-induced plasticity and dissipation have to be considered, as well as the displacement and the volume averaged effective stresses. Figure 3.43 shows the distortion of a cylinder during water quenching process.

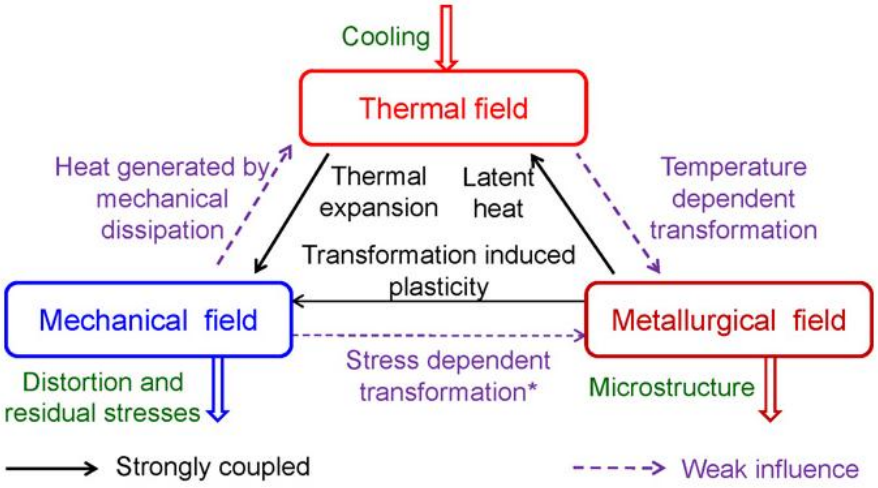

Figure 3.42 – Schematic representation of various couplings between physical fields (Nallathambi *et al.*, 2010).

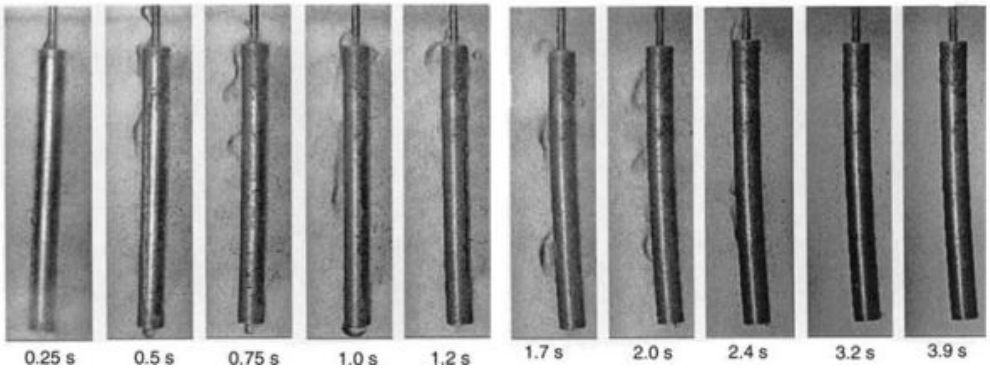

Figure 3.43 – Boiling behavior and distortion during quenching in still city water at 30°C (Arimoto *et al.*, 1998; in Narazaki *et al.*, 2002).

Freborg *et al.* (2007) conclude that dimensional and residual stress response during heat treatment can vary significantly based on the sensitivity of a steel part to thermal and transformation strains. Figure 3.44 shows the influence of the cooling condition on the final shape of a notched bar. The quench distortion of a AISI 5120 cut cilynder shape was investigated by Lee and Lee (2008), and is shown in Figure 3.45. A relationship between distortion and microstructure was defined. Ye *et al.* (2003) studied the quench distortion of an I-beam. These authors used a 2D FE simulation to predict the final shape, comparing to experimental values. Figure 3.46 shows the part characteristics and the comparison with experimental values, and Figure 3.47 represents distortion by means of plotting x and y displacement.

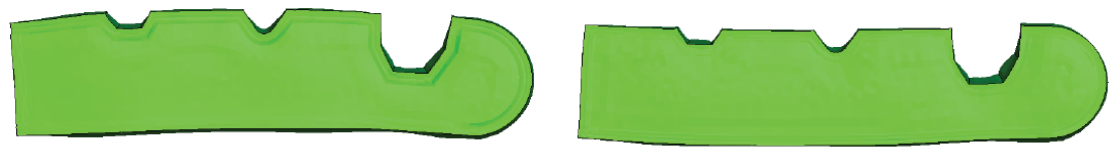

a) Oil Quenched Specimen *b) Intensively Quenched Specimen*

Figure 3.44 - Distortion response for notched bars; distortion magnified 10x (Freborg *et al.*, 2007).

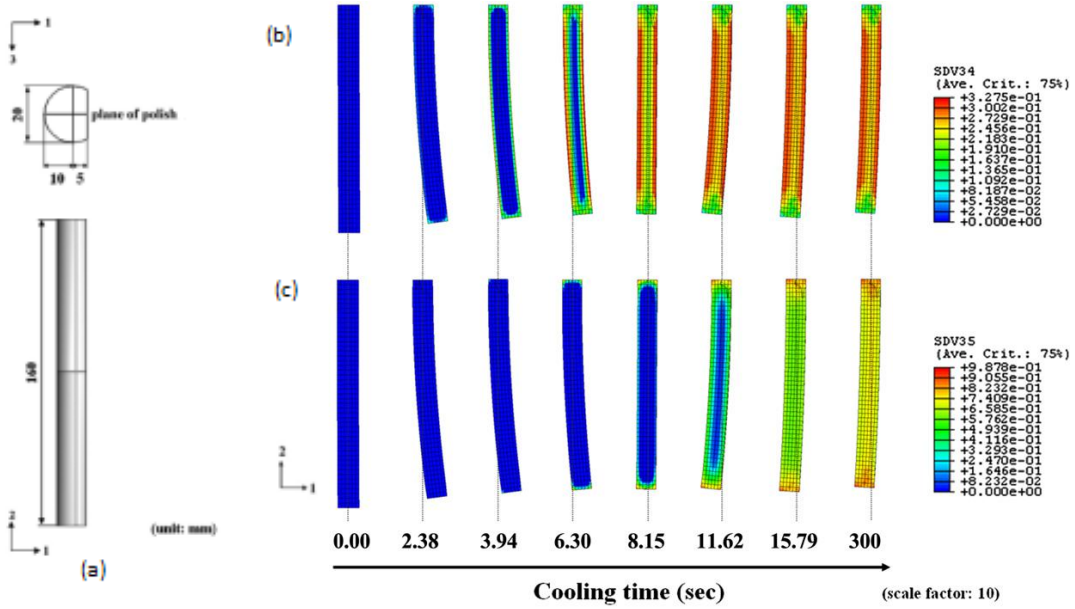

Figure 3.45 – Oil quenching of an (a) AISI 5120 cut cylinder specimen; relationship between the distortion and microstructure changes: (b) bainite and (c) martensite (Lee and Lee 2008).

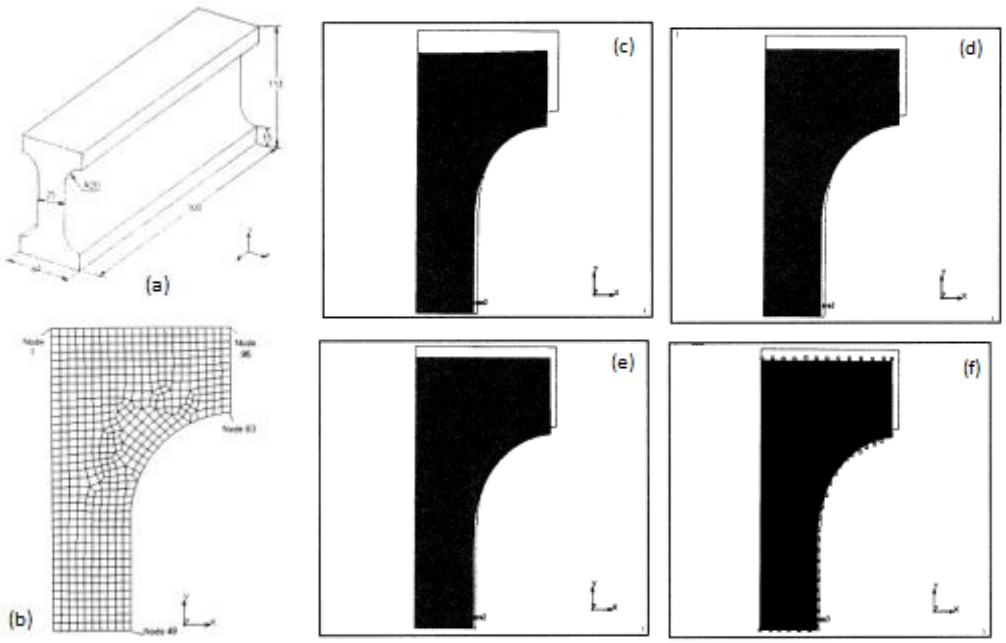

Figure 3.46 – Quench distortion prediction of an (a) I-beam part using (b) ¼ symmetric 2D mesh geometry. Original (white) and deformed (black) size of workpiece corresponding to: (c) 20 s, (d) 50 s, (e) 100 s, and (f) 270 s of cooling (Ye *et al.*, 2003).

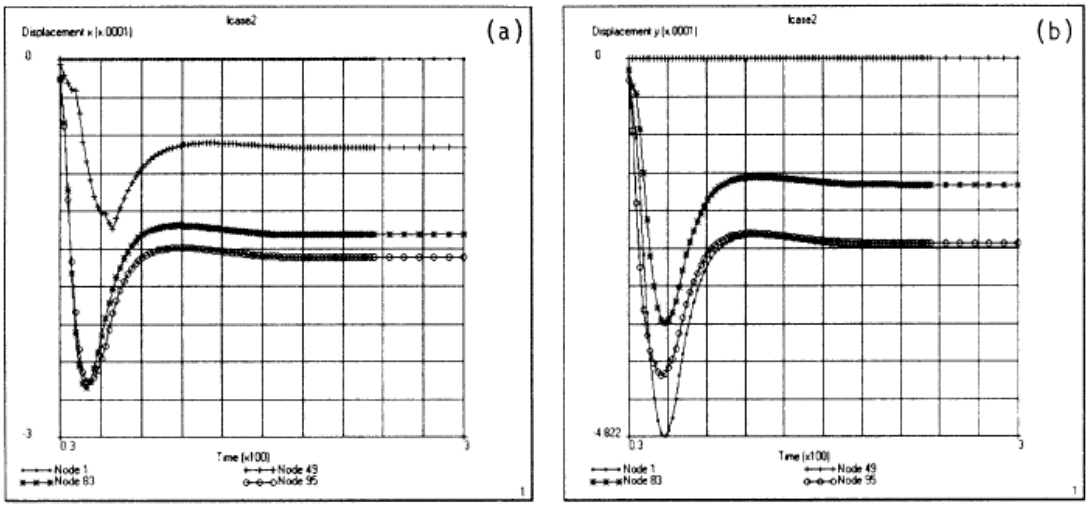

Figure 3.47 – Displacement of key nodes (see Figure 3.43) along x and y-axis direction (Ye *et al.*, 2003).

MacKenzie *et al.* (2007) used computational fluid dynamic (CFD) modeling to study the effect of quenchant flow on the distortion of carburized automotive pinion gears, correlating the parts position in the cooling system with the distortion (Figure 3.48). MacKenzie and Ferguson (2010) also stablished that FE modeling of the heat treatment

process steps provides a clear and efficient way to understand components response during heat treatment, which is also helpful for eliminating severe distortion problems. For the same automotive pinion gears, Figure 3.49 shows the distortion along the axis line correlated to the microstructure. Martensite formation provides larger distortion.

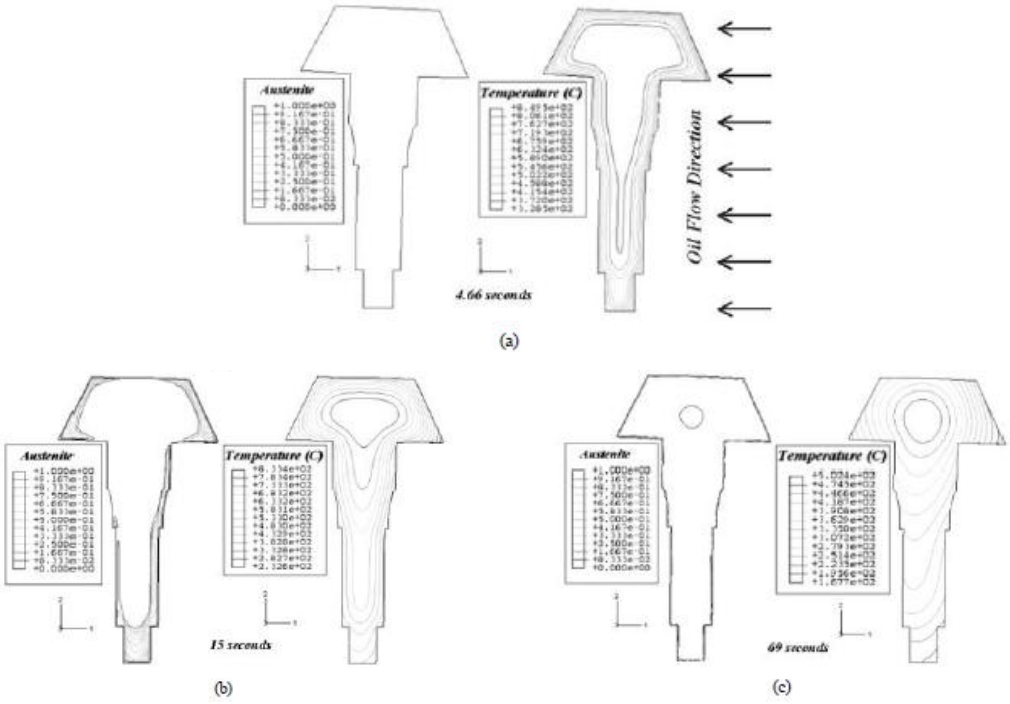

Figure 3.48 - Austenite and temperature distributions at different times in quench for an automotive pinion gear (MacKenzie *et al.*, 2007).

An approach has been applied by Arimoto *et al.* (2008) for explaining the mechanism of distortion and residual stress generation in carburized and quenched rings. Phenomena in the ring during heat treatment were simulated using a numerical model. Shapes of the distorted ring cross-section after the case carburizing were depicted as in Figure 3.50 using experimental and simulated results. The study has clarified how the transformation plasticity strain strongly affects to the quench distortion. The origin of distortion was explained by examining each simulated strain distribution, as shown in Figures 3.51 and 3.52 for axial and radial strain changes, respectively.

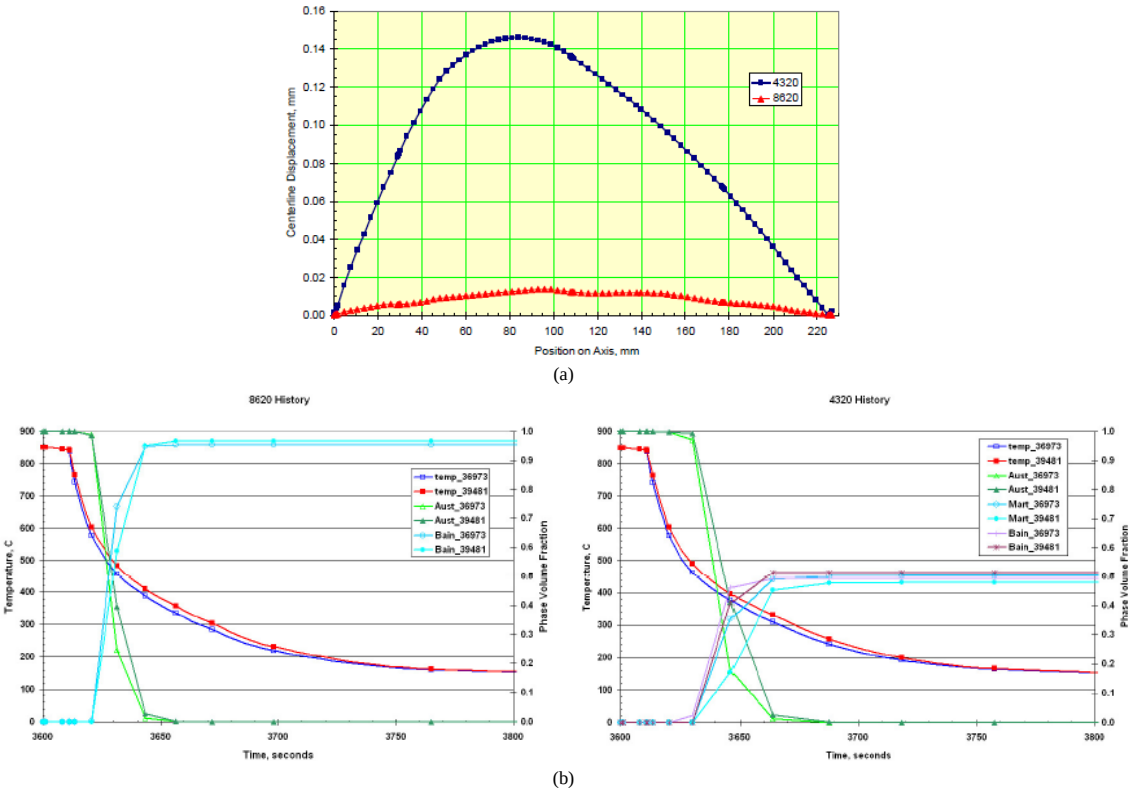

Figure 3.49 – Carburized and quenched AISI 8620 and AISI 4320 automotive pinion gears: comparison of (a) bowing and (b) transformation history (MacKenzie and Ferguson, 2010).

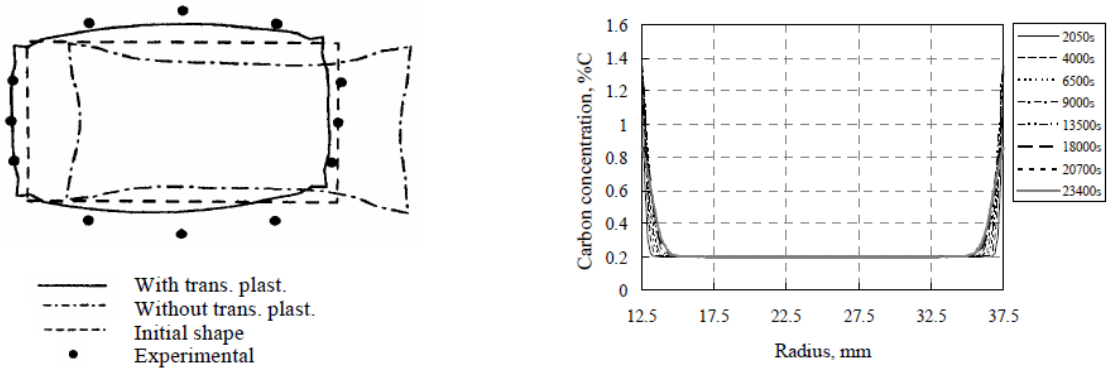

Figure 3.50 – (a) Simulated distortion of ring section, and (b) carbon concentration changes (Arimoto *et al.*, 2008).

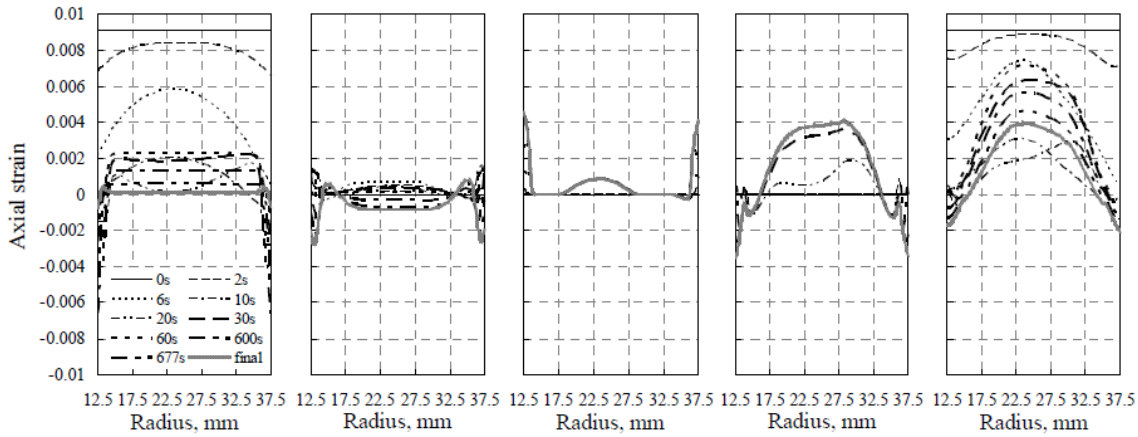

Figure 3.51 – Simulated axial strain changes: (a) thermo-phase transformation; (b) elastic; (c) plastic; (d) transformation plasticity; and (d) total (Arimoto *et al.*, 2008).

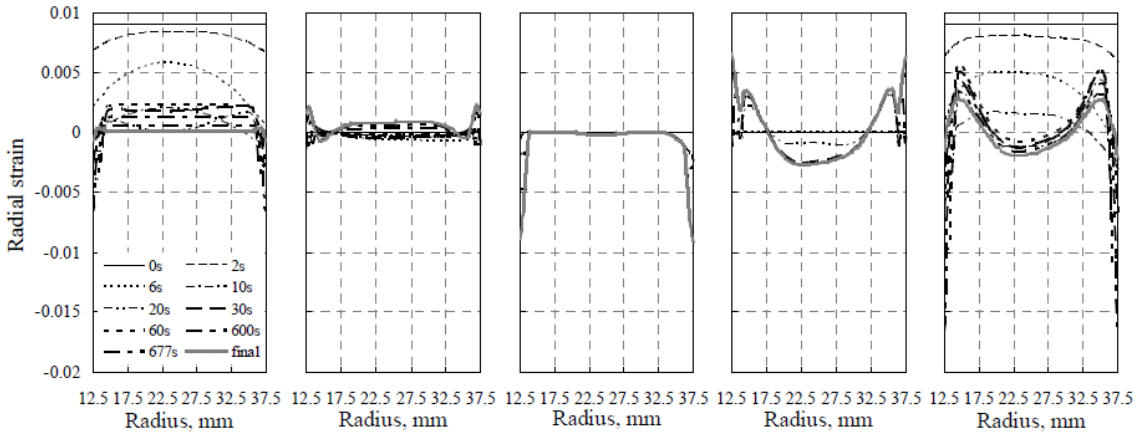

Figure 3.52 - Simulated radial strain changes: (a) thermo-phase transformation; (b) elastic; (c) plastic; (d) transformation plasticity; and (d) total (Arimoto *et al.*, 2008).

3.7.3. Test for Evaluating Quench Distortion (Navy C-Ring)

The so-called navy c-ring test is commonly used for evaluating quenching distortion. Since this work is based on the diameter distortion of hot rolled and heat treated rings, the navy c-ring is studied. Figure 3.53 shows a typical c-ring used for tests. Webster and Laird (1991) have used a high alloy-carbon alloy steel c-ring specimen to perform a conventional quenching in oil at 60°C. The obtained dimensional changes in A, B, C, D and E were 0.21, 0.24, 0.20, 0.61 and 0.075 mm, respectivelly.

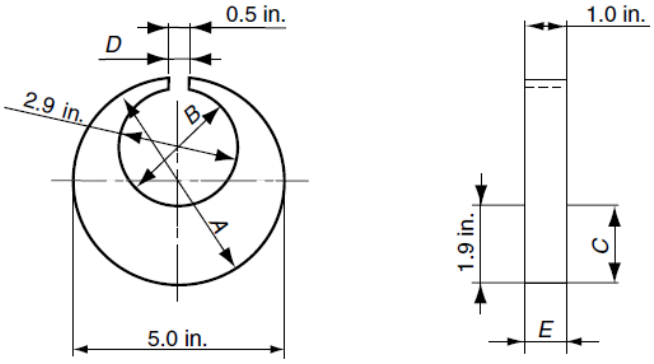

Figure 3.53 – Navy C specimen dimensions (Webster and Laird, 1991).

Grum *et al.* (2001) studied the influence of quenching agents on the cooling process and indirectly on the deformation of the heat treated 4140 steel c-rings (modifyed shape). Figure 3.54 shows an possible system to monitor the process information during quenching, and Figure 3.55 superposes cooling curves and CCT diagrams for diferent points in the c-ring and different quenchants. The hardnesses and distortions are reported in Table 3.4 – Changes in size measured at individual measuring points of the modified Navy C-ring made of 4140 steel in three cooling agents (Grum *et al.* , 2001). In adition, The alloy content is another factor that influences in the quenching distortion of steel. Fukuzumi and Yoshimura (1992) used navy c-ring tests to study the influency of aluminum and nitrogen in the distortion of SAE 8620 steels, and therefore minimize the distortion of automobile gears. Figure 3.56 shows the gap opening in function of aluminum content.

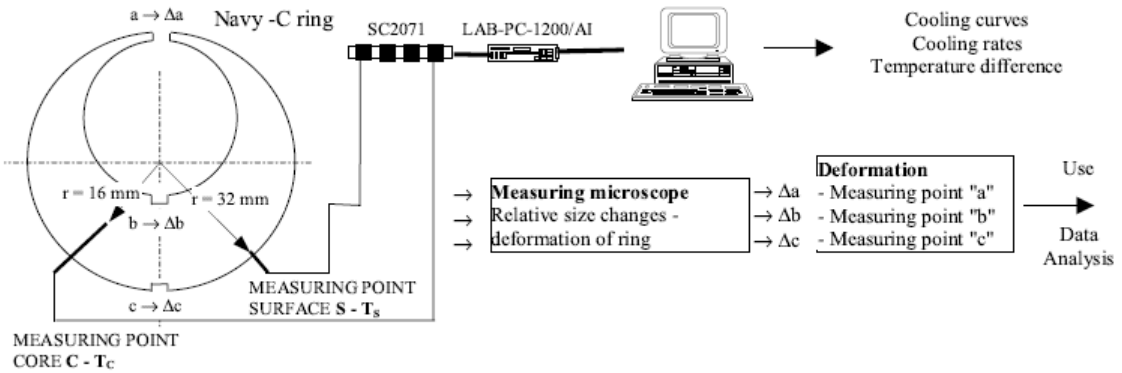

Figure 3.54 – Experimental set-up for capturing cooling curves and deformation on navy c-rings (Grum *et al.*, 2001).

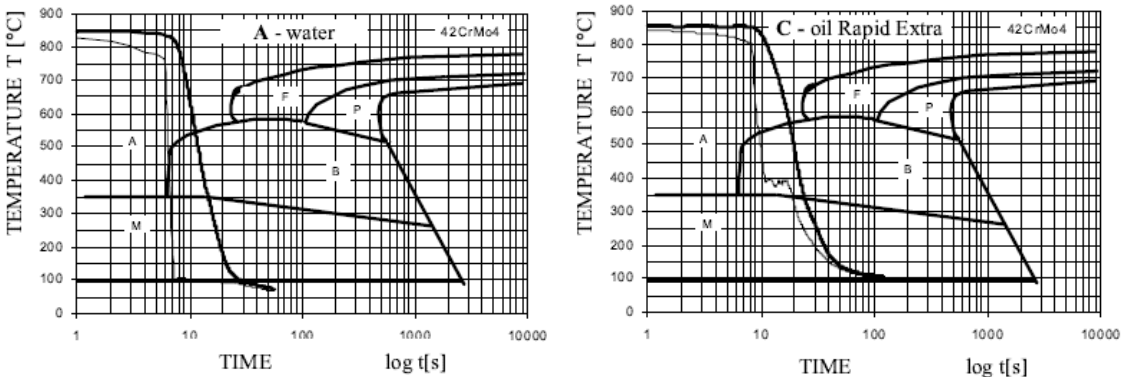

Figure 3.55 – Continuous cooling diagram of transformations with cooling curves plotted for individual points after quenching a navy c-ring (Grum *et al.* , 2001).

Table 3.4 – Changes in size measured at individual measuring points of the modified Navy C-ring made of 4140 steel in three cooling agents (Grum *et al.* , 2001).

Steel 4140	Hardness (HRC)			Dimensional changes (mm)		
Cooling agent	Max.	Min.	Differ.	Point "a"	Point "b"	Point "c"
Water	62	56	6	crack	crack	crack
10% polymer water solution	61	58.5	2.5	0.042	-0.044	0.050
Oil rapid extra	53	50.2	2.8	0.091	-0.112	0.054

(a) Values relative to Figure 3.51.

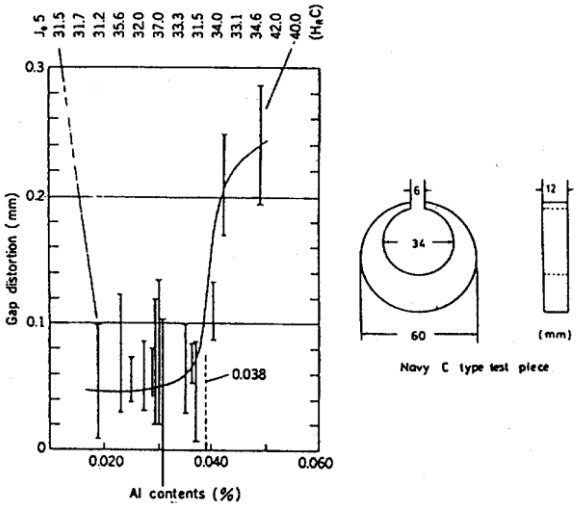

Figure 3.56 – Effect of aluminum content on gap distortion of SAE 8620H steels (Fukuzumi and Yoshimura, 1992).

Totten *et al.* (1993) reported navy c-ring tests for different materials. Table 3.5 shows the dimensional changes for gap and outside diameter (OD) for quenched c-rings. The

dimensions of the specimens are defined in Figure 3.57. Hardin and Beckermann (2005) simulated the navy c-ring tests for AISI 4140 and 8620 reported by Totten *et al.* (1993). Figure 3.58 shows the prediction of an AISI 4140 c-ring distortion when quenched in oil. The dimensional changes gap opening and OD are predicted based on the x-displacement at nodes "B" and "C", respectivelly. Figure 3.59 shows the dimensional changes for AISI 4140 and 8620 c-rings during heating and cooling process. Direct comparison between the measured and predicted dimensional changes show the simulated distortions to be substantially larger than the measurements. For the 4140 c-ring quenched in oil, the simulated gap opening was around 0.56 mm, while the experimental test reports a 0.041 mm gap opening. Hardin and Beckermann (2005) attribute this difference to the lack of carburization in the simulations, and also to the lack of detailed information about heating process. The amount of martensite is above 90% for all c-rings regions (nodes "A", "B" and "C"), indicating that the quenchant and specimen dimensions provide a high and homogeneous hardness (Figure 3.60).

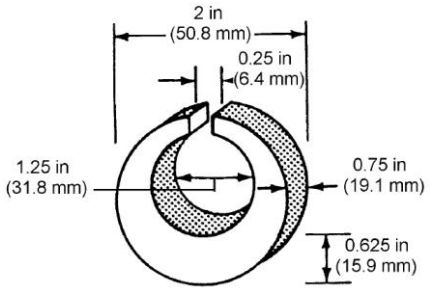

Figure 3.57 – Navy-C ring specimen dimensions for quench distortion experiments (Totten *et al.*, 1993).

Table 3.5 – Relative distortion of c-rings with different quenchants (Totten *et al.*, 1993).

AISI steel	**Quenchant**	**Dimensional change (mm)**	
		Gap opening	**OD**
1045	Petroleum oil (60°C)	0.013	-0.005
	UCON® Quenchant A (40°C)	0.018	-0.003
	Water (25°C)	0.008	0.008
4140	Petroleum oil (60°C)	0.041	0.015
	UCON® Quenchant A (40°C)	0.043	0.015
	Water (25°C)	Cracked	Cracked
8620 (carburized)	Petroleum oil (60°C)	0.018	0.005
	UCON® Quenchant A (40°C)	0.020	0.005
	Water (25°C)	0.046	0.018

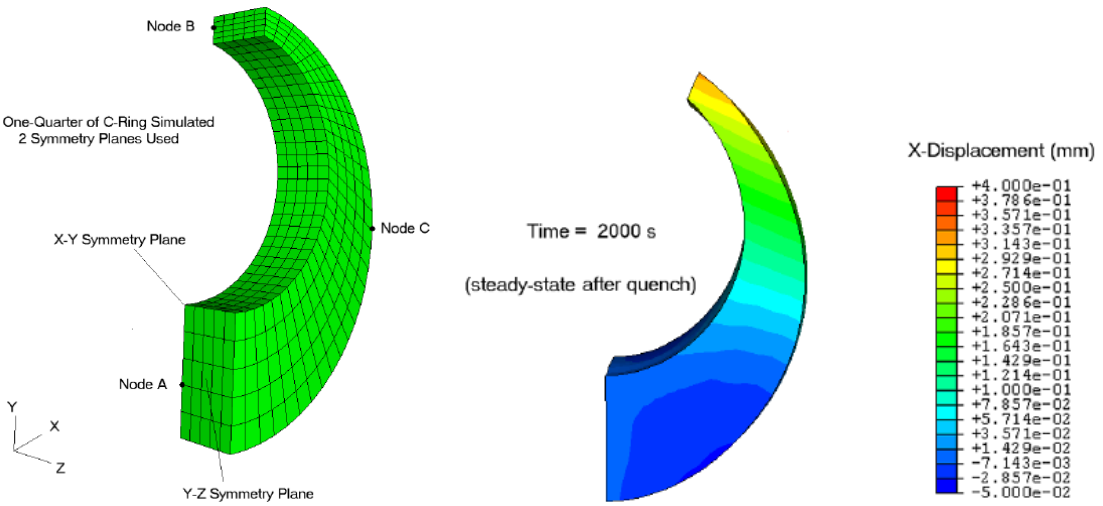

(a) (b)

Figure 3.58 – (a) Finite element model used to simulated the quenching of the c-ring: ¼ symmetric geometry; and (b) Simulated dimensional displacement in the x-direction for the oil quenched AISI 4140 c-ring; distorted geometry is magnified 30 times (Hardin and Beckermann, 2005).

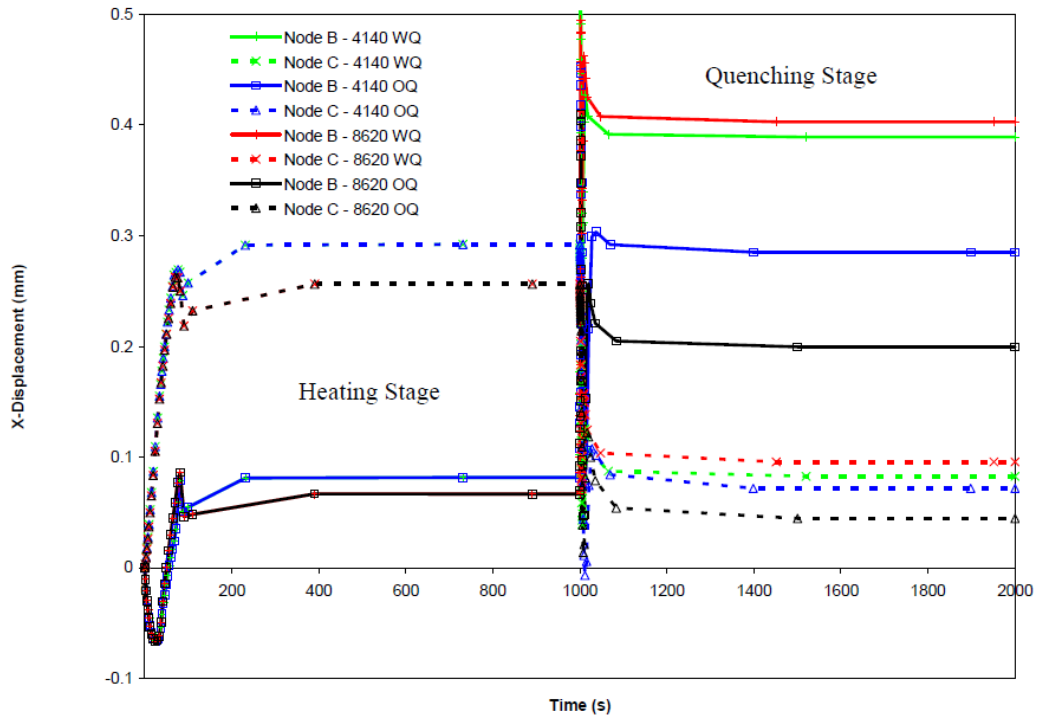

Figure 3.59 – Simulated dimensional displacement in the x-direction for all cases from start of heating through end of quench. Results are given at nodal locations “B” at the gap, and local at node “C” on the outside diameter (Hardin and Beckermann, 2005).

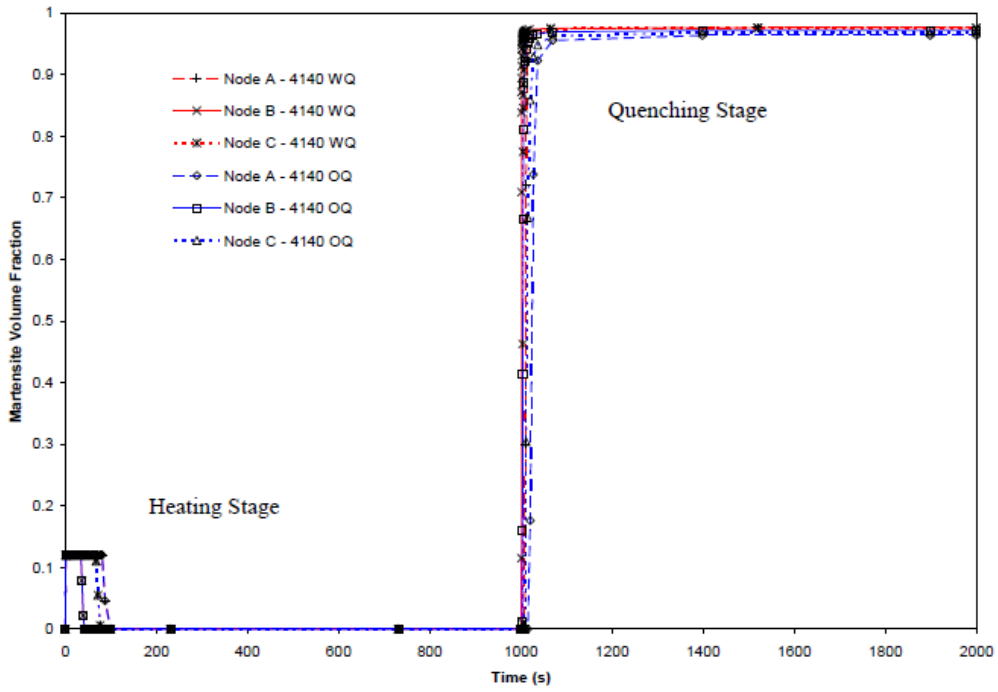

Figure 3.60 – Simulated martensite volume fraction for the 4140 alloy cases, from start of heating through end of quench. Results are given at nodal locations "A" at the center of the piece, "B" at the gap, and local at node "C" on the outside diameter (Hardin and Beckermann, 2005).

Brooks and Beckermann (2007) have predicted heat treatment distortion of cast steel c-rings, considering different c-ring shapes as shown in Figure 3.61. Software Dante (DCT - Deformation Control Technology, Inc.) and Abaqus (Simulia - Dassault Systèmes) were used for distortion simulations, and JMatPro (Sente Software Ltd.) for material properties prediction. Depending on the material, the gap may close due to thermal stresses. The study predicted general distortion trends seen in the experiments, but are not in complete agreement with the experimental results. In addition, dimensional measurements for different immersion directions and different alloys are compared and discussed. Cyril *et al.* (2009) have used the software Forge 2008 TTT® (Transvalor S.A.) to perform quenching simulation of thick c-ring parts. They defined a methodology with three steps to identify distortions (Figure 3.62): measurement of the discrete geometry of the part before and after heat treatment; relative comparison between measurement points before and after quenching; and linkage of the distortions

to physical and technological parameters: phase transformation, residual stress, steel grade. The distortions include gap opening and barrel effect (Figure 3.63).

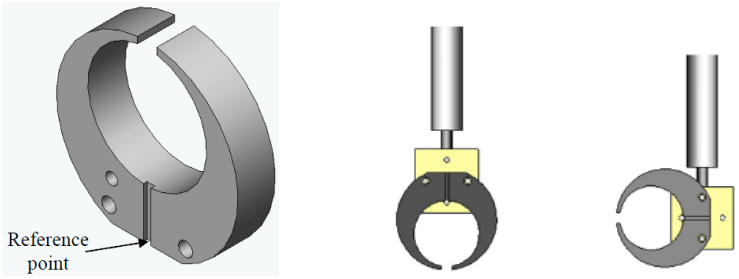

Figure 3.61 – (a) Model of a c-ring: system for (b) vertical and (c) side immersion (Brooks and Beckermann, 2007).

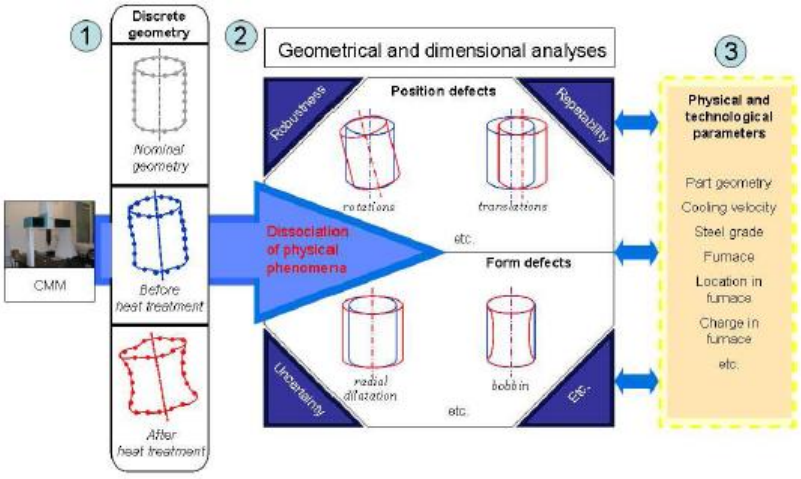

Figure 3.62 – Method for identifying distortions (Cyril *et al.*, 2009).

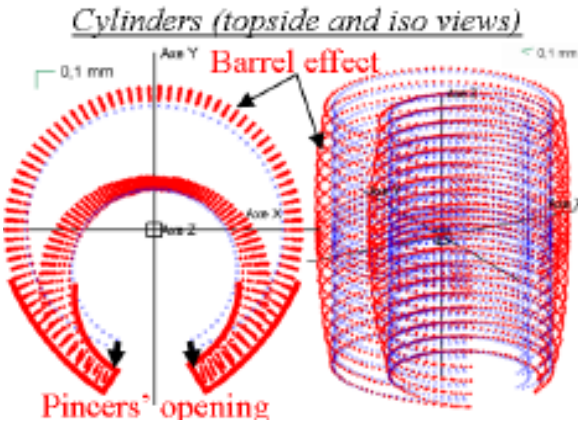

Figure 3.63 – C-ring distortions after heat treatment (Cyril *et al.*, 2009).

3.8. Rolled Rings

Rolled rings are seamless rings produced through ring rolling process. Its application, manufacturing and some defects are described as follows.

3.8.1. Application

Rolled rings have been used for many years in various applications. The most used materials for the rings include carbon and alloy steel, cobalt, aluminum, titanium, magnesium, nickel, also copper and bronze, and many types of tool steel. According to Bolin (2005), the ring's application can be organized in industry groups: transportation, aerospace, and energy. Another group can also be defined as commercial, which is a catch-all category for rings such as gears for large equipment, bearings for large cranes, food processing dies, and containment dies for forging.

Production of transportation components usually means high quantities. Bearings, ring gears, final drive gears, transmission components, clutch components, and wheel blanks are some examples. Parts for transportation systems include wheel bearings, railroad wheels, and tanker flanges. For aerospace industry, many jet engine and spacecraft parts are rolled from hard to form, heat-resistant alloys such as stainless steel, titanium, and nickel-base superalloys. Because of the high price of this material, difficulties in machining and the strict production controls, parts in this family are typically formed as contours in as close to net-shape form as possible to reduce machining and waste. Parts used in aerospace include rotating and nonrotating rings for fans, engine casings, and engine disks. Finally, energy is another large segment for rings. Lot sizes in this segment can be large or small, depending on application. Parts for this market segment include land-based turbine parts similar to aerospace components, flanges, spacers and blinds for the oil industry, vessel components, and nuclear reactor components. Another rapidly growing market segment is the wind power generation group of components including bearings, tower connector flanges, and electrical generator parts.

3.8.2. Forming of Rings

The forming process of seamless rings can be divided in two stages: blank preparation, where a bulk is forged in order to get an annular blank, and ring rolling, in which the annular blank is rolled into the finished ring. The formed part and the relevant volumetric calculation represent the starting point for developing the process plan of ring rolling (Milutinivic *et al*., 2005). A creative process is initiated in which a wide range of boundary conditions – such as starting diameter, material, prescribed strength levels, heat treatment, number of stations, distance between stations, press force,– must be considered simultaneously.

The starting round billets are sawed based on the target ring size. Usually, the surfaces of the billets are not machined. The sawed billets are then heated and soaked in a furnace. Additional heating may be needed depending on the billet size. The heated billets are upset, punched and pierced to obtain doughnut shaped pre-forms for the ring rolling machine. Gellhaus (2011) shown two different possibilities for the blank preparation, as it can be seen in Figure 3.64. The pre-forms are then re-heated to reach the temperature necessary for the ring rolling operation.

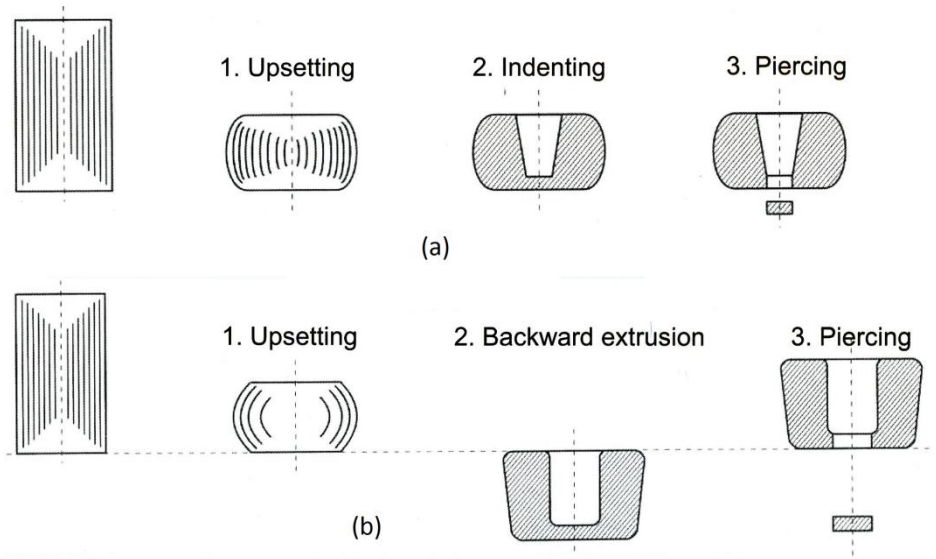

Figure 3.64 – Blank preparation for ring rolling process; (a) open-die and (b) pot-die operations (Gellhaus 2011).

After prepared, the blank is rolled in the ring rolling process. Altan *et al*. (1983) define ring rolling as a process whereby a circular blank (cold or hot) is formed into a ring. A main roll presses on the outside diameter of the blank, which is supported by a mandrel on the inside diameter. Shape cross sections are obtained by appropriate contouring of the mandrel and the roll. The height of the ring is controlled by an auxiliary roll. Guide rolls control the round shape. Figure 3.65 illustrates the ring rolling process, indicating its boundary conditions kinematics, and Figure 3.66 – Typical range of rings during ring rolling process (Brümmer, 2011). shows the ring rolling process of typical rings.

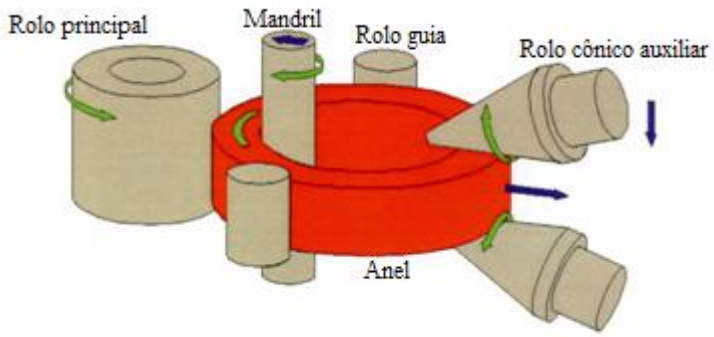

Figure 3.65 – Radial-axial ring rolling process (Gellhaus, 2011).

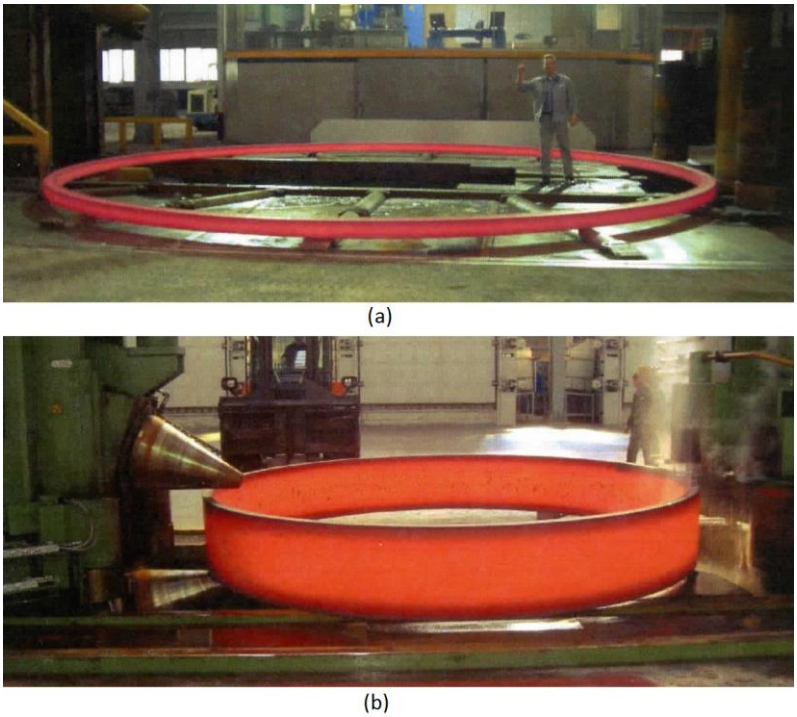

Figure 3.66 – Typical range of rings during ring rolling process (Brümmer, 2011).

3.8.3. Heat Treatment of Hot Rolled Rings

After being rolled at forging temperature most rings are heat treated. The steps commonly followed in heat treatment are: normalizing, quenching, and tempering. Figure 3.67 shows a schematic of the most common steps after ring rolling. Hot rolled rings are disposed in stacks of 4 to 6 rings and heated. Normalizing is conducted to achieve uniformity in grain size and composition throughout an alloy. The target temperature will depend on the composition of the steel. This process may be omitted in case the microstructure is considered to be uniform enough after rolling process. Figure 3.68 (a) shows rings in stacks inside the furnace, prepared for the heating procedures. After 2 hours inside the furnace at a normalizing temperature, the rings are removed from the furnace (Figure 3.68 (b)) to be air cooled. The next stage is the quenching process. The ring is heated at a temperature around 850°C and held at this temperature for 2 hours to achieve a complete austenitizing of the ring material. Then, it is cooled very fast inside a quenching tank. Figure 3.69 shows an example of quenching tanks for rings.

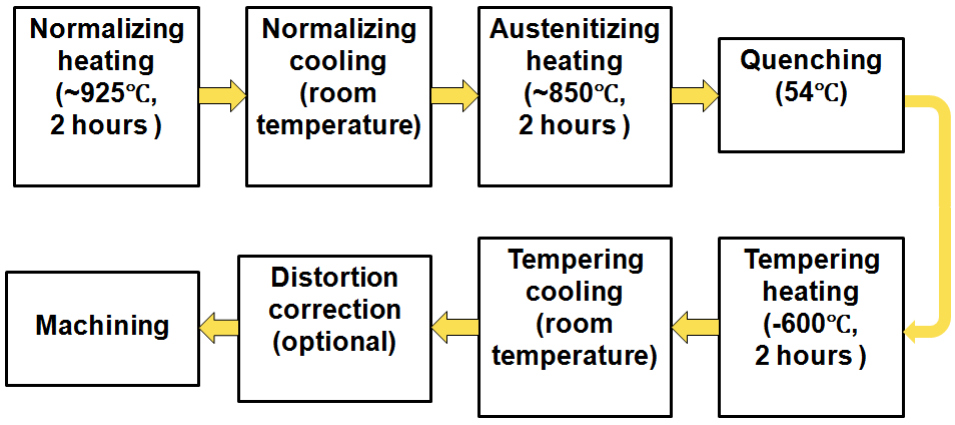

Figure 3.67 – Most common processes used for rings after ring rolling stage.

Tempering processes can be performed on quenched rings. Usually, the rings are heated at 600°C and air cooled. Distortions obtained during quenching process are not corrected with tempering process. Therefore, correction procedures are conducted in order to reach the geometry tolerances for the rings. However, residual stresses are

decreased during tempering. Procedures to correct distortion may also decrease the residual stresses. Machining process is performed in order to achieve the final product geometry. If there are still significant residual stresses in the ring, the part may distort after machining.

(a) (b)

Figure 3.68 – Rings in stacks during heating process; (a) rings prepared for heating and (b) after heating (McINNES Rolled Rings, 2011).

Figure 3.69 – Tanks for quenching of hot rolled rings (Rotek® Rings, 2011).

3.8.4. Heat Treatment Distortion of Rings

The subsequent process to ring rolling is normalizing. During the air cooling, a non homogeneous cooling condition may lead the ring to distort. Some of these distortions include contraction and rotation of the ring section. Pascon *et al.* (2004) has used 2D simulations based on FEM (Finite Element Method) to obtain different distortions of the

ring section. These authors have varied the shape of the rings, the number of ring's faces that change heat with the environment, and also the cooling rate magnitude.

A comparison between the distortion of a thick and a thin-walled AISI 4140 steel ring after quenching (water with polymer solution) process is predicted in Figure 3.70. The thick ring exhibits large distortions, including a rotation that does not occur in the case of the thin ring. The distortion can be explained based on the volume fraction of the material phases after cooling (Figure 3.71). The bulk of the thin ring is much lower than that of the thick one. Therefore, the thin ring has a higher cooling rate and a higher proportion of bainite and martensite.

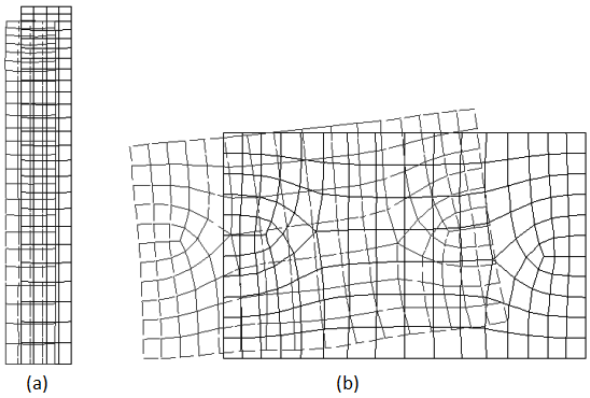

Figure 3.70 – Distortion of two different ring sections; (a) Thin-walled ring and (b) thick-walled ring; displacement is magnified 10x (Pascon *et al.*, 2004).

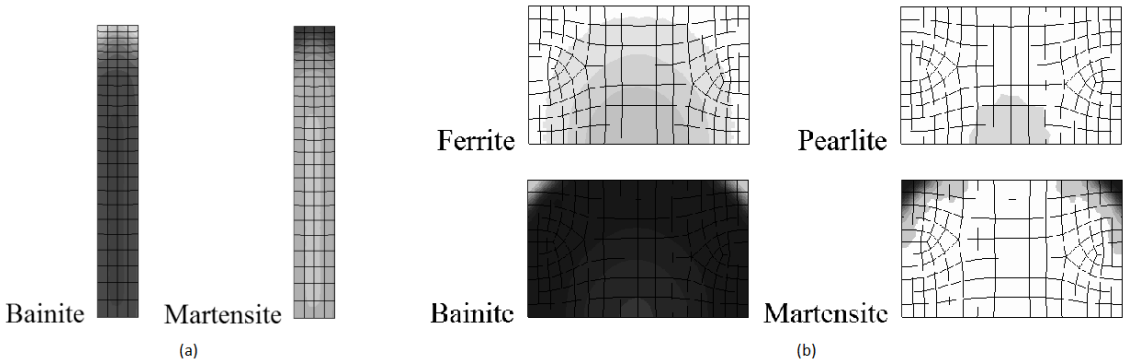

Figure 3.71 – Material phases percentage after quenching of AISI 4140 steel rings (scale: black color = 100%); (a) phases distribution in the tall and thin ring (without

ferrite or pearlite formation); and (b) phases distribution in the plate and thick ring (Pascon *et al.*, 2004).

Other types of distortions may occur during the quenching of rings. At some ring companies the rings are quenched in tanks, disposed in stacks with more than one ring each stack. Due to the high production rate necessity, many rings are quenched at the same time, at the same quenching tank. Figure 3.72 shows a typical arrangement of ring stacks in the quenching tank. The rings may be set in the stacks separated or not by spacers. A very precise control of this parameter in a system like this is complex. Several parameters influence the quenching process, including: temperature, polymer concentration, bacteria quantity and velocity (agitation inside the tank) of the quenchant, and size, position inside the tank and number per stack of the rings. Due to the described parameter, for the same ring, there is always a non-homogeneous heat transfer between ring and environment along the ring surface.

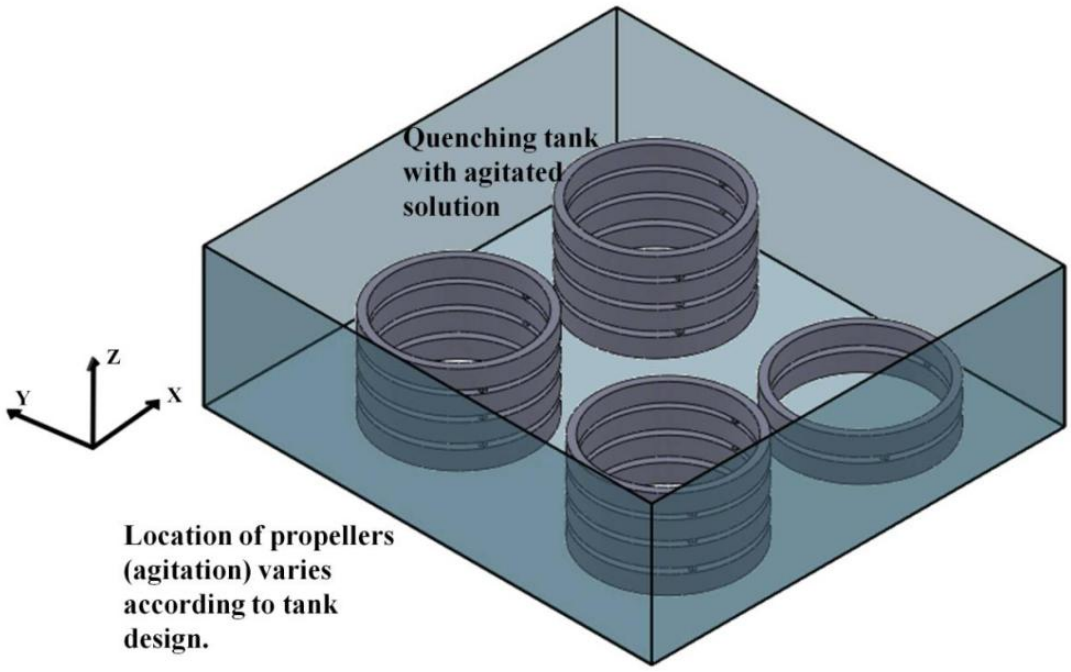

Figure 3.72 – Typical arrangement of ring stacks in the quenching tank.

The system illustrated in Figure 3.72 can create in the rings the distortions already discussed in this topic, and also other ones. The rings might undergo torsion strains, distorting across their horizontal plan. Another defect due to the distortion phenomena

occurs in special with thin-walled and large outside diameter rings. Since the heat transfer between ring and quenchant varies with the ring surface temperature, ring region inside the tank and time, the rings may reach an out-of-roundness shape. This out-of-roundness shape is also called “ovality”. Making an analogy with defects provided by the hot rolling of the rings, the quench ovality is similar to the ovality that can be caused by the ring rolling process. Figure 3.73 illustrates the ovality, a ring defect obtained after forming stage. Buhl (2011) has defined the ovality as the difference between maximum OD (outside diameter) and minimum OD. In addition, at least three diameters should be measured to check the ring ovality. The same ovality is observed after quenching processes in thin-walled and large OD rings. No ovality is observed due to the normalizing process.

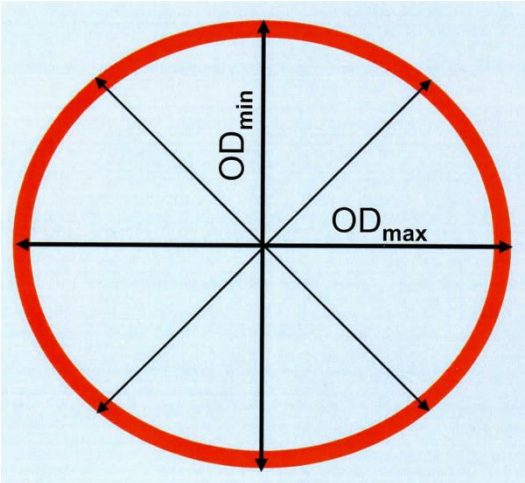

Figure 3.73 – Ring ovality caused by an inadequate hot rolling process (Buhl, 2011).

Even if the finished rings meet dimensional tolerances, residual stresses resulting from heat treatment may become a problem during subsequent machining. Additional deformation and distortion may be caused by residual stresses. So, the heat treatment should be well controlled to prevent residual stresses.

3.8.5. Correction of Ring Ovality (Circumferential Distortion)

In case the heat treatment systems cannot prevent distortion, corrections based on small plastic deformation may be performed afterwards. Some systems have already been designed to correct the illustrated ovality in the Figure 3.73. One of these systems is a very sophisticated expander, schematically demonstrated in Figure 3.74 (a). The distorted ring is positioned on the expander, which applies forces at the internal surface of the ring. According to the ring dimension, the expanders may change the number of tools to better adequate to the process. Simpler systems, such as compressers (Figure 3.74 (b)), are also used to correct ovality.

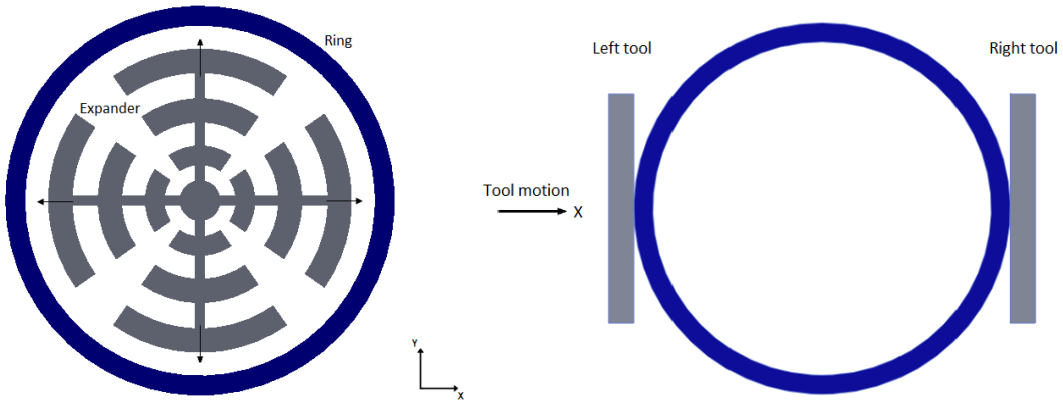

(a) (b)

Figure 3.74 – Schematic of systems used to correct ring ovality; (a) an expander and (b) a compresser.

The operation of the systems in the Figure 3.74 is based on trial and error. The learning curve is long, since each ring has a different material and ovality, and the necessary stroke to achieve plastic strain is tricky. Most of the time, this process is operator experience dependent. The sophisticated expanders are very expensive systems, and its learning curve process is also long and expensive. In another way, compressers are alternative less expensive systems. The learning curve is also long. The absence of a well established procedure to operate the equipments, which is ring characteristics dependent, leads the production to time losses. In special, for the compressers, the trial and error methodology can cause mistakes during the compression stroke, and the rings need to be reworked. In addition, inadequate strokes can cause cracks and break the parts. As a result, there are cost increases and production rate decreases.

3.9. AISI 4140 Steel

3.9.1. Characteristics and Properties

AISI 4140 is a chromium, molybdenum and manganese low alloy steel noted for toughness, good torsional strength and good fatigue strength. It is used in applications requiring a combination of moderate hardenability and good strength and toughness, but in which service conditions are only moderately severe. Tables 3.6 and 3.7 gives the AISI 4140 chemistry and references, respectively.

Table 3.6 – AISI 4140 chemistry (ASM International, 1993).

Element	C	Mn	P	S	Si	Cr	Mo
Weight (%)	0.38-0.43	0.75-1.00	0.035max	0.04 max	0.15-0.30	0.80-1.10	0.15-0.25

Table 3.7 – AISI 4140 cross-reference (ASM International, 1993).

United States (SAE)	Fed. R. of Germany (DIN)	Japan (JIS)	United Kingdom (BS)	France (AFNOR NF)	Italy (UNI)	Sweden (SS14)
4140	1.3563, 43CrMo4 1.7223, 41CrMo4 1.7225, 42CrMo4 1.7225, GS-42CrMo4 1.7227. 42CrMoS4	G4052 SCM4H G4052 SCM440H G4103 SNCM4 G4105 SCM4 G4105 SCM440	3100 Type 5 4670 711M40 970 708A40 970 708A42 (En19C) 970 708H42 970 708M40 970 709A40 970 709M40	40CD4 A35-552 42CD4, 42CDTS A35-553 42CD4, 42CDTS A35-556 42CD4, 42CDTS A35-55742CD4, 42CDTS	3160 G40CrMo4 5332 40CrMo4 7845 42CrMo4 7847 41CrMo4 7874 42CrMo4	2244

The AISI 4140 steel is available as bar, rod, forgings, sheet, plate, strip, and castings (Philip and McCaffrey, 1993). It is used for many high-strength machine parts (some of them nitrided) such as connecting rods, crankshafts, steering knuckles, axles, oil well drilling bits, piston rods, pump parts, high-pressure tubing, large industrial gears, flanges, collets, machine tool parts, wrenches, tong jaws, sprockets, and studs.

The workability of this steel alloy is commented at Metal Suppliers Online (2012). The alloy readily cold works in the annealed condition by conventional methods. As with all the low alloy steels, forming may be done by conventional methods with the alloy in the

annealed condition. These alloys have good ductility, but are tougher than plain carbon steel and thus usually require more force, or pressure, for forming. AISI 4140 hot forming range temperature is 850-1100 °C. For welding processes, all of the conventional methods may be used. Finally, machinability of this alloy is good in the annealed condition. In the heat treated and quenched condition, machining is best limited to finish grinding.

The heat treatment processes for the 4140 steel are performed as follows (TATA Steel, 2011):

- annealing: heat to 830-850 °C and cool in furnace;
- normalizing: heat to 870-900 °C, and cool in still air;
- stress relieving: heat to 600-650 °C (annealed) or 500-550 °C, and cool in still air;
- hardening: heat to 830-880 °C, and quench in oil or polymer;
- tempering: heat to 450-500 °C, and cool in still air; tempering within the range 200-420 °C will result in temper brittleness and should be avoided;
- flame and induction hardening: heat quickly to the required case depth at 860-890 °C, and quench immediately in water or oil;
- and nitriding: heat to 500-530 °C and hold for sufficient time to develop the depth of case required.

Typical mechanical properties of the AISI 4140 material are shown in . The hardenability diagram of 4140 is shown in Figure 3.75, obtained from the Jominy test. The true stress-strain curve is shown in Figure 3.76. This material is commonly supplied in the hardened and tempered condition. The level of hardness of the material is selected to give useful strength while still maintaining the ability to machine the material into finished components. Figure 3.77 provides true stress-strain curves for 4140 steel as-quenched and tempered at different temperatures, obtained from monotonic and cyclic tension and compression tests.

Table 3.8 – Typical Mechanical Properties of AISI 4140 (Huyett, 2004).

Treatment	UTS (MPa)	Y (MPa)	Elongation (%)	Reduction (A%)	Hardness (HB/HRC)
Normalized	1020	655	17.7	46.8	302/32
Annealed	655	417	25.7	56.9	197/(14)

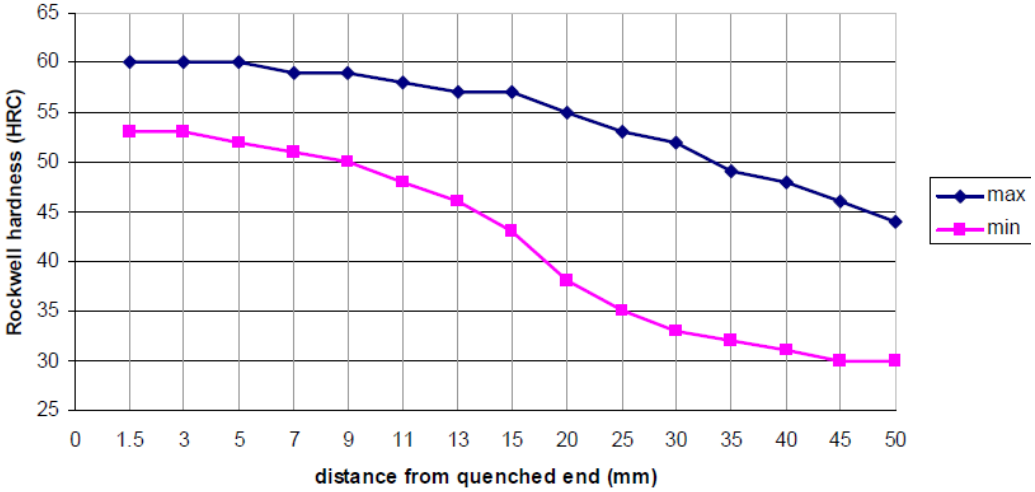

Figure 3.75 – Hardenability diagram of 4140 (Atlas Specialty Metals, 2005).

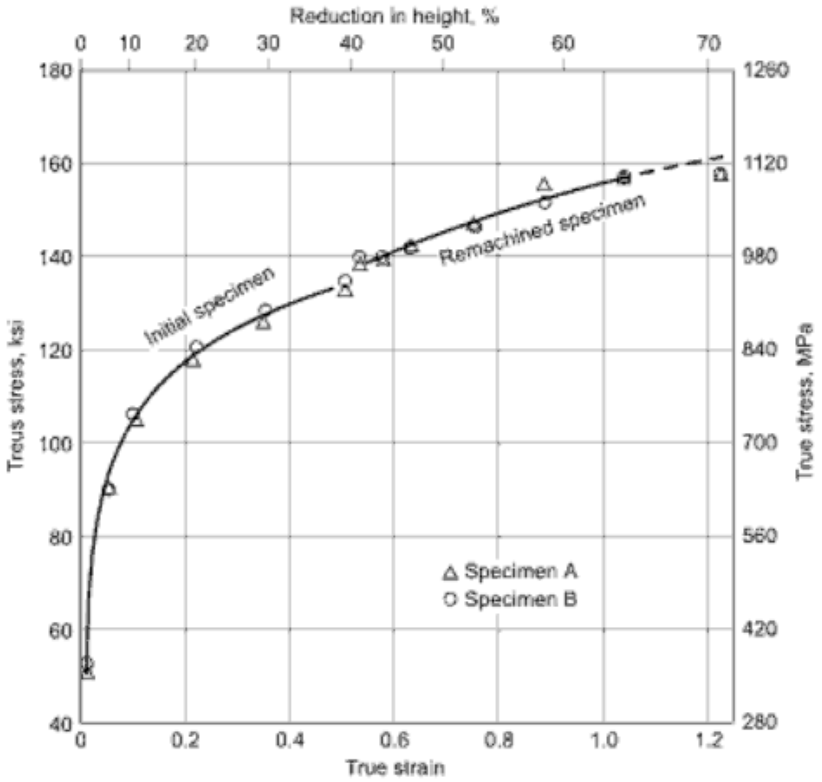

Figure 3.76 – True Tress-Strain curve for the 4140 steel; compression test on the specimen taken hot-worked process (Crawford, 1975; in ASM International, 2002).

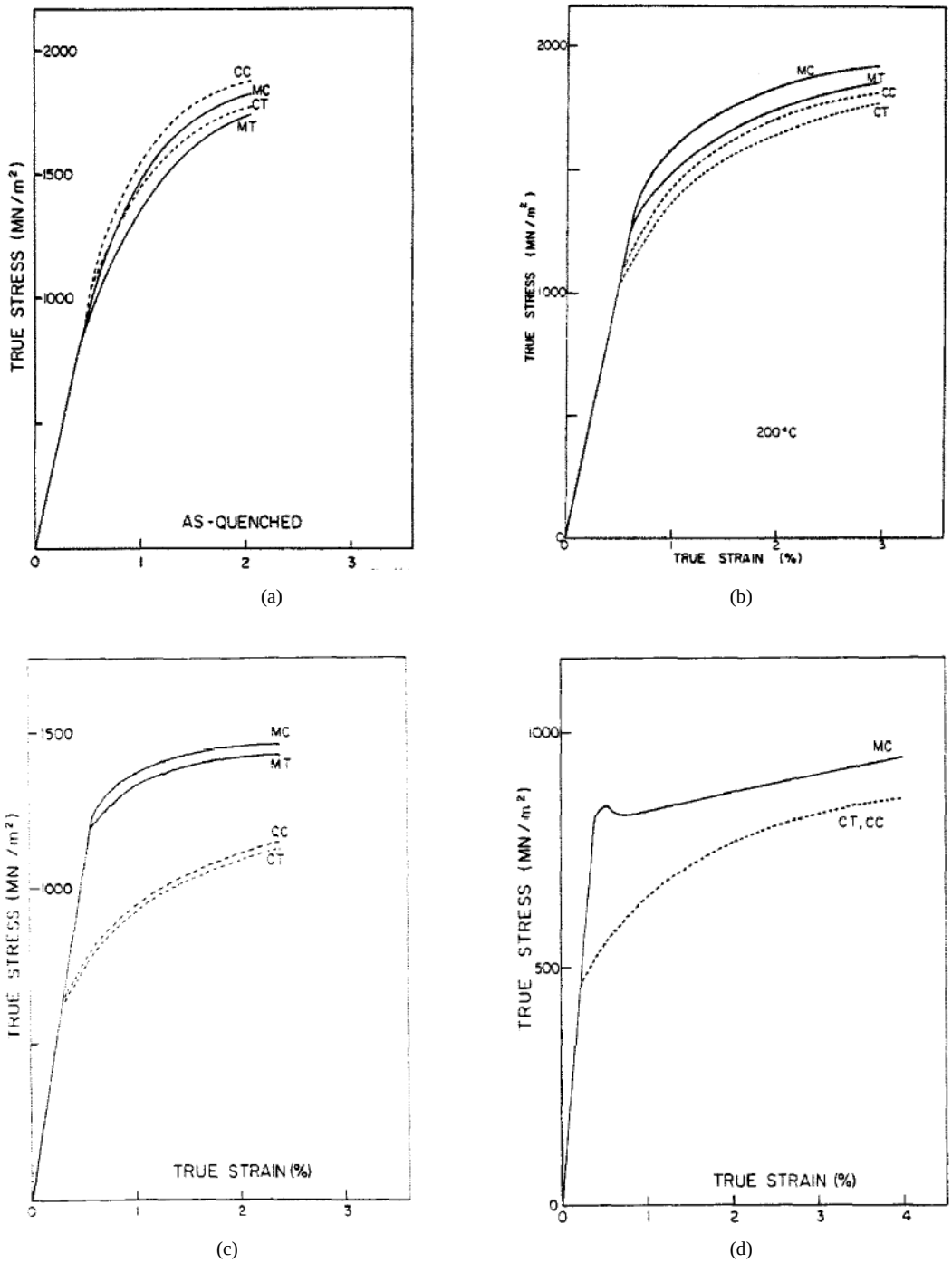

Figure 3.77 – Monotonic and cyclic true stress-true strain curves for 4140 steel. (a) As-quenched condition; (b) tempered at 200 °C; (c) tempered at 400 °C; and (d) tempered at 650 °C. MT = monotonic tension; MC = monotonic compression; CT = cyclic tension; CC = cyclic compression (Thielen *et al.*, 1976).

3.9.2. Material Phases

Austenite, ferrite, pearlite, bainite and martensite are the main microstructures of the AISI 4140 steel. The existence and quantity of each phase in the steel depends on the process that is applied to it. Figure 3.8 showed the microstructure evolution of the 4140 steel when cooled from austenite for two different cooling rates. The TTT and CCT curves have already been discussed in section 3.2.2. Figure 3.78 shows a typical TTT diagram for AISI 4140 steel. The microstructure composition and aspect are illustrated in Figure 3.79. The final hardness of the material changes according to the cooling rate. Figure 3.80 correlates the CCT diagram and the hardenability diagram to different quenchants.

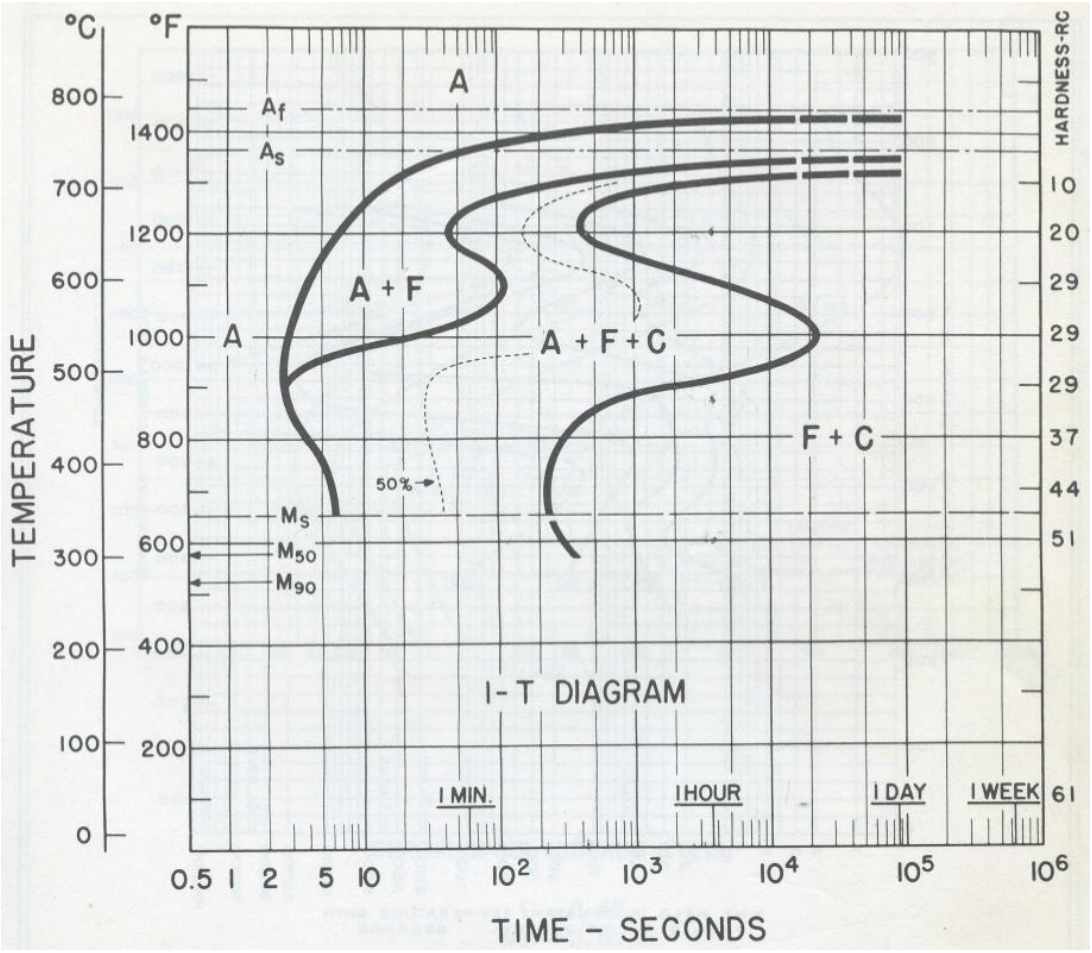

Figure 3.78 – TTT diagram for AISI 4140 (American Society for Metals, 1977).

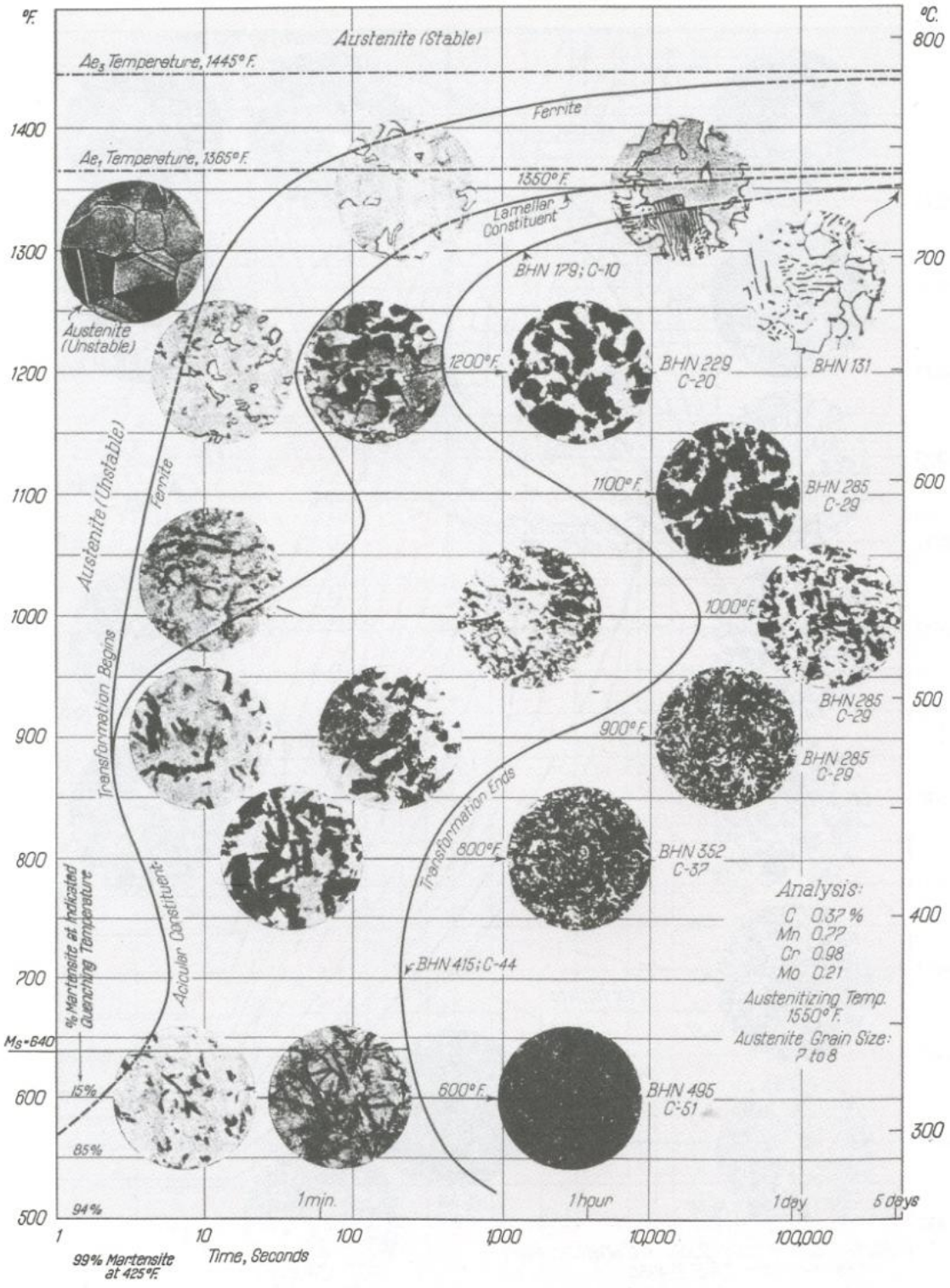

Figure 3.79 – AISI 4140 microstructure evolution at isothermal temperatures (Voort, 1991).

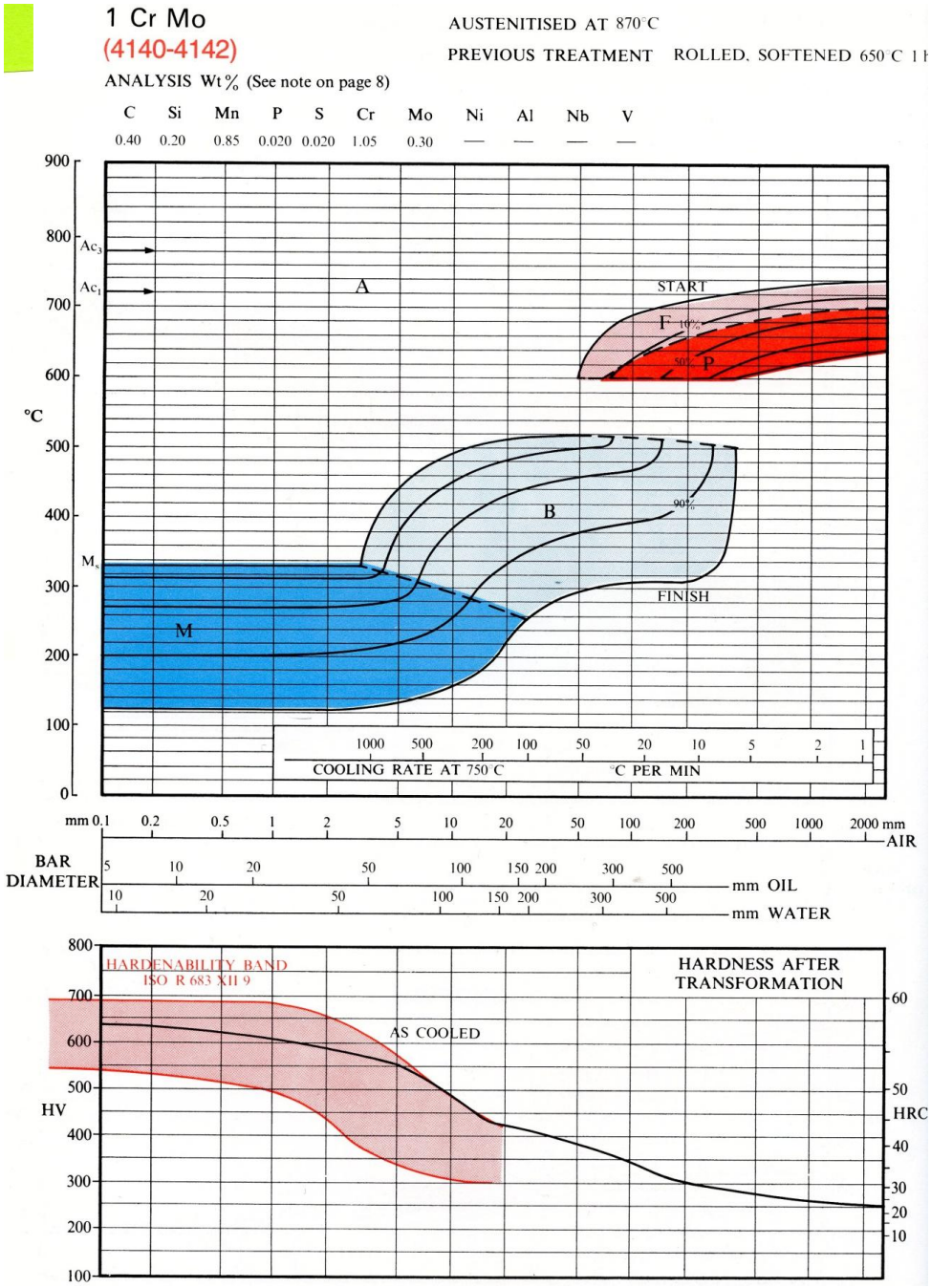

Figure 3.80 – CCT and Hardenability diagram for 4140 steel (Atkins and Met, 1980).

Each phase has different properties, and the final steel property is defined by the mix of the present phases. Properties for AISI 4140 (yield stress and density) are correlated to the phases and temperatures in Figure 3.81. Since the cooling rate influences the phase transformation of the steel, different properties are obtained for different cooling rates. Figure 3.82 exemplifies different AISI 4140 steel properties for different cooling rates.

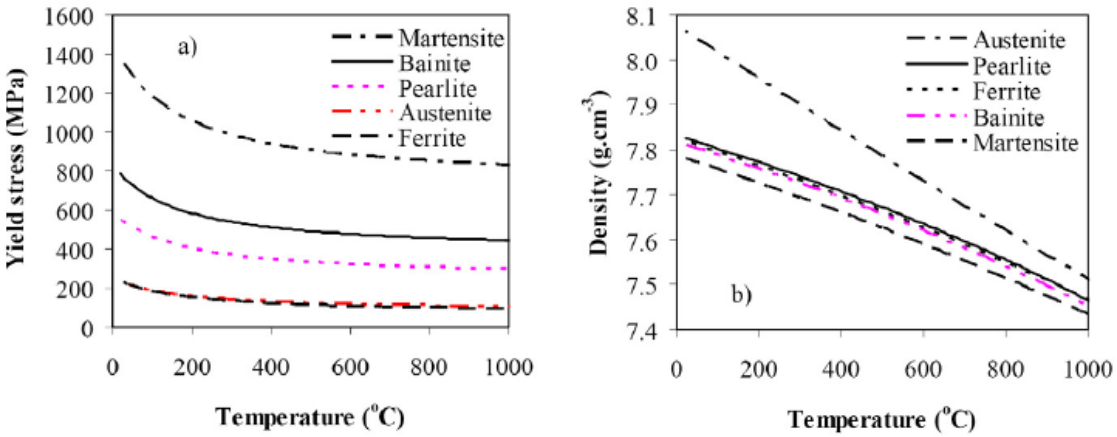

Figure 3.81 – Properties for each phase during cooling of steel 4140; (a) yield stress and (b) density (Guo *et al.*, 2009).

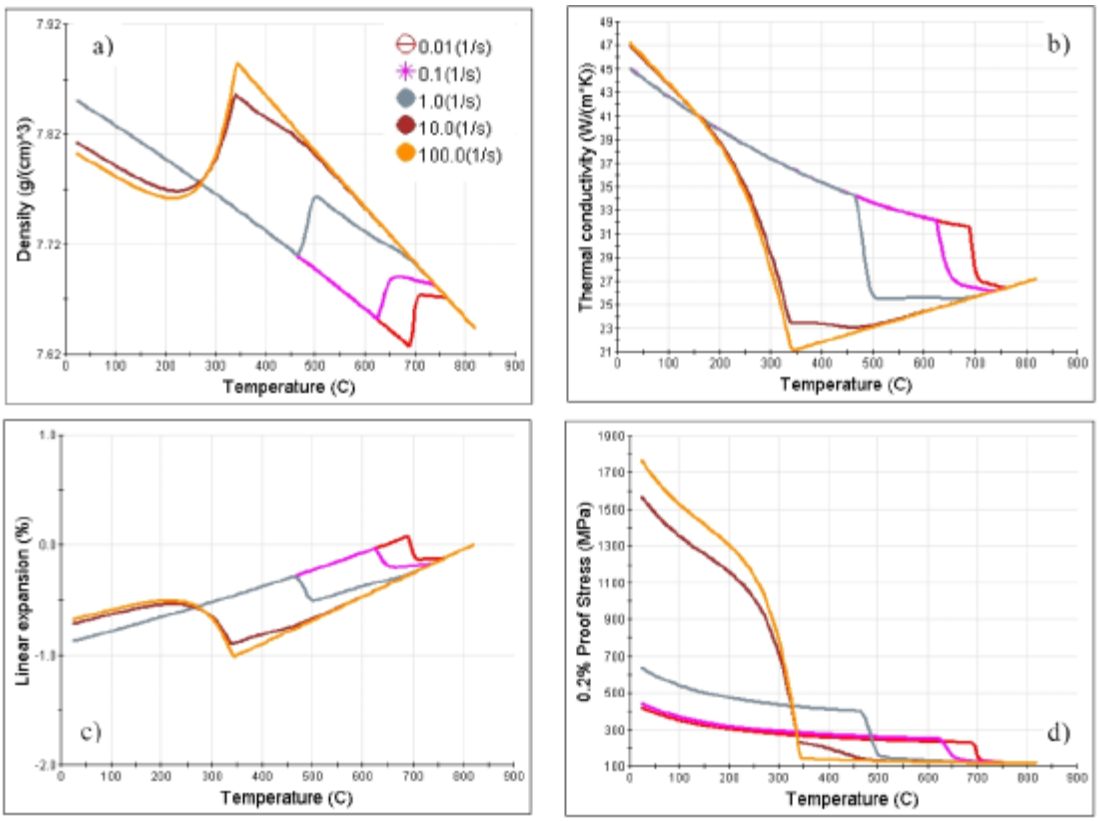

Figure 3.82 – Properties calculated for 4140 steel at cooling rates from 0.01 to 100 °C/s; (a) density; (b) thermal conductivity; (c) linear expansion (Guo *et al.*, 2009).

Gür and Tuncer (2004) have investigated and reported the 4140 steel miscrostructure. Hardness measurements can be used as a direct indicator of the phases obtained. The microstructure having the highest hardness is martensite with 674 HV (59 HRC). By

tempering, hardness of martensite drops dependent on tempering temperature. While hardness of martensite tempered at 200°C reduces slightly to 636 HV (57 HRC), tempering at 600°C reduces the hardness significantly to 386 HV (40 HRC). Hardness of the bainitic microstructure is 330 HV (34 HRC). Hardness value of ferrite–fine pearlite is 270 HV (25 HRC). That of ferrite-coarse pearlite is 199 HV. Figure 3.83 shows the discussed microstructures. In addition, the hardness can be correlated to the martensite percentage (Figure 3.84).

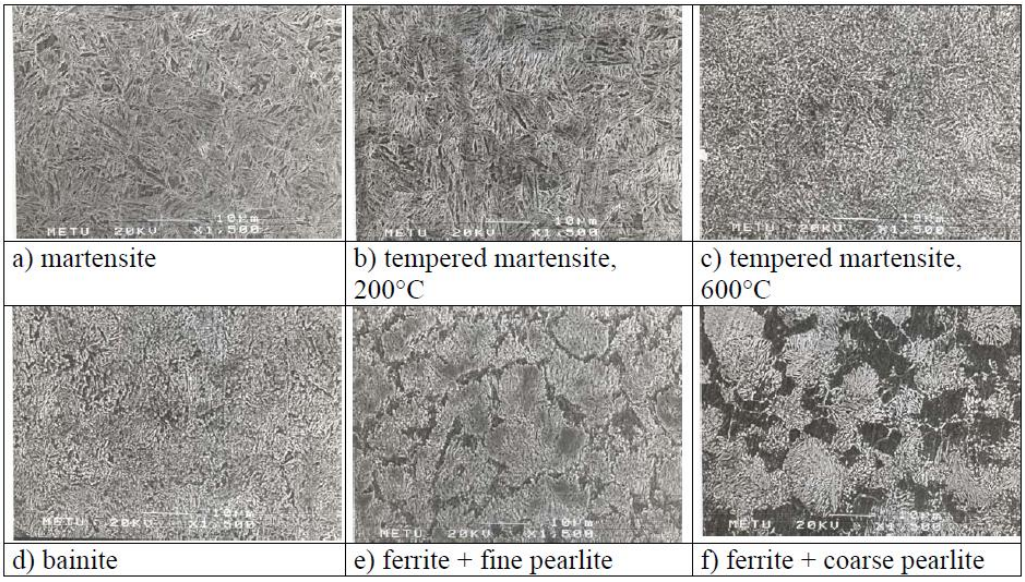

Figure 3.83 – Microstructures of heat treated AISI 4140 specimens (Gür and Tuncer, 2004).

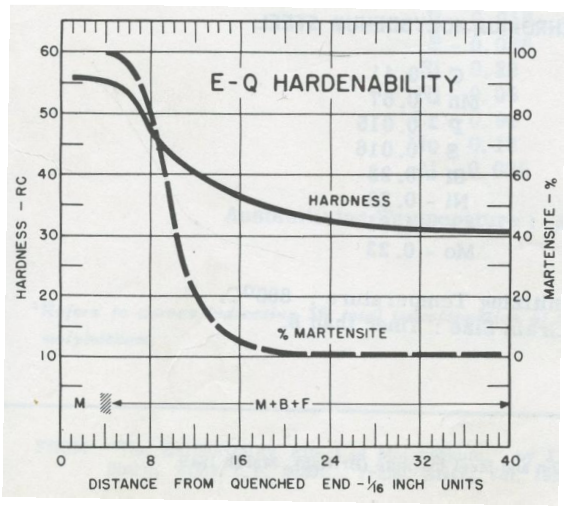

Figure 3.84 – Hardenability diagram and martensite percentage for the AISI 4140 (American Society for Metals, 1977).

3.10. Finite Element Method

The finite element method (FEM) is a numerical approach by which partial differential equations for engineering problems can be solved approximately. The FEM may be used to solve systems such as structures and manufacturing processes. Basically, the studied body/system is divided in finite elements, or elements, connected by nodes, and load and displacements are calculated.

3.10.1. Historical Background and Application

According to Fish and Belytschko (2007), the FEM was developed in the 1950s by the aerospacial industry, including Boeing and Bell Aerospacial (USA), and Rolls Royce (UK). M. J. Turner, R. W. Clough, H. C. Martin and L. J. Topp published in 1957 the first papers about this new method. In the beginning, the matrices of elements were developed, but the term finite element was used later by Ray Clough, who became famous as one of the FEM developers. Initially, the scientific society was skeptic about the FEM. However, later, many studies could prove the advantages of the method.

Mathematicians demonstrated, in the beginning of the 1960s, that the solution based on finite elements converges to precise results for the partial differential equations. Therefore, the more elements used in the problem, the higher is the tendency of the solution, in the limit, be precise. Figure 3.85 exemplifies the Finite Element Method application. The finite element mesh and the process of making the mesh is called mesh generation.

E. Wilson developed one of the first softwares based on the FEM, which was widely used. This program was limited to bidimensional stress analyses, and was improved by research and industrial groups. In 1965, the NASA started the development of general FEM software: NASTRAN. This computer program included a large array of capabilities, such as bi and tridimensional stress analyses, beam and shell elements, for analyzing complex structures, such as airframes, and analysis of vibrations and time-dependent response to dynamic loads.

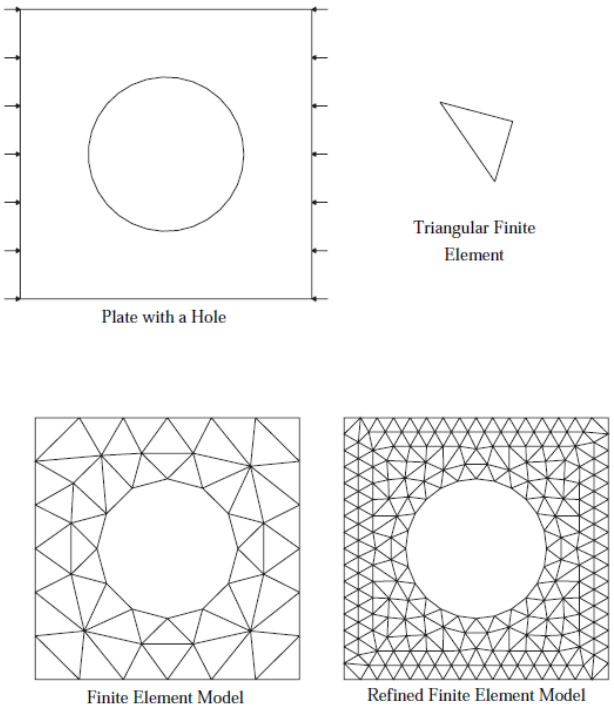

Figure 3.85 – Geometry, loads and finite element meshes (Fish and Belytschko, 2007).

The FEM has changed the engineering projects. The need for costly shop floor trials and redesign of tooling and processes has been reduced. Also the improvement of tool and die design have reduced production and material costs. Such aspects have shortened lead time in bringing a new product to market. The use of more complex equations to predicted loads and dislocations became possible due to the process capability of the computers. Also, tridimensional models became possible to be solved. As can be seen from Figure 3.86, the increase in computational power has been linear on a log scale, indicating a geometric progression in speed. In addition, it is important to say that while the computers have evolved, the prices have been decreasing. Such factors have helped in the FEM development and its popularity.

Kobayashi *et al.* (1989) mention that in the late 1970s and 1980s the use of computer-aided techniques (computer-aided engineering, design, and manufacturing) in the metal forming industry increased considerably. Also, the trend to the following years was toward ever wide application of this technology for process simulation and process design. This trend has been concretized. Furrer and Semiatin (2010) give some examples of computer codes developed over the years. In the 1970s, the development of

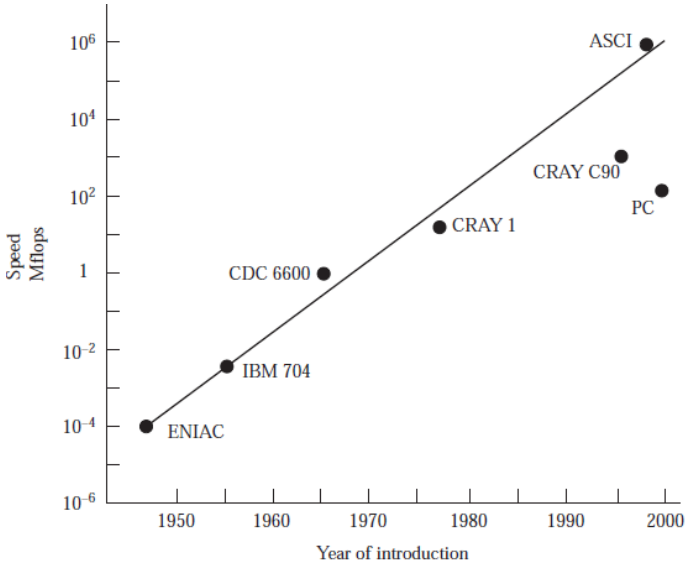

Figure 3.86 – Historical evolution of speed of computers (Fish and Belytschko, 2007).

computer codes to simulate solidification was initiated; commercial codes such as AFS-Solids became available to industry shortly thereafter, followed by many other software packages, including ProCast, MagmaSoft, and SOLIDCast. During this time period, codes for deformation processes, such as ALPID, were being developed to enable industrial engineers to simulate metal flow and predict the occurrence of flow defects. A number of commercial codes are now available for use by industry, including DEFORM, FORGE, and Simufact.

The range of applications of finite elements is too large to list, but the following list provides an idea of its versatility (Fish and Belytschko, 2007):

- stress and thermal analyses of industrial parts such as electronic chips, electric devices, valves, pipes, pressure vessels, automotive engines and aircraft;
- seismic analysis of dams, power plants, cities and high-rise buildings;
- crash analysis of cars, trains and aircraft;
- fluid flow analysis of coolant ponds, pollutants and contaminants, and air in ventilation systems;
- electromagnetic analysis of antennas, transistors and aircraft signatures;
- and analysis of surgical procedures such as plastic surgery, jaw reconstruction, correction of scoliosis and many others.

The metalworking industry has used simulation tools for a number of years. For example, forging process modeling has been used initially to assess bulk metal flow and to predict metal-flow defects, such as laps/folds during deformation. Furrer and Semiatin (2010) also exemplify that simulation can be applied to heat treatment processes for metallic components to predict the required final component microstructure and mechanical properties. The simulation of thermal processes provides detailed temperature and stress histories. Simulation tools are also providing greater understanding of equipment and processes and are being used to guide the application of process controls to further enhance the repeatability of thermal processes. Prediction of thermally induced residual stresses is being accomplished with the simulation of thermal histories within manufactured components. Understanding of bulk residual stresses is having a profound impact on how components are machined and how components are being analyzed for service performance.

3.10.2. Metal Forming Simulation

The FEM is applied to metal forming process for many objectives, such as: develop a new product; develop a new manufacturing process; improve the quality of the product; improve process efficiency; tooling design; and predict tooling failure and wear. Usually, there are 4 main steps during a project based on simulation. The first step is based on CAD tools, and the subsequent steps on CAE tools:

1. 3D model: the final product is designed. Its geometry, material properties and others aspects are defined;
2. Pre processor: the FE setup is defined. Mesh generation and boundary conditions are applied to the system. Material properties and routines are established;
3. Simulation: the FE model is run. The numerical calculation is conducted and the process is predicted and stored.
4. Post processor: the simulated process is analyzed. Stresses, strains, damages, defects, temperatures, geometries, material properties, loads, and other aspects are observed during and after the proposed process.

A complete design of any specific process approaches the 3D model, the FE analysis, the tool design, and the final product. Figure 3.87 exemplifies the design process of metal sheet components part of a car product. However, to account for the complicated thermomechanical responses to the manufacturing process, four FEM modules, as shown in Figure 3.88, are loosely coupled. They are the deformation model, the heat-transfer model, the microstructural model, and, in the case of steel, a carbon diffusion model (Oh *et al.*, 2010).

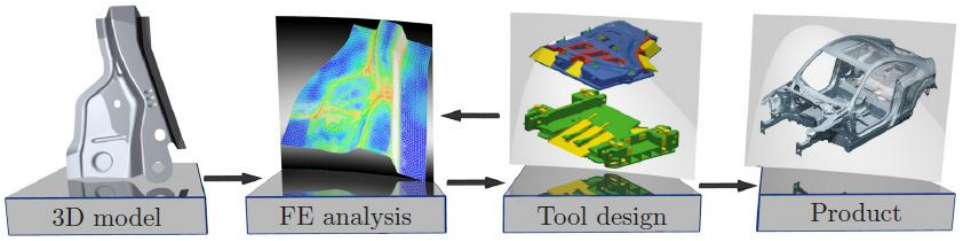

Figure 3.87 – Design process schematic (Burchitz, 2008).

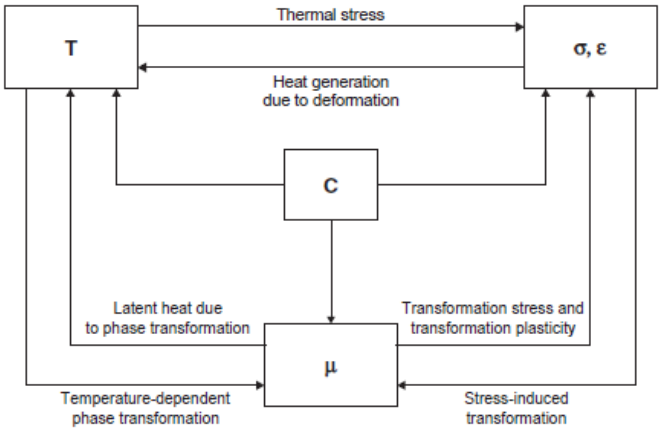

Figure 3.88 – View of the various coupled phenomena within metal forming (Oh *et al.*, 2010).

In order to predict the temperature evolution accurately during metalworking processes, Oh *et al.* (2010) list several important thermal boundary conditions must be considered:

- Radiation heat with view factor to the surrounding environment;
- Convection heat to/from the surrounding environment, including the tool contact, free air, fan cool, water or oil quench;

- Friction heat between two contacting bodies. It is also noted that friction heating is the primary heat source in the friction-stir welding process.
- Deformation, latent heat, and eddy current are the primary volume heat sources. Deformation heat is important for large, localized deformation and fast processes, because the adiabatic heat will increase the local temperature quickly, and material is likely to behave differently at elevated temperatures. It plays an important role in metalworking, inertial welding, translational friction welding, and the cutting process. The latent heat comes from the phase transformation or phase change, and eddy-current heat is generated by electromagnetic fields.

The FE setup may consider different formulations (SFTC, DEFORMTM 3D Version 10.1.2. User's Manual, 2010):

- Rigid: usually used for dies, which are modeled as non-deformable materials. This option is applied in order to perform a more efficient simulation. In this case, stress and deflection data for the dies is not available during deformation;
- Elastic: elastic objects are used if the knowledge of the tooling stress and deflection are important throughout the process. However, if yield stress for the tooling is exceeded, stress and deflection results will be incorrect.
- Plastic: modeling as rigid-plastic or rigid-viscoplastic material depending on characteristics of materials. The plastic material behavior of the object is specified with a material flow stress function or flow stress data.
- Elasto-plastic: objects are treated as elastic objects until the yield point is reached. Then, any portions of the object that reach the yield point are treated as plastic, while the remainder of the object is treated as elastic. Also, provides a realistic simulation of elastic recovery (springback), and strains due to the thermal expansion.
- Porous: the same as plastic objects (compressible rigid-viscoplastic materials) except that the material density is calculated and updated as part of the simulation.

Linear analysis, such as elastic formulations, may be used in analyzing the stress, strain, elasticity modulus, and deformation behavior of a component. Using linear

approximations, mathematical models are made, which are used for design and analysis purposes. Technically, all physical processes that involve a mechanical component are non-linear in nature. Non-linear analysis, such as plastic and elasto-plastic formulations, also allows a comprehensive, multi-dimensional analysis within the limits of the system.

Many metal forming processes may consider rigid-viscoplastic formulations. A forging process sequence in demonstrated through simulation in Figure 3.89. Figure 3.90 shows the stress analysis in the workpiece during a wire drawing simulation. An elasto-plastic system is exemplified in Figure 3.91. Modeling the simple act of taking an ordinary steel paper clip, "unbending" it, and then "bending" it back, requires consideration of both nonlinear material and nonlinear geometry. The heat exchange with the surrounding environment should also be considered (Figure 3.92).

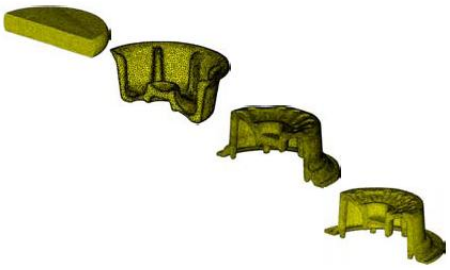

Figure 3.89 – Simulation of a hot forging process for aerospacial component (Ngaile and Altan, 2004).

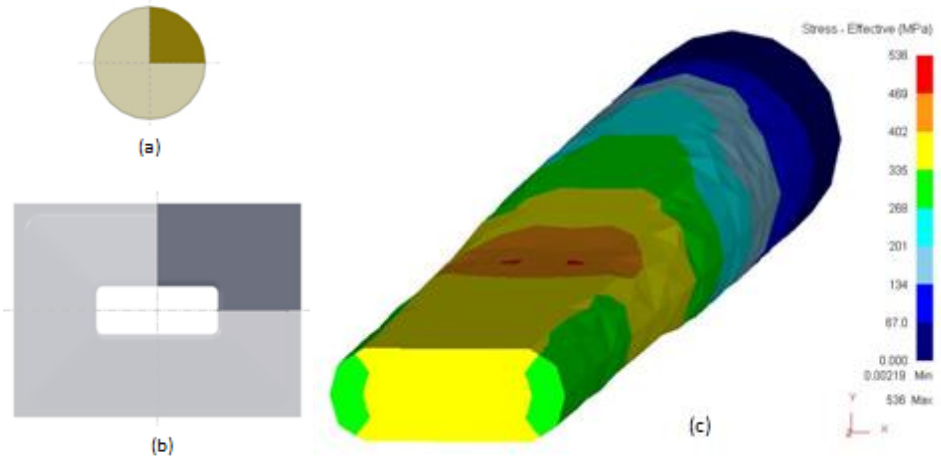

Figure 3.90 – Wire drawing process simulation: (a) initial cross-section of the wire, (b) wire gage, and (c) effective stress in the wire during the process (da Silva, 2009).

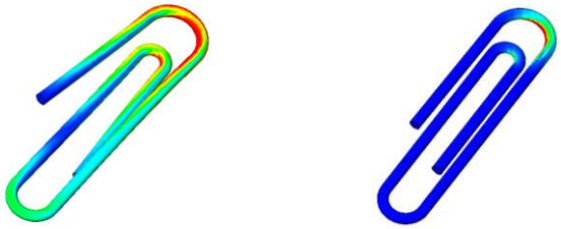

(a) (b)

Figure 3.91 – (a) Analysis of paper clip bending requires nonlinear material and nonlinear geometry analysis. Paper clip in "unbent" position shows plastic stresses; (b) Paper clip bent back into the original shape shows residual stresses (Dassault Systèmes SolidWorks Corp., 2008).

(a)

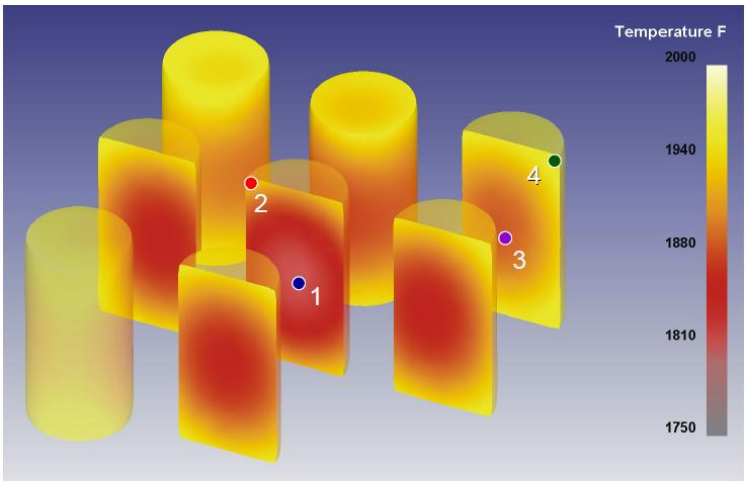

(b)

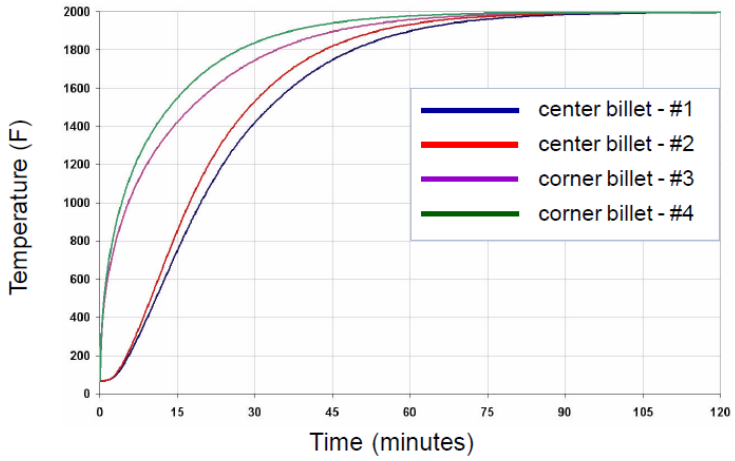

Figure 3.92 – (a) Model of nine billets being heated is shown above; the shadowing effect of the center billet is captured with the view factor. (b) Time to temperature is shown below. High energy cost justifies modeling the heating processes (SFTC, 2005).

3.10.3. Heat Treatment Simulation

FE models for heat treatment simulations consider a complex interaction between deformation, temperature, transformation and diffusion. There is coupling between all of the phenomenon, as illustrated in Figure 3.93. When the objective of the simulation is related to part distortions, the model has to take into account the deformation based on the strain rate components stated in Equation 3.16. Each strain rate component was discussed in the section 3.4.

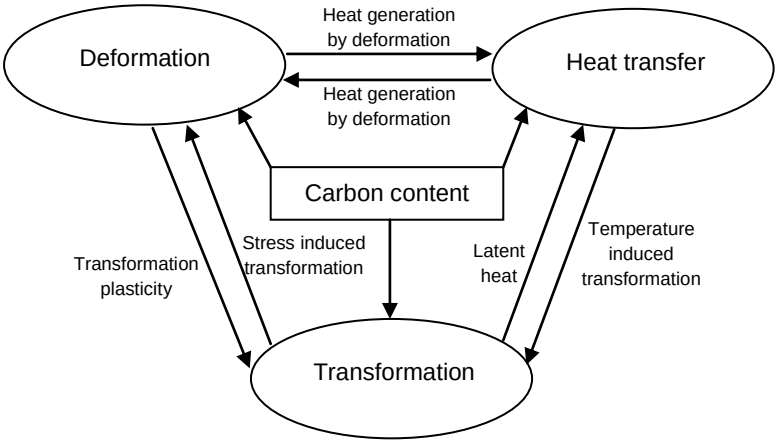

Figure 3.93 - Coupled phenomena considered during the quenching simulations.

Heat treatment simulations have to consider thermal effects within the simulation, including heat transfer between objects and the environment, and heat generation due to deformation or phase transformation, performing the transformation between phases due to thermomechanical and time effects. Section 3.6 has exemplified different heat transfer coefficients as a function of part surface temperature, obtained from experimental tests, and able to be applied to FE models.

In order to obtain adequate simulation results the material data should be accurate. According to Guo *et al*. (2009) the following information on materials properties have to be known for distortion prediction caused by quenching through numerical simulations:

- phase transformation kinetics, *i.e.*, TTT and CCT diagrams;

- temperature dependent thermo-physical properties for each phase formed, such as density, Young's modulus, thermal expansion coefficient, and thermal conductivity;
- temperature dependent mechanical properties of each phase formed, including tensile strength, yield strength, and hardness.

The above data involves long and expensive laboratory testing; an alternative is the use of software focused on material properties simulation, which are usually based on the chemical composition of the material.

In order to consider phase transformation during simulations, the material data should be composed by different material datas, obtaining a mixture of materials/phases. An inter-material data should define the relationships between the phases of a mixture. The relationships between the phases are defined in terms of the following transformation characteristics: transformation kinetics model; latent heat of transformation; transformation induced volume change; and transformation plasticity. According to (SFTC, DEFORMTM 3D Version 10.1.2. User's Manual, 2010), transformation is modeled by defining the volume fraction for each possible phase in each element of a meshed object. Each phase is defined by its own set of material properties. These material properties define the elastic and plastic behavior of the phase, the thermal properties of the phase. The relationship between the transformation from one phase to another is defined in terms of a kinetics model (in order to determine rate of phase transformation) and a few relational properties such as latent heat and volume change.

A kinetics model is a function that defines the conditions and manner in which one phase may transform into another. The transformation is driven by the diffusion processes depending on the temperature, stress history, and carbon content. The diffusionless transformation from austenite to martensite involves a shear process which depends on the temperature, stress, and carbon content.

CCT and TTT curves may be used for the kinetics model of diffusion transformation. For this work, TTT curves are considered in the inter-material data. For cooling processes of an austenitized AISI 4140, for example, Figure 3.94 shows TTT curves for

the transformation from austenite into ferrite, pearlite, and bainite (the temperature of the beginning of martensite transformation is also indicated). For each phase, two curves are used to define the volume fraction transformed for a given dominant atom content. Each curve corresponds to the appropriate specified volume fraction.

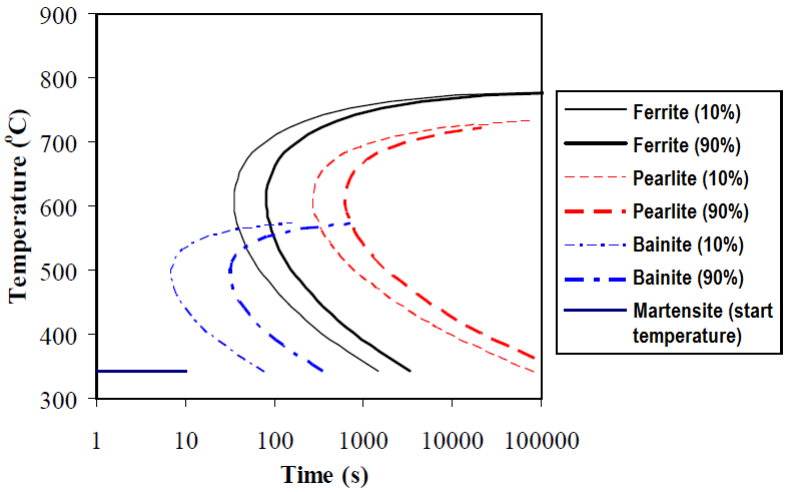

Figure 3.94 – TTT curves of steel 4140, corresponding to 10% and 90% of the transformation (Guo *et al*., 2009).

The volume fraction transformed, ζ, is calculated based on an Avrami equation, which has the form

$$\zeta = 1 - exp(-f_T(T) f_S(\sigma_m) f_C(C) t^n), \tag{3.46}$$

where, σ_m is the mean stress, C is the carbon content, t is the time, and n is the transformation dependent Avrami number. $f_T(T)$, $f_S(\sigma_m)$ and $f_C(C)$ are functions of temperature T. $f_T(T)$ can be expressed by the simplified formula

$$f_T(T) = A_{T1} \left(\frac{T - A_{T2}}{A_{T3}}\right)^{A_{T4}} \left(\frac{A_{T5} - T}{A_{T6}}\right)^{A_{T7}}, \tag{3.47}$$

where, the coefficients from A_{T1} to A_{T7} are determined by using 50% transformed line of TTT curve diagram. $f_S(\sigma_m)$ and $f_C(C)$ describe the stress and carbon content dependency of transformation, respectively, as

$$f_S(\sigma_m) = exp(A_S \sigma_m), \tag{3.48}$$

$$f_C(C) = exp\big(A_{C1}(C - A_{C2})\big), \tag{3.49}$$

where, the coefficient A_S is specified according to the stress dependency of TTT curves, and A_{C1} and A_{C2} are determined by carbon content dependency.

The latent heat accounts for the net energy gain or loss when a phase change occurs from one phase to another. The volume change due to transformation is induced by a change in the lattice structure of a metal, and the strain is calculated as discussed in section 3.4.3. The transformation plasticity, a phenomenon where the material plastically deforms at a stress lower than the flow stress, was also discussed in section 3.4.3.

Material hardness is also an indication of the phases present in heat treated materials. To predict hardness through computational simulation, Jominy tests can be used in the model. In section 3.2.5, the Jominy test was discussed. An alternative in the prediction of hardness is to input the hardness of each material phase, and the final hardness will consider the final mix of phases. Section 3.9.2 shows Jominy tests and phase's hardness for the AISI 4140.

Examples of FEM application to heat treatment processes have already been shown in this text. Section 3.6.4 discusses inverse analysis techniques based on FE simulation to determine the heat transfer coefficient, HTC. Approaching quench distortion prediction, section 3.7 shows several examples of distorted metal components after simulation.

4. METHODOLOGY

In order to define the methodology to correct the ring distortions, it is necessary to predict the distortion caused by the heat treatment process. The prediction of the ring distortion was conducted throughout a numeric simulation based on the Finite Element Method (FEM). The code to be used for the FE (Finite Element) simulation is the DEFORM-3D^{TM}, version 10.1 (Scientific Forming Technology Corporation, Columbus, Ohio, USA). The same software was used to perform the correction of the geometric defect by forming process.

The heat treatment simulation has to be validated. So, a Navy C-ring test was experimentally conducted and also simulated. The obtained distortion for experimental and simulated cases were compared.

4.1. Validation of the Heat Treatment Simulation Methodology using a Navy C-Ring Test

4.1.1. Experimental test

AISI 4140 steel Navy C-rings were machined for the quenching process, considering the dimensions given in Figure 4.1. The nominal composition of the alloy steel employed for the C-ring is defined in Table 4.1, which was certified by the supplier.

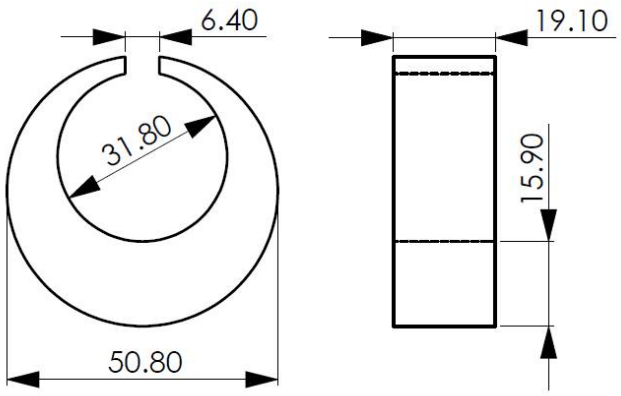

Figure 4.1 – C-ring geometry (all dimensions in mm).

Table 4.1 – Nominal composition of AISI 4140 steel (in wt%).

C	Si	Mn	Cr	Mo
0.40	0.20	0.85	0.95	0.20

The measurements of the ring dimensions before and after the heat treatments were performed in a Mitutoyo Shadowgraph PJ A3000 Model with an accuracy of 0.01 mm. Two dimensional changes weree analyzed: gap opening, *G*, and outside diameter, *D*. Based on Figure 4.2, the dimensional changes may be expressed as:

$$G = n' - n \,, \tag{4.1}$$

and,

$$D = m' - m \,. \tag{4.2}$$

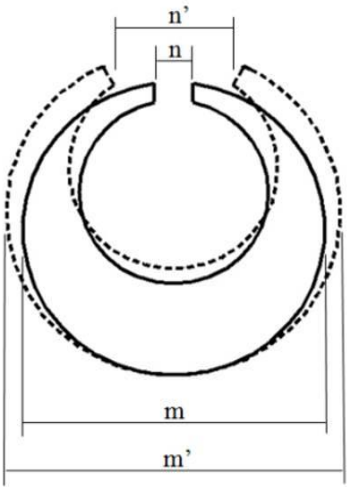

Figure 4.2 – C-ring specimen before heat treatment (*m* and *n* dimensions) and after heat treatment (*m'* and *n'* dimensions).

The C-rings were heated to 900 °C in a tubular furnace where an Argon gas flow was maintained for minimizing the oxidation of the material. This temperature was held for 1 hour (3600 s) in order to attain a homogeneous austenitic microstructure. After austenitized, the quenching was performed through the fast vertical movement of the ring (thickest part of the ring at the bottom and ring gap at the top) into the quenching oil (CASTROL OILQUENCH 1) at 25 ºC, being held for at least 300 s.

The microstructure of the quenched C-rings was evaluated at various points of the longitudinal and transversal cross-sections of the C-rings, as illustrated in Figure 4.3. Sample preparation involved conventional surface grinding, polishing and etching with Nital 2%. Hardness measurements (HRC – Rockwell "C") were also taken at various locations in the sections indicated in Figure 4.3.

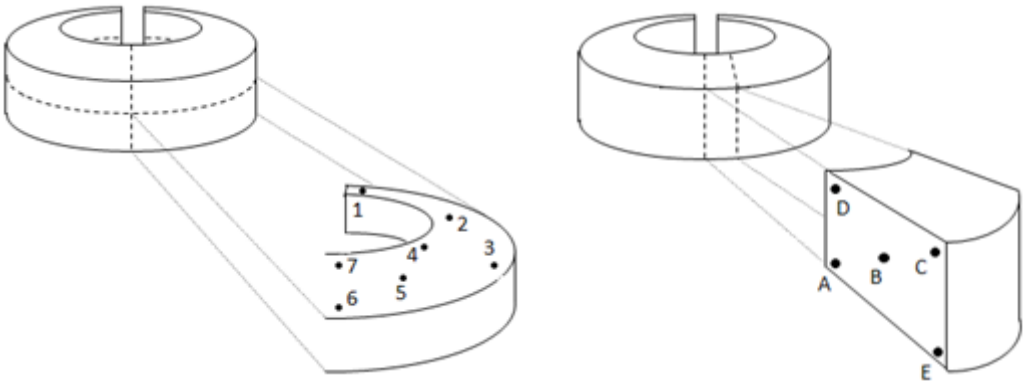

(a) (b)

Figure 4.3 – Location of the regions where the microstructure of the quenched C-rings was examined (a) in the longitudinal cross-section and (b) in the transversal cross-section.

4.1.2. Numerical Simulation

The simulation of the C-ring test was conducted using the DEFORM^{TM}-HT module. The acquisition of the material data necessary for heat treatment simulations involves long and expensive laboratory testing. An alternative is the use of software focused on material properties simulation, which are usually based on the chemical composition of the material. JMatPro (Sente Software Ltd., Surrey, United Kingdom) is one of the available software with the capability of simulating all the necessary material properties for the FE simulation of forming and cooling processes based o the material chemical composition. In the case of JMatPro, there is already an interface for exporting files to be used in DEFORM^{TM}, as shown in Figure 4.4.

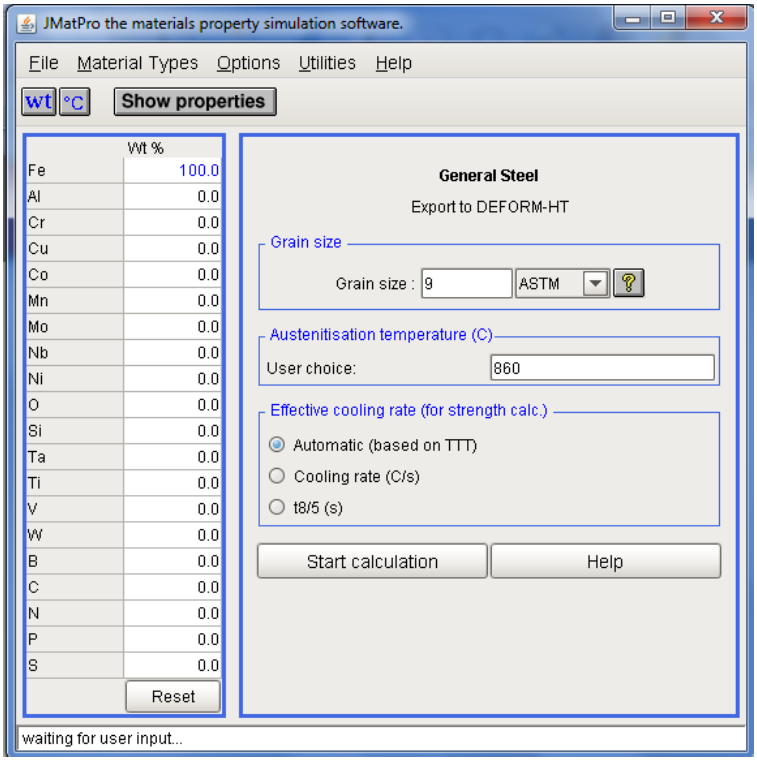

Figure 4.4 – JMatPro's interface for exporting material data to DEFORM™ (Sente Software Ltd.).

The simulation of the initial heating stage of the C-ring involved the prediction of the ring expansion due to the temperature increase from 20 to 900 °C. The coefficient of thermal expansion for the 4140 steel was obtained from the DEFORM™ library (1.23×10^{-5}/°C). Once expanded at 900 °C, the specimen was considered as completely austenitized (100% austenite).

The AISI 4140 data for the quenching stage simulation was provided by Sente Software Ltd. (JMatPro software). The mechanical and thermo-physical properties for the various material phases and constituents (austenite, martensite, bainite, ferrite and pearlite) were taken into consideration. The phase transformation kinetics is based on TTT curves. Also, all of the transformation aspects were taken into account, including latent heat, volume change and transformation plasticity. Jominy curves were used for hardness prediction.

Since that the C-ring has a relatively small size and the quenching process was performed in still oil, the heat transfer coefficient was considered as constant along all of the C-ring surface and as a function only of the ring surface temperature. The heat transfer coefficient between AISI 4140 and oil as a function of temperature has already been determined by Hardin and Beckermann (2005), given in Figure 4.5, and were used for the simulation.

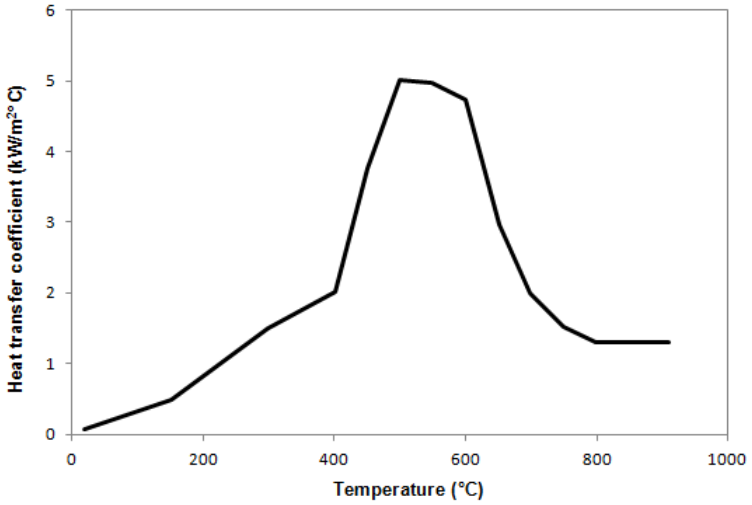

Figure 4.5 – Heat transfer coefficient between AISI 4140 and still oil (Hardin and Beckermann, 2005).

Due to the part symmetry, only ¼ of the part was simulated. Summarizing the FE setup for the simulations, Table 4.2 gives the main parameter used for the model.

Table 4.2 – FE setup for the simulations of the Navy C-Ring Test.

Operation	Parameter	Value
1 – Heating (furnace)	Code	DEFORM-3D™
	C-ring geometry	Figure 4.1
	Material	AISI 4140 from DEFORM-3D™ library
	Initial temperature	20 °C
	Furnace temperature	900 °C
	Object type	Elastic
2 – Quenching (oil)	Code	DEFORM-3D™
	C-ring geometry	Expanded - Operation 1
	Material	AISI 4140 from JMatPro
	Initial temperature	900 °C
	Quenchant temperature	25 °C
	Heat transfer coefficient	Function of temperature (Figure 4.5)
	Object type	Elasto-plastic

4.2. Prediction of Ring Distortion during Heat Treatment Processes

Once the methodology to predict heat treatment distortion of steel parts using DEFORM-HT code is validated through the simulation of the C-ring test, the same methodology was used to obtain ovality (distortion) during the heat treatment of hot rolled rings. The normalizing and quenching stages were simulated.

Since the objective of this work is the definition of a methodology to predict and correct geometric distortion and residual stresses of hot rolled and heat treated rings, a case study was considered. The thin-walled ring given in Figure 4.6 was defined for the development of this work. The obtained ovality and residual stresses of the ring after the simulations were calculated.

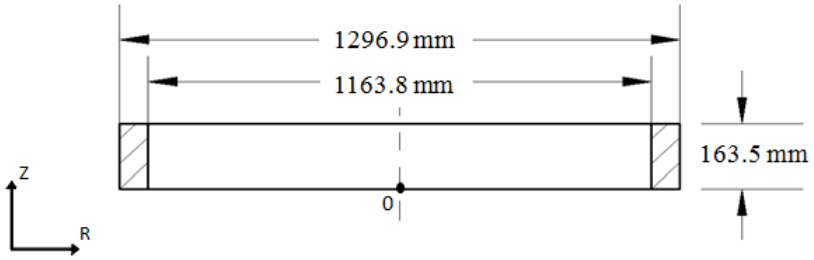

Figure 4.6 – Thin-walled ring to be used as a case study (cross section).

4.2.1. Numerical Simulation of Normalizing

Once the methodology to simulate heat treatment processes for AISI 4140 steel parts and predict eventual distortion defects was defined, it was verified whether distortion occurs or not during the normalizing process.

After hot rolled, the rings are air cooled. Then, for normalizing, the rings are heated up to the austenitizing temperature and air cooled. For the cooling stage, the rings are positioned one beside the other. In order to verify if a ring may distort due to the irradiated heat received from another ring, two rings were numerically air cooled, being positioned next to each other. For this simulation, the heat transfer by convection between ring surrounding, and the heat transfer by radiation between the rings were

taken in consideration. Figure 4.7 shows a schematic drawing of two rings during the air cooling procedure. Both rings lose heat to the surrounding by convection and radiation, but also receive radiated heat from the other ring. The FE model considered a conservative system, positioning one ring 10 mm distant from the other.

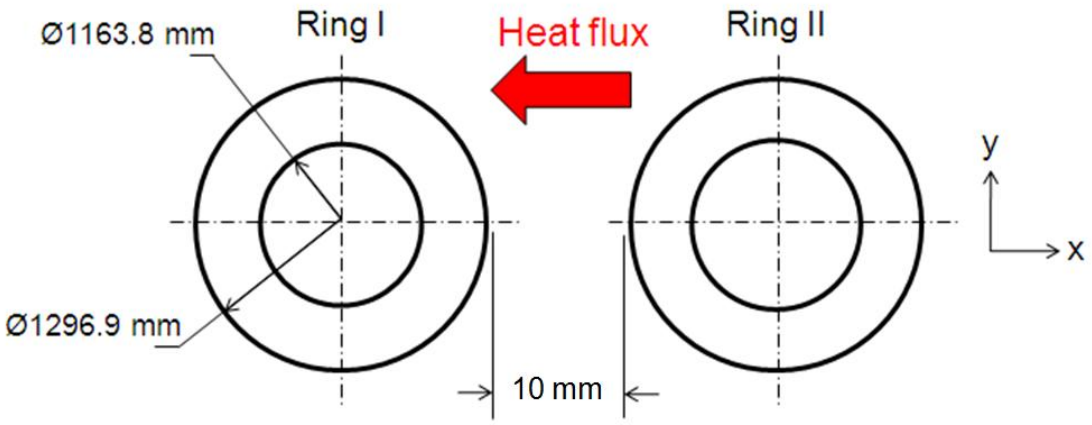

Figure 4.7 – Schematic drawing of two rings during air cooling; Ring I is losing heat to the surrounding by convection and radiation, and receiving heat from Ring II by radiation.

A FE model with two rings was simulated. Each ring had ½ of the geometry due to the symmetry. The heat transfer coefficient between ring and surrounding, for air cooling, to be considered in the simulation is given in Figure 3.29 for oxidized steel. Figure 4.8 shows the heat transfer coefficient as a function of the surface temperature to be inserted in the FE model, including convection and radiation. In addition, the heat exchange between the two rings by means of radiation was taken in account throughout a view factor function The view factor was activated by the input of a “dat” file. The main parameters of the FE setup to simulate the normalizing process are given in Table 4.3.

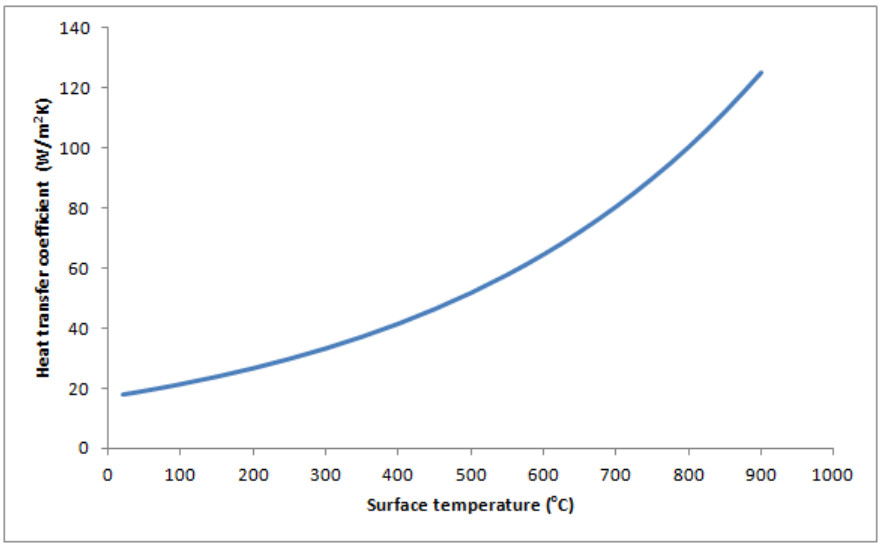

Figure 4.8 – Heat transfer coefficient for oxidized steel during air cooling (Bamberger and Prinz, 1986).

Table 4.3 – FE setup for the simulations for normalizing process considering the heat exchange between two rings.

Operation	Parameter	Value
1 – Heating (furnace)	Code	DEFORM-3D™
	Ring geometry	Figure 4.6
	Material	AISI 4140 from DEFORM-3D™ library
	Initial temperature	20 °C
	Furnace temperature	927 °C
	Object type	Elastic
2 – Air cooling + heat exchange between parts	Code	DEFORM-3D™
	Ring geometry	Expanded - Operation 1
	Material	AISI 4140 from JMatPro
	Initial temperature	927 °C
	Quenchant temperature	20 °C
	Heat transfer coefficient	Function of temperature (Figure 4.8)
	Object type	Elasto-plastic

4.2.2. Numerical Simulation of Quenching

The quenching process is performed after the normalizing stage. No ovality is expected due to the normalizing process. Therefore, for the quenching simulation, the nominal geometry of the ring was used for the simulation with no residual stresses. The ring was

heated to an austenitizing temperature. At 900 °C, with a 100% of austenite, and then cooled quickly.

Since the objective of this thesis is the definition of a methodology to predict and control ring ovality, some assumptions were taken for the FE model, without the necessity of including real values. For quenching of rolled rings, a typical heat transfer coefficient between AISI 4140 steel and quenchant (8% Aqua-Quench) was considered. Houhgton Corp. provided the heat transfer coefficient in function of surface temperature given in Figure 4.9.

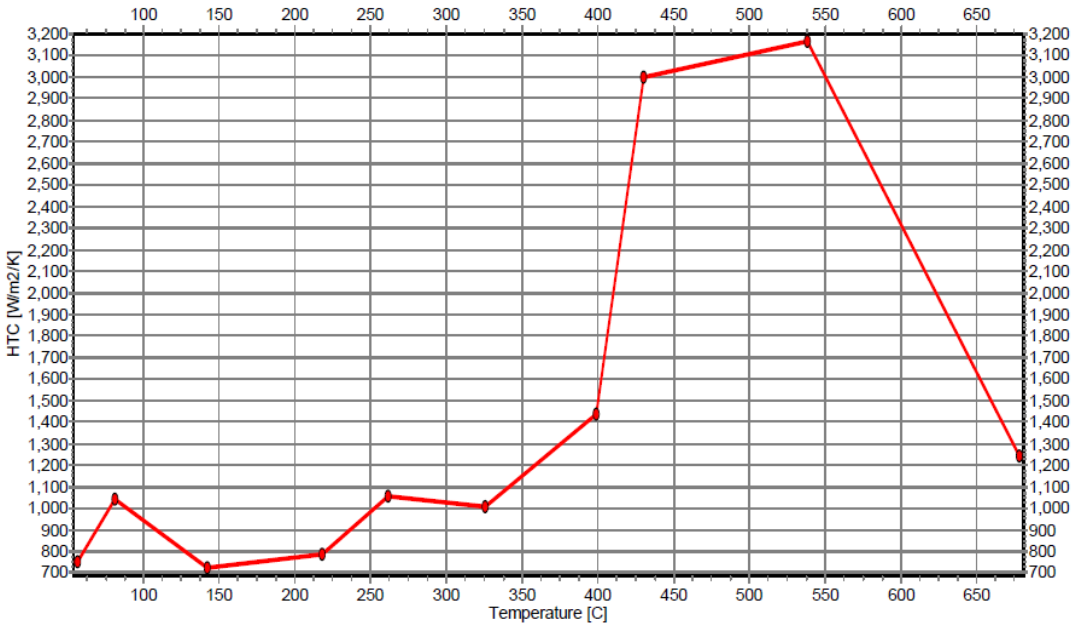

Figure 4.9 – Heat transfer coefficient between AISI 4140 steel and still 8% Aqua-Quench quenchant (provided by Houghton Corp.).

It is already known that the ovality occurs during the quenching process. The variation of the number of rings in the tank, the size of the rings, the quenchant conditions, and the high production rate influence in the heat treatment conditions. The heat transfer coefficient varies along the ring surface, being a function of different parameters such as quenchant agitation, temperature, time and position. Due to the complexity of the quenching process, assumptions were taken and a hypothetical model was defined.

Figure 3.35 shows that the heat transfer coefficient around a cylinder may varies as a function of the quenchant flow. This principle was used for the hypothetical model to predict the ovality of the rings. Figure 4.10 illustrates the hypothetical model for the quenching simulation: a propeller is assumed next to the ring; the ring surface was divided in regions, and for each region, a different heat transfer coefficient was applied to. For the inside surface of the ring (green line in Figure 4.10), the heat transfer coefficient was applied as given in Figure 4.9. For external, top and bottom surfaces, the heat transfer coefficient was applied as shown in Figure 4.10: for region DA (green color), the heat transfer coefficient was applied as it is; for regions AB and CD (yellow color), the heat transfer coefficient was increased two times; and for region BC (red color), it was increased eight times. Figure 4.11 shows a schematic drawing of the ring's cross section indicating the heat transfer coefficient for all surfaces.

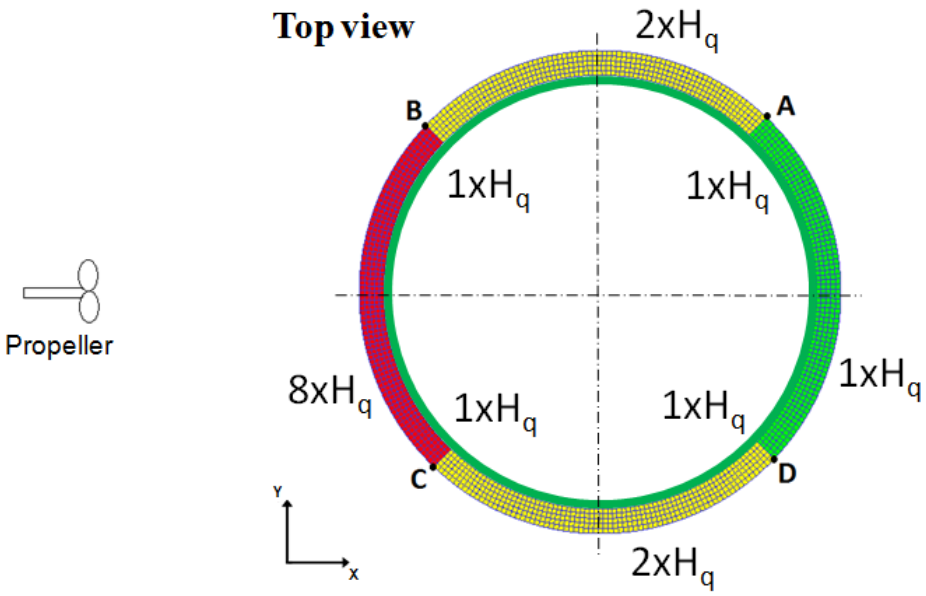

Figure 4.10 – Heat transfer coefficient distribution on the ring surface. Inside surface is represented by a green line; and regions DA (green), AB and CD (yellow), and BC (red) represent top, bottom and outside surfaces, respectively.

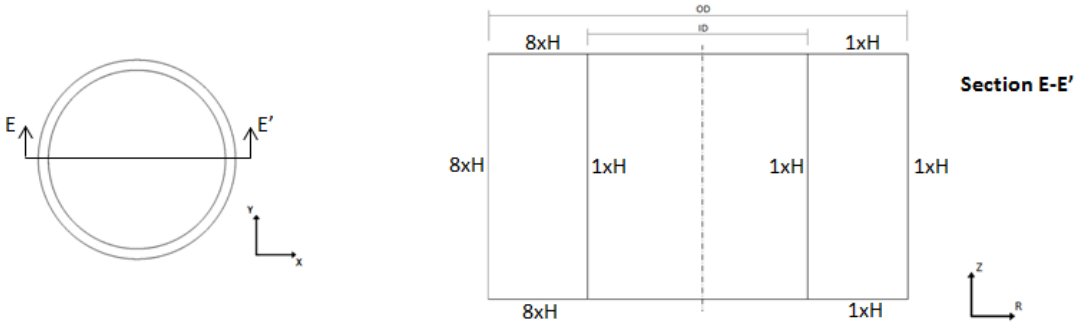

Figure 4.11 – Schematic drawing of the ring's cross section showing the heat transfer coefficient distribution on the surface.

The obtained ovality was measured after the simulation of the fast cooling stage. In addition, the residual stresses and also the hardness were calculated. The main parameters of the FE setup are given in Table 4.4.

Table 4.4 – FE setup for the simulation of quenching process.

Operation	Parameter	Value
1 – Heating (furnace)	Code	DEFORM-3D™
	Ring geometry	Figure 4.6
	Material	AISI 4140 from DEFORM-3D™ library
	Initial temperature	20 °C
	Furnace temperature	900 °C
	Object type	Elastic
2 – Quenching (tank)	Code	DEFORM-3D™
	Ring geometry	Expanded - Operation 1
	Material	AISI 4140 from JMatPro
	Initial temperature	900 °C
	Quenchant temperature	25 °C
	Heat transfer coefficient	Function of temperature (based on Figure 4.10)
	Object type	Elasto-plastic

4.3. Correction of Distortion

The distortion of rings, obtained during heat treatment processes, is a defect. Defects such as ovality have specified tolerances for shipping to the customers. In the case of the rings, the industry has reported ovalities in a range between 2 and 18 mm. Therefore, for this study, it is assumed that ovalities higher than 2 mm are not acceptable for shipping to the customers.

In this work, a procedure to correct the ovality was developed based on the system in Figure 3.74 (b), which is, basically, a machine with two flat tools. The rolled ring industry corrects the ring distortions compressing it. This procedure is already in use in the industry. However, it is based on the operator of the system's experience, developed in a trial and error practice.

In order to simulate de correction of the oval rings, first it is necessary to define a procedure to perform the correction in the industrial process. A schematic assembly of the compressing process is shown in Figure 4.12, in which the left die moves toward the ring, compressing it and obtaining small plastic deformations to correct the out-of-roundness shape.

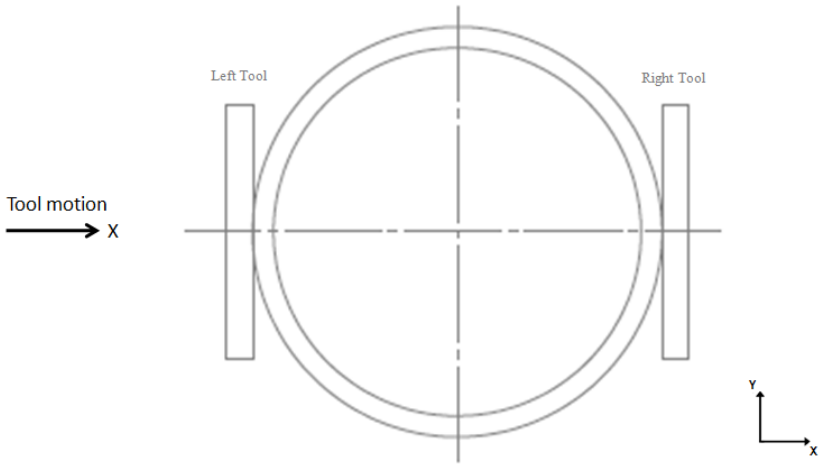

Figure 4.12 – Schematic compression of ring process.

The trial and error practice in the industry leads to a high number of steps in the process, and lower production rates as a consequence. In some cases, the distortion is too high to be corrected, and the ring might be scrapped. A new methodology should be proposed to optimize the process and increase the production rate. Considering the wide range of ring geometries and materials at the shop floor, each one with its respective distortion, the methodology should be as simple as possible.

The new proposed methodology consists in making at least 8 marks on the ring, with the same distance between each one, which was used for ring dimensions measuring. Figure 4.13 shows 8 marks 45° distant from each other. The methodology is set as follows:

1. The distorted ring should be marked as shown in Figure 4.13, with equal distances between them. Note: if possible, one of the marks should be on the direction of the largest dimension;
2. The distances between opposite marks are measured before compression procedure;
3. The ring is positioned in the machine considering that the first step compression will be performed on the direction of the largest measured dimension;
4. First step is conducted. The objective is to achieve, for the compressed dimension, the nominal ring diameter magnitude. Therefore, the stroke magnitude should be satisfactory for achieving the nominal diameter after the tools move back (ring relaxation).
5. All the dimensions are measured again. If the distortion is higher than the tolerance for shipping to the costumers, a second step should be conducted.
6. For the second step, the ring is rotated and positioned with the largest measured dimension on the compression direction.
7. Stages 4, 5, and 6 are repeated until the ring obtains an acceptable round shape for shipping to the costumers.

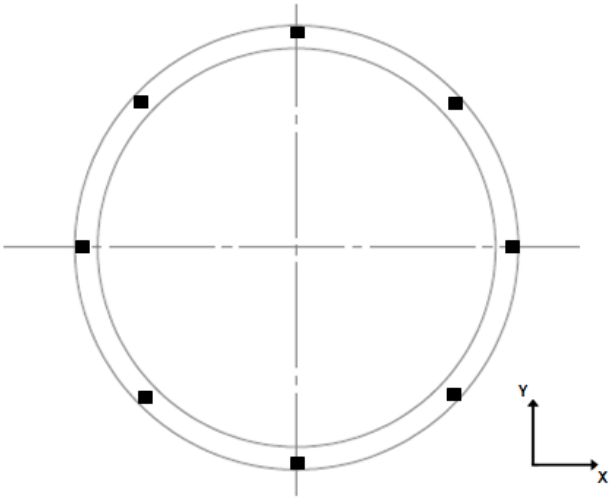

Figure 4.13 – Ring marks for compression of ring process.

The proposed methodology to correct the ring ovality in the industry is not complete yet. During the ring compression, the necessary die stroke is not proportional to the ovality magnitude. The elasto-plastic behavior of the material provides a relaxation of the ring after the compression as a consequence. Therefore, simulations of this process should be performed in order to correlate the necessary die stroke with the ring ovality and the ring geometry and material.

In order to establish the complete methodology of distortion correction, including the simulation stage, the distorted ring after the quenching process was used. The compression of the distorted ring was simulated, defining the necessary die stroke for the specific ovality.

It is important to consider that the quenched ring is hardened. Because of that, it is necessary to obtain a new true stress-strain curve in order to establish a correct FE model for the compression of the hardened ring. The correct procedure would be the performing of tensile tests for the ring material after the quenching process. However, this would be a destructive and very expensive test – alloy steel rings have a minimum price of 10,000 dollars, and titanium or nickel alloys may achieve 80,000 dollars each. Since the objective is focused on the methodology, and not the results, an alternative way is used to obtain the true stress-strain curve. It was seen in the item 3.5.2 how to determine the true stress-strain curve with Yield and Ultimate Tensile Strengths. Therefore, it is necessary to obtain the Yield Strength and the Ultimate Tensile Strength for the hardened material of the quenched ring.

Pavlina and Van Tyne (2008) defined a linear relationship for Yield Strenght (YS) and Ultimate Tensile Strength (UTS) in function of hardness. This relationship was used to calculate the YS and UTS based on the average simulated hardness of the quenched ring. The YS and UTS in function of hardness are presented as follows:

$$YS = -90.7 + 2.876 \cdot HV, \quad \text{and} \tag{4.3}$$

$$UTS = -99.8 + 3.734 \cdot HV, \tag{4.4}$$

where YS is Yield Strength (MPa), UTS is the Ultimate Tensile Strength (MPa), and HV is Vickers hardness (HV), also known as diamond pyramid hardness (DPH).

With the YS and the UTS values defined based on the average simulated hardness of the quenched ring, the flow stress may be calculated. The Young's modulus for the AISI 4140 steel is obtained from DEFORM^{TM} library. Therefore, the compression process may be simulated. Many strokes should be tested in order to define the correct one to decrease the correct the ovality. Table 4.5 gives the main parameters of simulation for correcting the ring distortion.

Table 4.5 – FE setup for the simulation of quenching process.

Operation	Parameter	Value
1 – Compression	Code	DEFORM-3D^{TM}
	Ring geometry	Quenched ring
	Material	Calculated AISI 4140 based on hardness
	Temperature	20 °C
	Object type	Elasto-plastic
2 – Relaxation	Code	DEFORM-3D^{TM}
	Ring geometry	Compressed - Operation 1
	Material	Calculated AISI 4140 based on hardness
	Temperature	20 °C
	Object type	Elasto-plastic

5. RESULTS AND DISCUSSION

This chapter presents and discusses the results of the proposed methodology. The Navy C-Ring Test (quenching) was performed and also predicted by numerical simulation, comparing the results for distortion, microstructure and hardness. This first stage of this work has validated a methodology to simulate heat treatment processes. Therefore, the normalizing and quenching of hot rolled rings were simulated, predicting the distortion so-called ovality. Due to the heat treatment process, the ring became oval and a new procedure for correcting this distortion was developed, based on a straightening process, and simulated.

5.1. The Validation of Heat Treatment Simulation using a Navy C-Ring Test

5.1.1. Experimental Test

In order to establish a correct methodology to simulate the heat treatment of hot rolled rings, a Navy C-Ring Test was conducted for validation proposes. An AISI 4140 steel bar was machined to obtain C-ring specimens with the dimensions given in Figure 4.1. The C-rings were heated to 900 °C in a tubular furnace where an Argon gas flow was maintained for minimizing the oxidation of the material. This temperature was held for 1 hour (3600 s) in order to attain a homogeneous austenitic microstructure. After austenitized, the quenching was performed through a fast vertical movement of the ring (thickest part of the ring at the bottom and ring gap at the top) into the still oil at 25 ºC, being held for at least 300 s.

The C-ring was measured before and after the heat treatment process. The geometry of the specimen changed, obtaining new dimensions. This phenomenon characterizes a quench distortion. The distortion was evaluated based on the gap opening and outside diameter values, described in Figure 4.2. The gap of the C-ring opened 0.43 mm, and the outside diameter increased 0.09 mm.

Table 5.1 displays the values of hardness measured at the various locations in the cross-sections of the C-rings indicated in Figure 4.3. All values lie between 54 and 55 HRC, confirming the formation of high fractions of martensite (Gür and Tuncer, 2004). This is confirmed by the various metallographic results given in Figures 5.1 and 5.2.

Table 5.1 – Measured hardness after oil quenching process.

Property	C-ring region											
	A	B	C	D	E	1	2	3	4	5	6	7
Hardness (HRC)	54	54	54	55	55	54	55	54	54	55	54	54

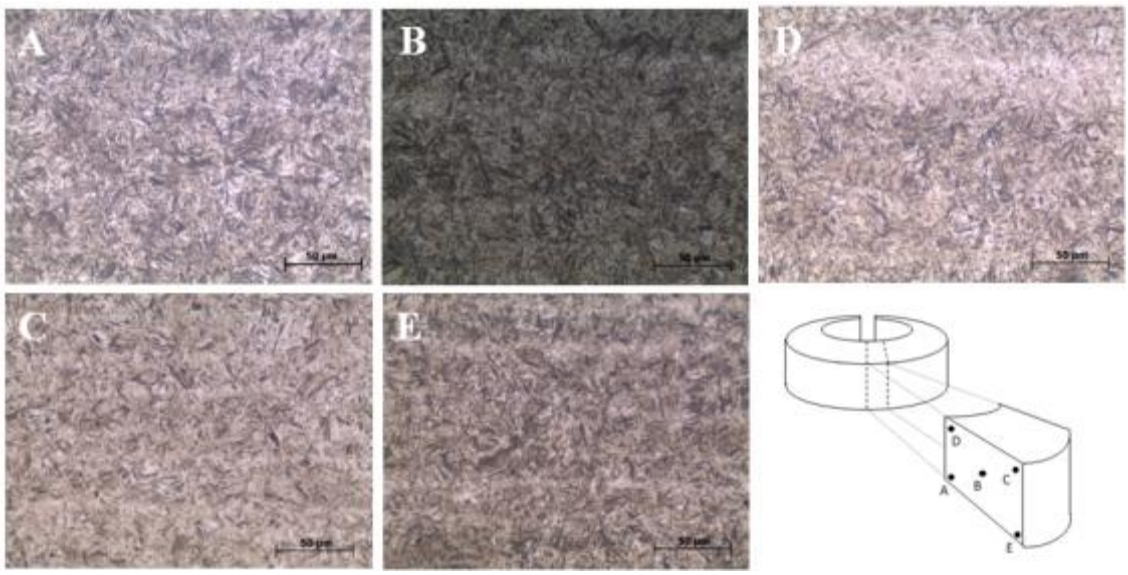

Figure 5.1 – Micrographs from various points in the transversal cross-section of a C-ring, indicating the presence of martensite in all locations (optical microscopy).

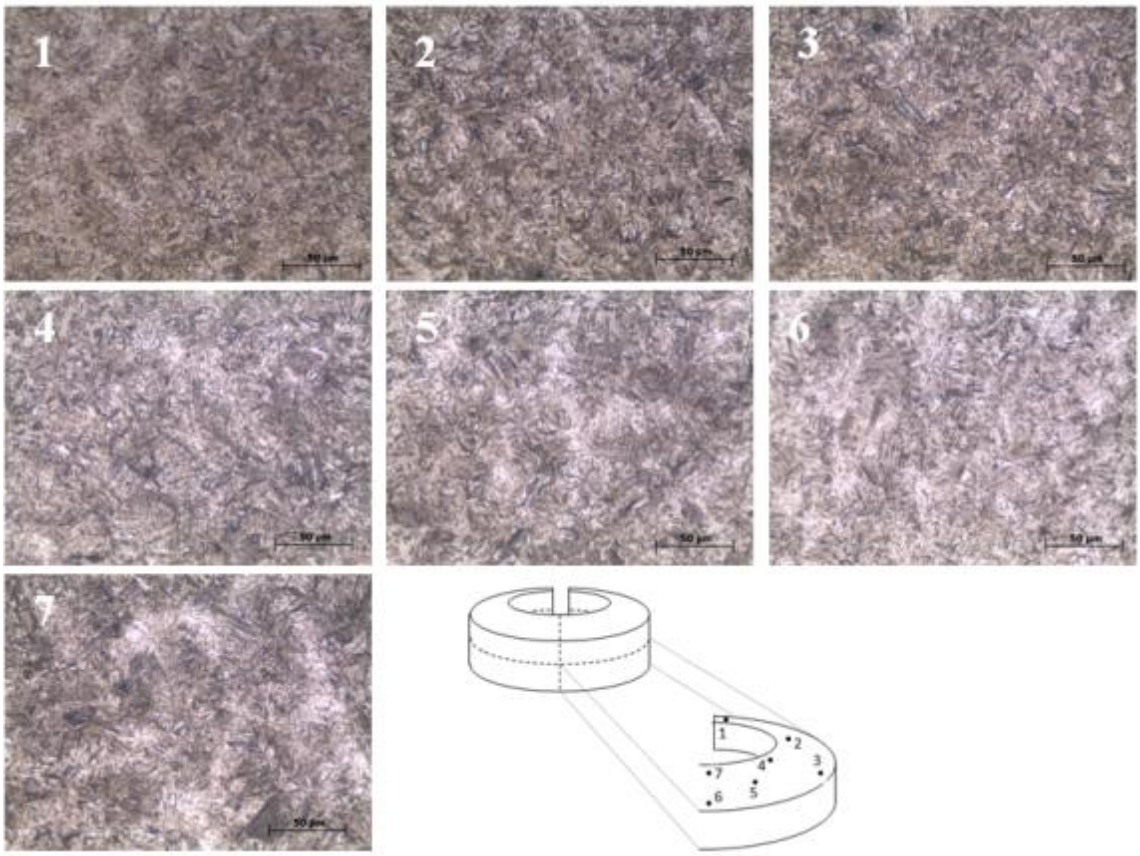

Figure 5.2 – Micrographs from various points in the longitudinal cross-section of a C-ring, indicating the presence of martensite in all locations (optical microscopy).

5.1.2. Numerical Simulation

Looking for the definition of a methodology to simulate heat treatment processes, the Navy C-Ring Test described in the previous item was simulated using DEFORM-3D™ (Scientific Forming Technologies Corporation, Columbus, Ohio, USA). The material data was provided by Sente Software Ltd. (Surrey, United Kingdom), based on the software JMatPro.

Due to the part symmetry, only ¼ of the part was simulated. Brick elements were used (7,000), as shown in Figure 5.3. Nodes *M* and *N* were utilized for outside diameter and gap opening measurements, respectively.

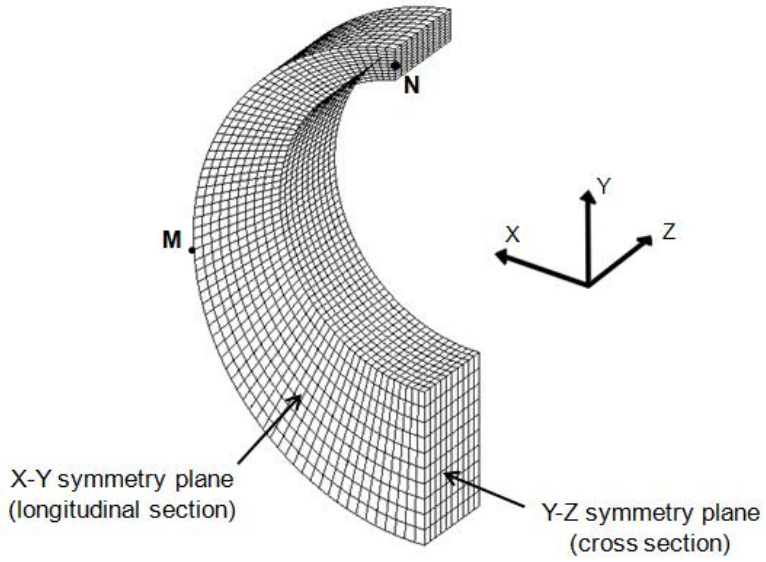

Figure 5.3 – Meshed ¼ C-ring symmetric geometry, used for the simulation. Nodes *M* and *N* were used for outside diameter and gap opening evaluation, respectively.

After simulated, the C-ring was analyzed. Figure 5.4 shows the simulated distribution of the displacement in the *x* direction. There is a tendency for the "opening" of the ring, as observed experimentally. Figure 5.5 displays the simulated displacements in the *x* direction of nodes *M* and *N* in the C-ring for a period of 150 s after the beginning of the quenching process. It is seen that after about 100 s, there is a stabilization of the displacements predicted for both nodes. Taking into account that a symmetric FE model has been used, the x-displacement, given in Figure 5.5 represents only half of the total dimensional change. Thus, the ring gap opens 0.402 mm and the outer diameter expands about 0.084 mm. Table 5.2 presents a comparison between the experimental and predicted values for the ring distortion. It is seen that the relative differences for gap opening and outside diameter increase are smaller than 7%.

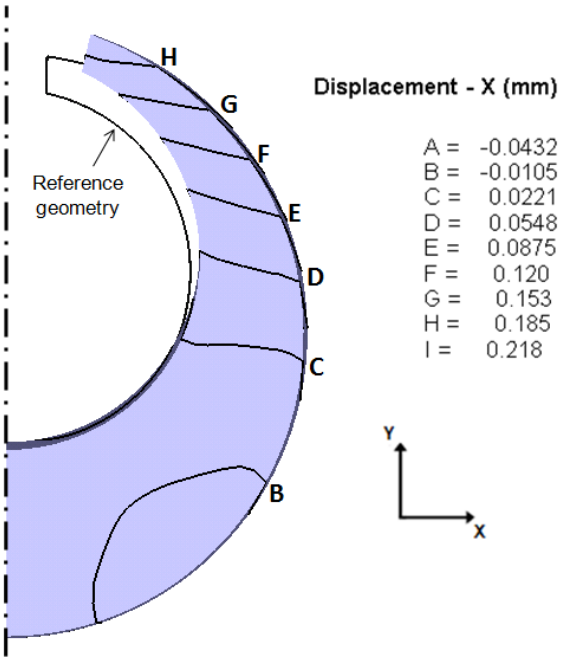

Figure 5.4 – Simulated displacement in the *x* direction of the points in the longitudinal cross-section of the C-ring (displaced geometry magnified 20x).

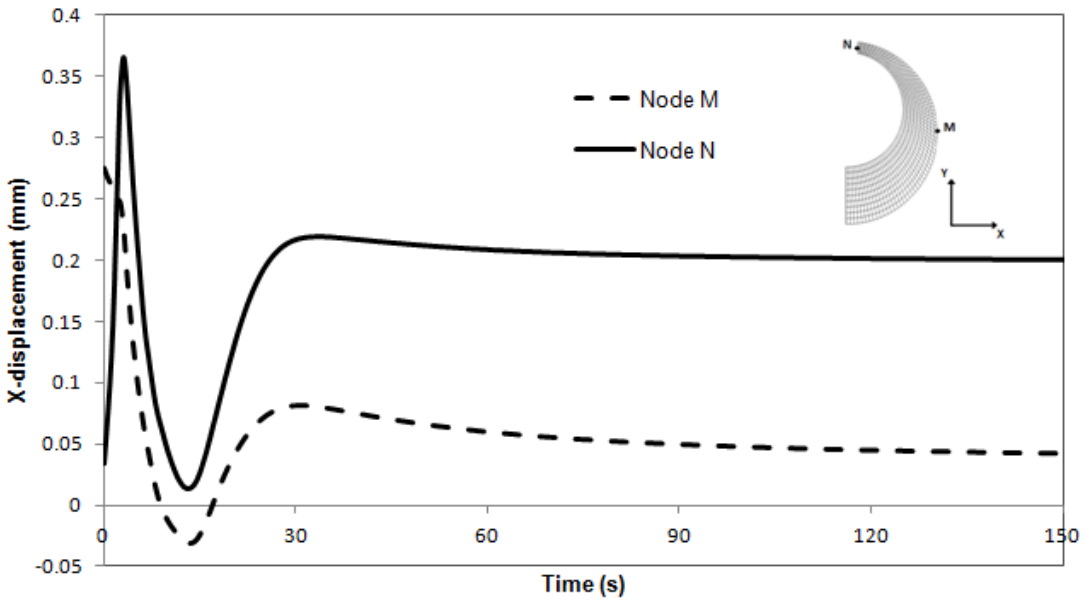

Figure 5.5 – Simulated displacements in the *x* direction for Nodes *N* and *M* of the C-ring, during the oil quenching process.

Table 5.2 – Comparison of the experimental and simulated results for the geometric distortions of the C-ring.

Dimensional changes	Method		Prediction difference
	Experimental	Simulation	
Gap opening (mm)	0.43	0.402	6.5%
Outside diameter (mm)	0.09	0.084	6.7%

Luo and Totten (2011) and Eshraghi-Kakhki *et al.* (2011) have recognized that distortions caused by heat treatments may be controlled and/or avoided throughout proper selection of quenching media, but under some circumstances this may be impracticable (Gonzalez-Mendez *et al.*, 2012). The present simulation can consider various quenching media (through their heat extraction characteristics), allowing satisfactory predictions of quench distortions and their inclusion in the design and manufacturing steps. In addition, adequate post-heat treatment forming operations that would eliminate the distortions may also be designed.

Figure 5.6 shows the simulated distribution of martensite on the C-ring surface and of the displacement. The specimen was initially thermally expanded and austenitized. From 4 s after the quench initiation, it is possible to visualize in Figure 5.6 the beginning of martensite formation in the region close to the C-ring gap. After 10 s, practically all thermal expansion is absent, but martensite formation is still in progress, being now responsible for further ring distortions. The situation after 25 s of cooling shows that the martensite formation in the thicker portion of the C-ring is associated with the final opening of the ring gap and of the external diameter of the ring.

Figures 5.7 and 5.8 display the simulated results for the evolution of martensite volume fraction for various points in the transversal and longitudinal cross-sections of the C-ring, respectively. Very high volume fractions of martensite are predicted, in agreement with the hardness and metallographic results displayed in Table 5.1 and Figures 5.1 and 5.2, respectively. The simulated hardness values lie around 56 HRC, again in agreement with the experimentally measured values.

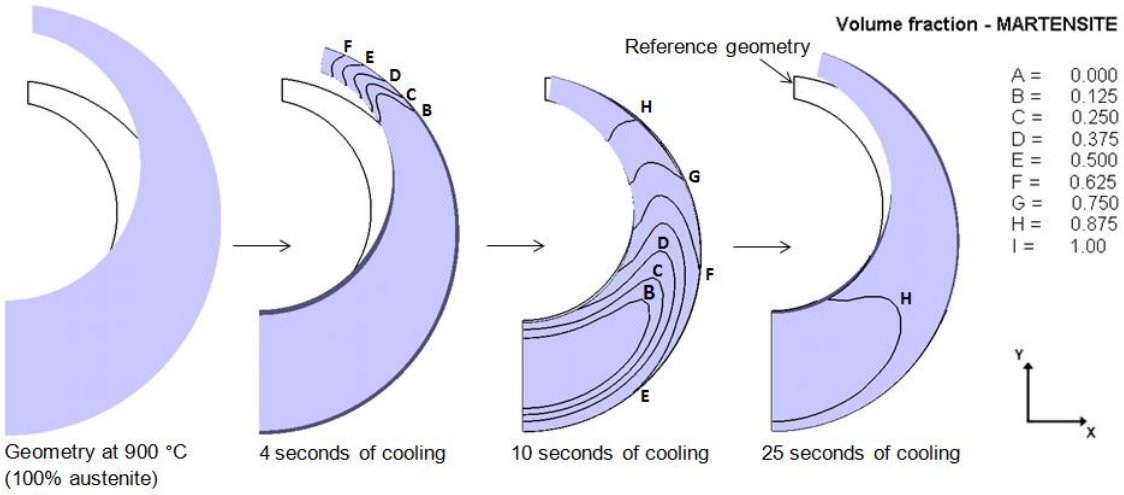

Figure 5.6 – Martensite formation (displaced geometry magnified 20x) on the C-ring during the cooling simulation.

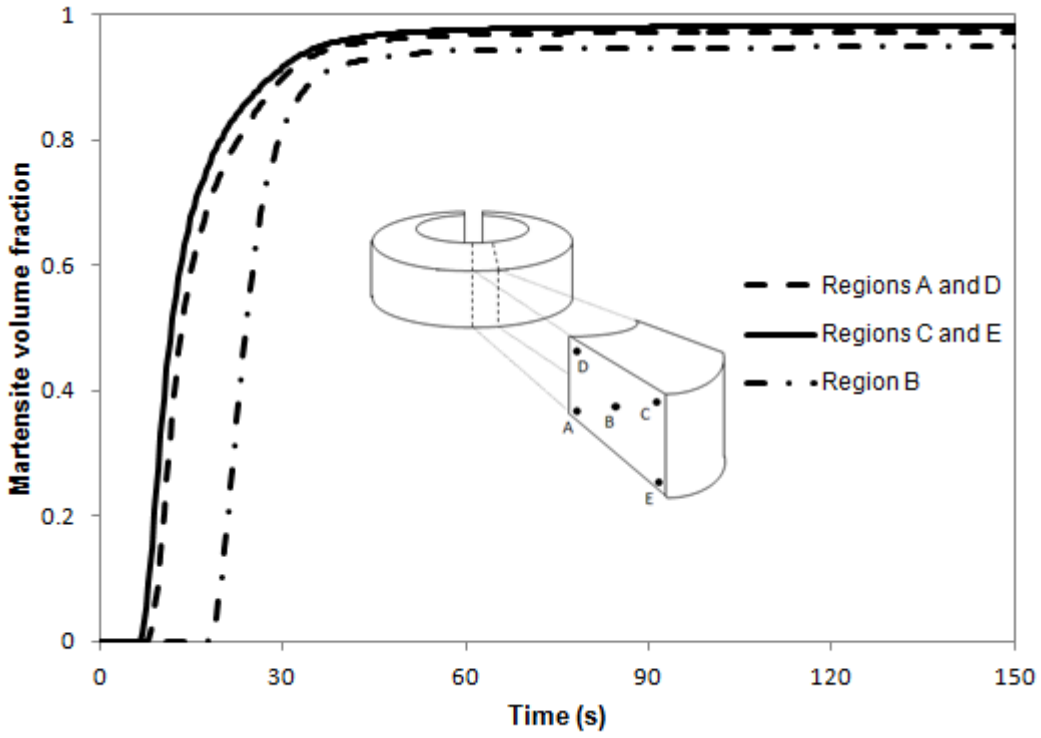

Figure 5.7 – Simulated evolution of the martensite volume fraction at several points in the transversal cross-section of the C-ring during oil quenching.

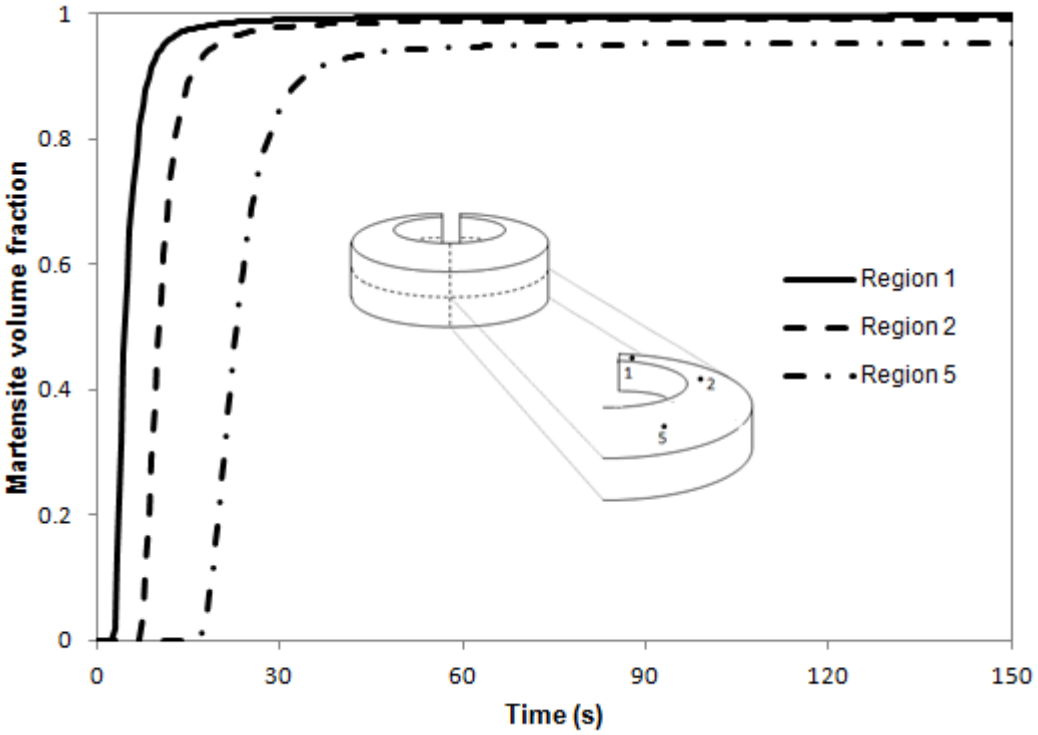

Figure 5.8 – Simulated evolution of the martensite volume fraction at several points in the longitudinal cross-section of the C-ring during oil quenching.

The simulation of quenching, using the DEFORM^{TM} software and material data from JMatPro, led to results very similar to those obtained experimentally, for both geometric distortions and final microstructures and hardness.

5.2. Prediction of Ring Distortion during Heat Treatment Processes

The ring ovality is reported by the industry as a result of the quenching process. However, it is an industrial interest to verify whether, during the normalizing process, one ring may influence in the cooling process of another ring or not, considering the proximity between them. Therefore, normalizing and quenching processes were simulated, and the ovality defect was predicted.

5.2.1. Normalizing of Hot Rolled Rings

After the hot rolling process, the ring is normalized. The geometry given in Figure 4.6 was considered for the prediction of the heat treatment process simulation. The same tools and procedures used for the simulation of the Navy C-Ring Test were applied. Due to the part symmetry, ½ of the geometry was meshed for the simulation. Brick elements were used (15,000), as shown in Figure 5.9.

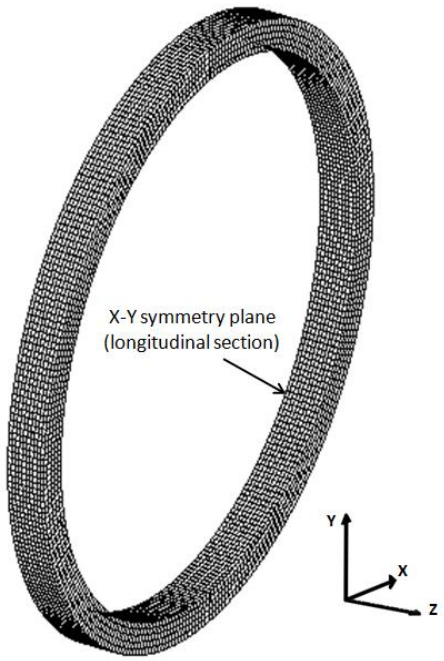

Figure 5.9 – Meshed ½ ring symmetric geometry used for the simulation.

The meshed geometry was heated to 927 °C. The heated and expanded mesh was duplicated in order to take in account the influence of the radiation energy between two parts during the air cooling stage. Therefore, the two equally meshed geometries were positioned very close to each other (10 mm distant). The heat transfer coefficient for air cooling given in Figure 4.8 was applied for the surface of both rings (environment temperature is 20 °C). In addition, a "view factor" function was activated for the simulation, and heat between the ring's surfaces was exchanged by radiation.

During the process, the cooling of the ring is non-uniform, since one side of the ring receives heat by radiation from the other ring. Figure 5.10 shows the simulation of the

normalizing (initial temperature of 927 °C), with the two rings during the air cooling stage (38 minutes of air cooling) exchanging heat with the surroundings and between them. The same temperature distribution is shown in Figure 5.11 for a 3D perspective.

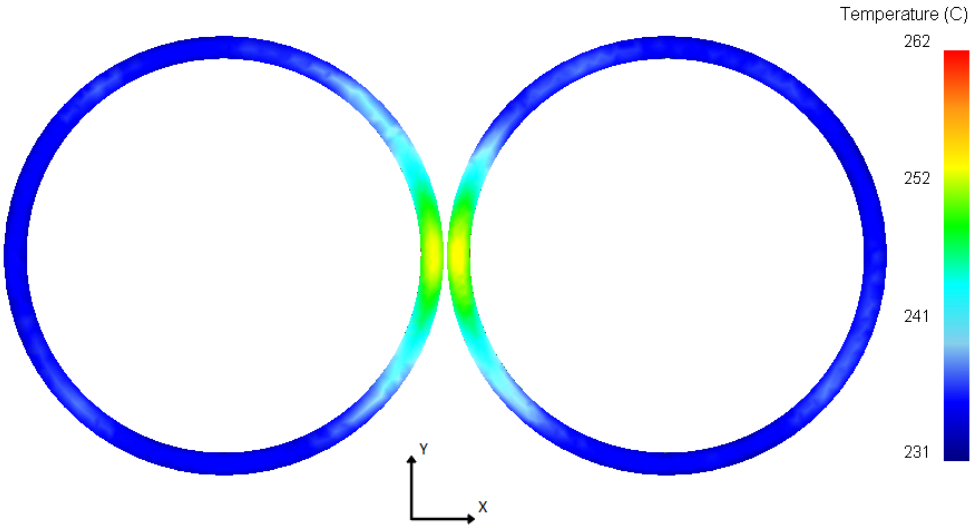

Figure 5.10 – Simulated temperature distribution on the rings after 38 minutes of air cooling (top view).

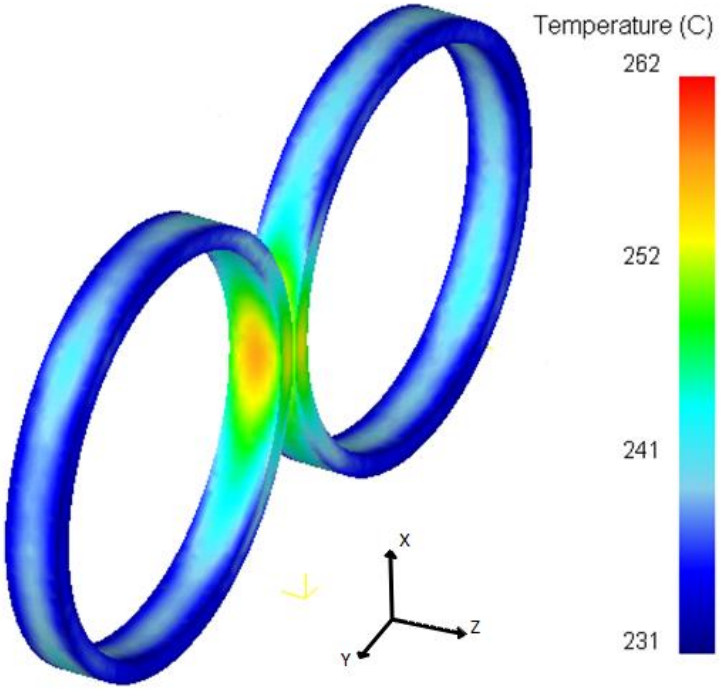

Figure 5.11 – Simulated temperature distribution on the rings after 38 minutes of air cooling (3D view).

Despite the temperature variation in the ring during the air cooling simulation, no ovality was observed in the simulated parts. The non-uniformity of the air cooling process due to the proximity between two rings is not capable to create considerable residual stresses and, as a consequence, the ovality defect.

5.2.2. Quenching of Hot Rolled Rings

As a sequence of the hot rolling and normalizing processes, the rings are hardened through quenching. Since there was no ovality due to the normalizing process, the quenching process was simulated considering a ring with no initial residual stresses. The same generated mesh shown in Figure 5.9 was used for the quenching simulation. The ring was heated to 900 °C, expanding its geometry as shown in Figure 5.12. In this case, the ring OD increased 14 mm.

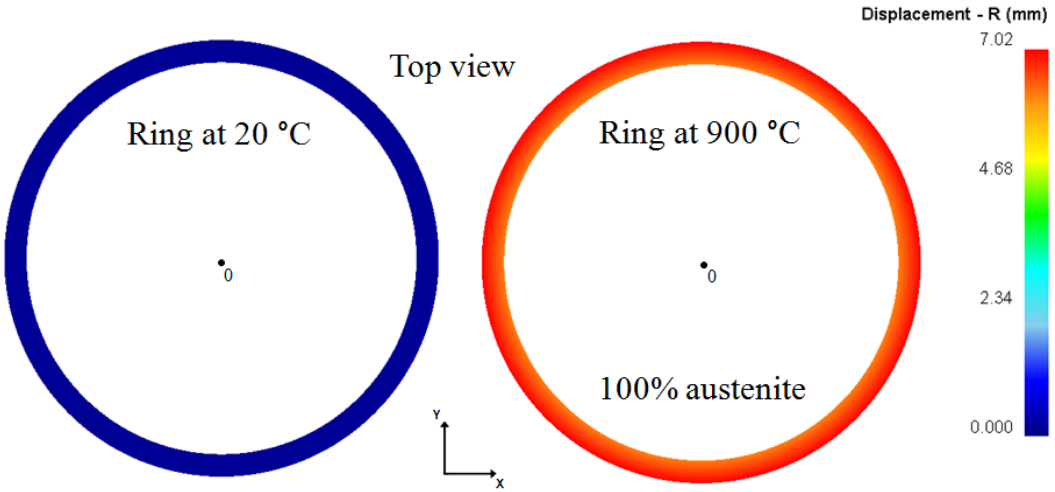

Figure 5.12 – Heating simulation of hot rolled ring. The geometrical expansion increases the ring radius.

For the simulation of the quenching process, the heated ring is considered completely austenitized at 900 °C. For the fast cooling stage, the heat transfer coefficient was applied to the ring surface in function of temperature and position on the surface, following the hypothetical configuration defined in Figure 4.10. The ring was measured at the end of the quenching simulation. The maximum and minimum dimensions were 1304.2 mm and 1291.4 mm, respectively. As a result, the obtained ovality was 12.8

mm. Figure 5.13 shows the simulated oval ring after the quenching process. The blue geometry (dark) has its displacement magnified 10x, and is superimposed on the "reference geometry" with no magnification.

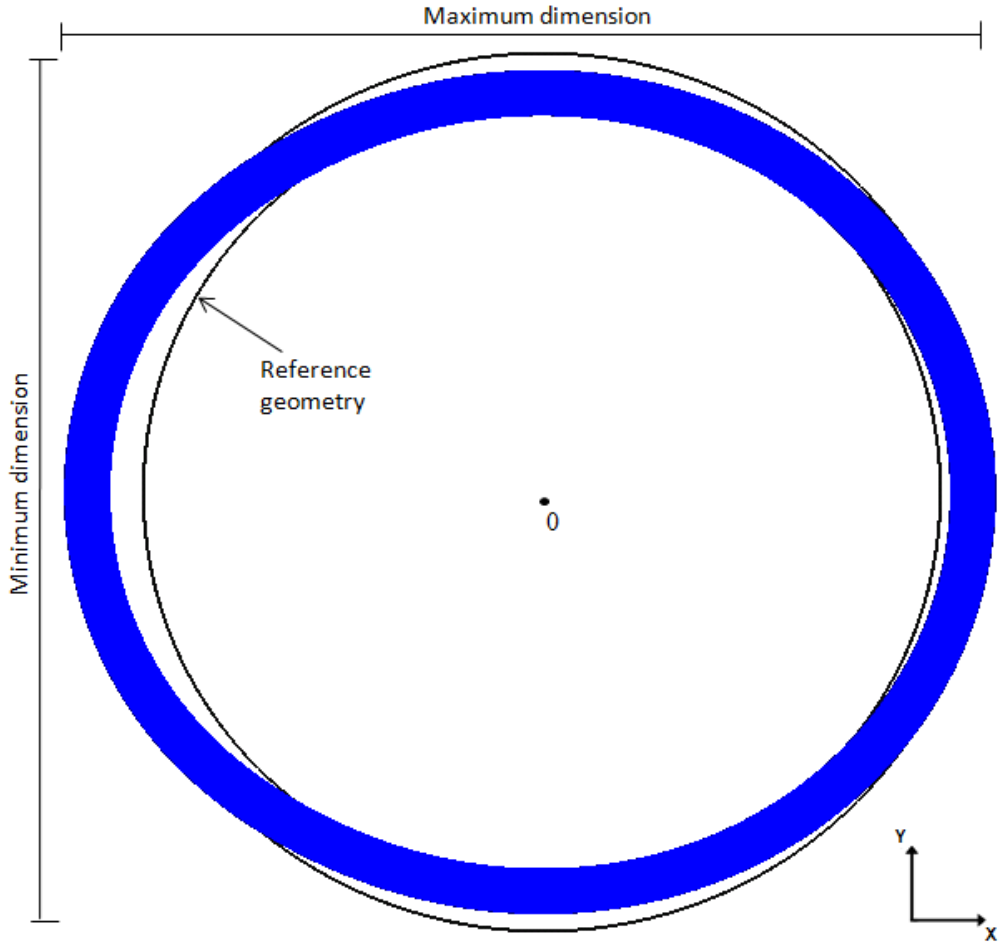

Figure 5.13 – Quenched distorted ring for hypothetical case (Displacement magnified 10x).

The reason for the obtained distortion is the residual stress distribution in the ring. As shown in Figure 5.14, the residual stress is non-homogeneous along the ring circumference. However, it is necessary to conduct a more specific analysis of the residual stress in the ring to better understand the ovality formation.

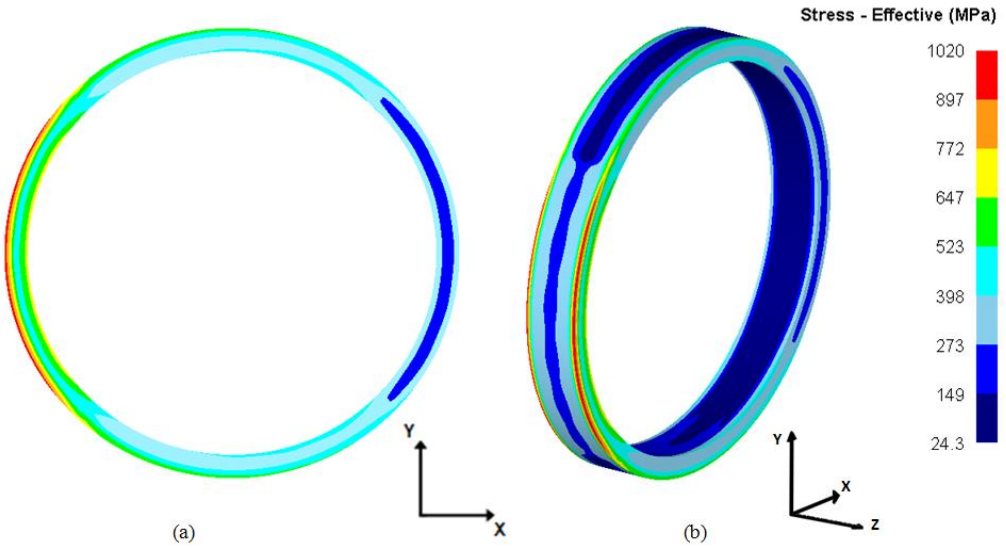

Figure 5.14 – Residual stress in the distorted ring after quenching simulation: (a) top and (b) 3D views.

The hypothetical case considers a heat transfer distribution along the ring surface as shown in Figures 4.10 and 4.11. A schematic drawing of the ring cross section is shown in Figure 5.15, indicating a center-line for measuring the results. The volume fraction of martensite and bainite along the center-line is shown in Figure 5.16. The right side of the ring has the same heat transfer coefficient for all the four surfaces ($1xH_q$), and 100% of bainite along the center-line. In another hand, the left side has the heat transfer coefficient eight times higher for the outside, top and bottom surfaces. As a consequence, there is a formation of martensite in the region closer to the outside surface.

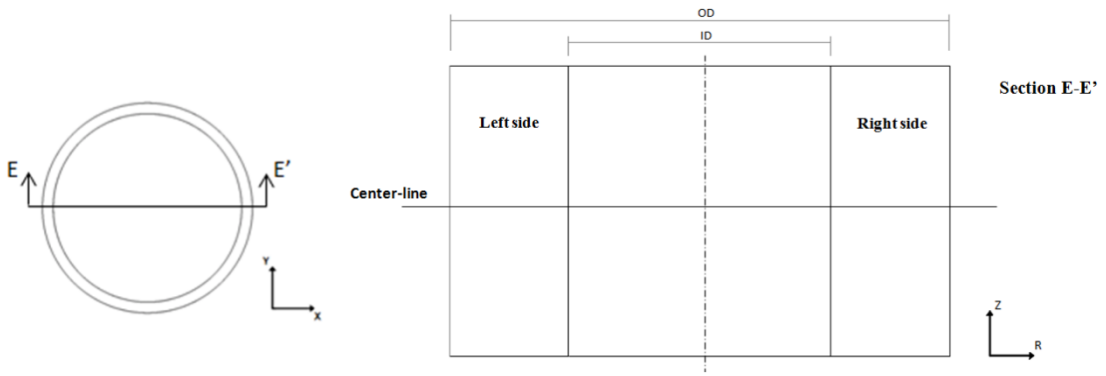

Figure 5.15 – Schematic of the ring cross section: the indicated center-line is used to analyze the simulation.

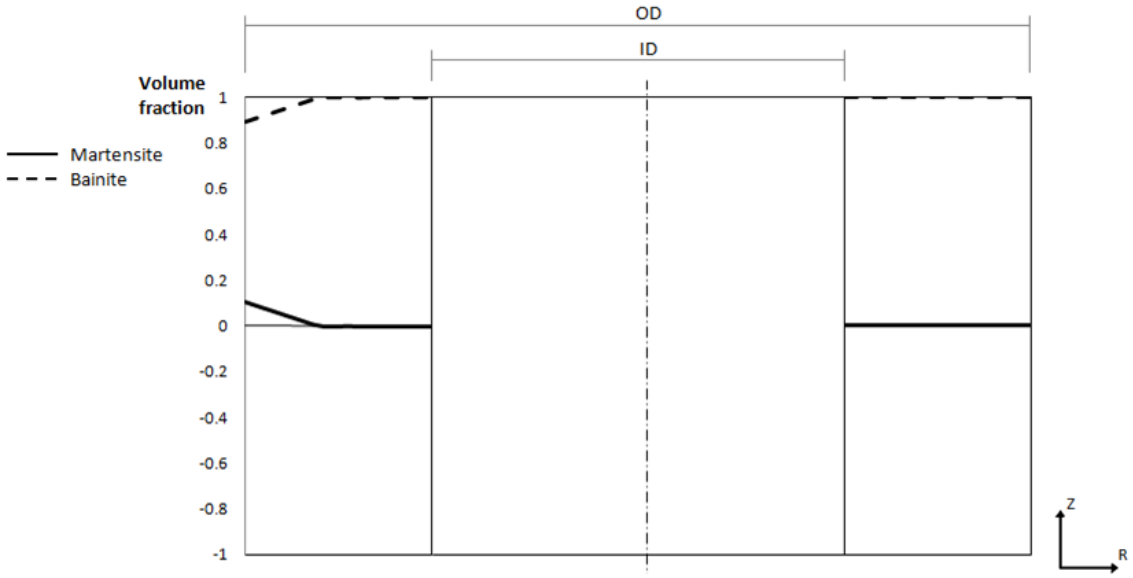

Figure 5.16 – Volume fraction of bainite and martensite on the center-line of the ring cross section.

Analyzing Figure 5.17, it is possible to verify that the circumferential stress profile on the right side of the ring is nearly-symmetric. This characteristic is related to the homogeneity of the heat exchange around the ring at that region, where the heat transfer coefficient is the same for all the four surfaces. On the other hand, the left side displays a non-symmetric circumferential stress profile due to the martensite formation closer to the outside surface, which expands this portion of material, creating compressive stresses on the outside surface and tensile stresses on the inside surface. The result is the ovality distortion already shown in Figure 5.13.

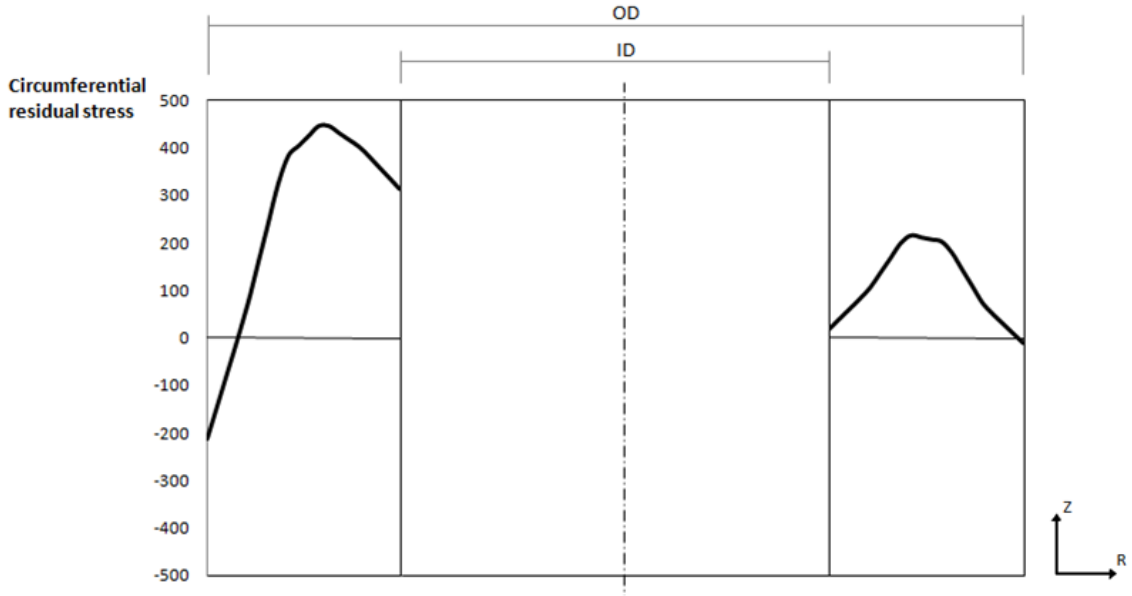

Figure 5.17 – Circumferential stress on the center-line of the ring cross section.

The hardness distribution on the cross section of the ring is shown in Figure 5.18. The hardness may also be related to the volume fraction of martensite and bainite. On the right side there is a symmetric profile of the final hardness, while on the left side the hardness increases closer to the outside surface. The predicted average hardness of the whole ring is 52 HRC (550 HV).

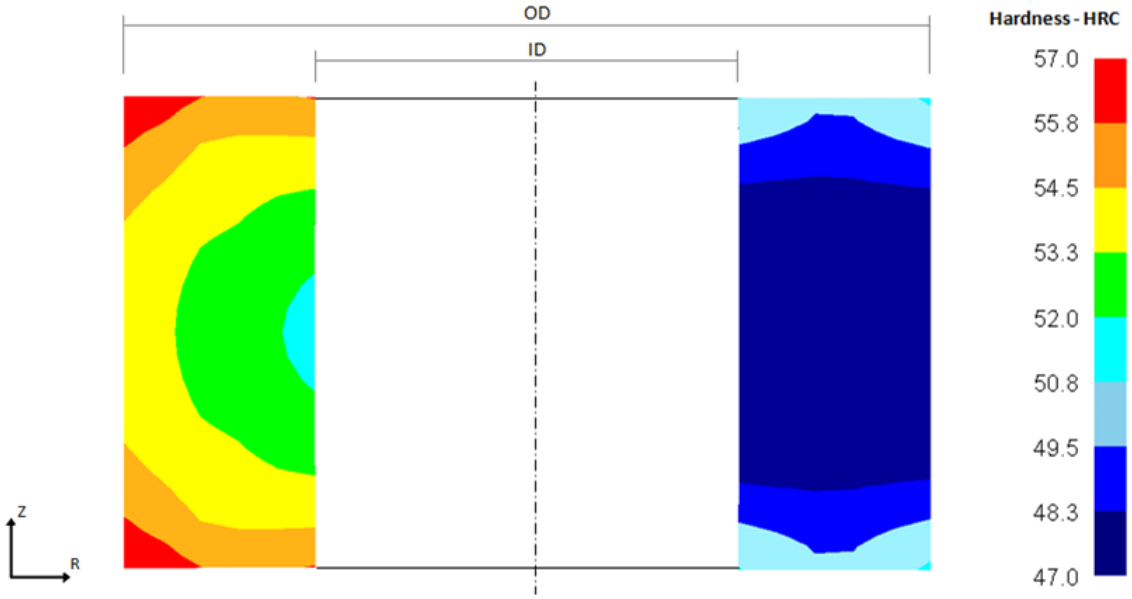

Figure 5.18 – Hardness (HRC) distribution on the cross section of the ring.

5.3. Correction of Ring Distortion

A methodology for the straightening process of the distorted ring was developed and proposed in the Item 4.3. This methodology should be calibrated throughout industrial tests, which are expensive and time consuming. Therefore, computational tools have been used to simulate the straightening process of distorted rings based on a compresser system.

In order to set the FE model for the straightening process, it was necessary to define a new material data for the ring, but the mechanical properties of the new hardened AISI 4140 steel are unknown. Mechanical tests for the new material would benecessary and would involve destructive mechanical tests on the material of the quenched rings. In the present work, an alternative procedure was taken for defining the flow stress of the hardened AISI 4140 steel material. Based on Equations 4.3 and 4.4, the Yield Strength (YS) and Ultimate Tensile Strength (UTS) of the material were defined. For an average hardness of 520 HV (52 HRC), it was calculated a 1490 MPa for the YS, and 1950 MPa for the UTS. The Young's modulus of the AISI 4140 steel specified in the DEFORM^{TM} library was also used. Therefore, the new flow stress was calculated according to the methodology presented in Item 3.5.2. Figure 5.19 gives a comparison between the true stress-strain curves for the calculated hardened AISI 4140 steel and the AISI 4140 steel from DEFORM^{TM} library (non-hardened material).

The distorted mesh, including all the data information such as stresses and strains, was compressed using two flat tools through simulation. The FE model was set up according to the assembly of the process, shown in Figure 4.12. The proposed marks in Figure 4.13 are represented by nodes 1 through 8 shown in Figure 5.20. The dimensions between opposite nodes were defined as *A*, *B*, *C*, and *D*, which were monitored during the simulation of the process.

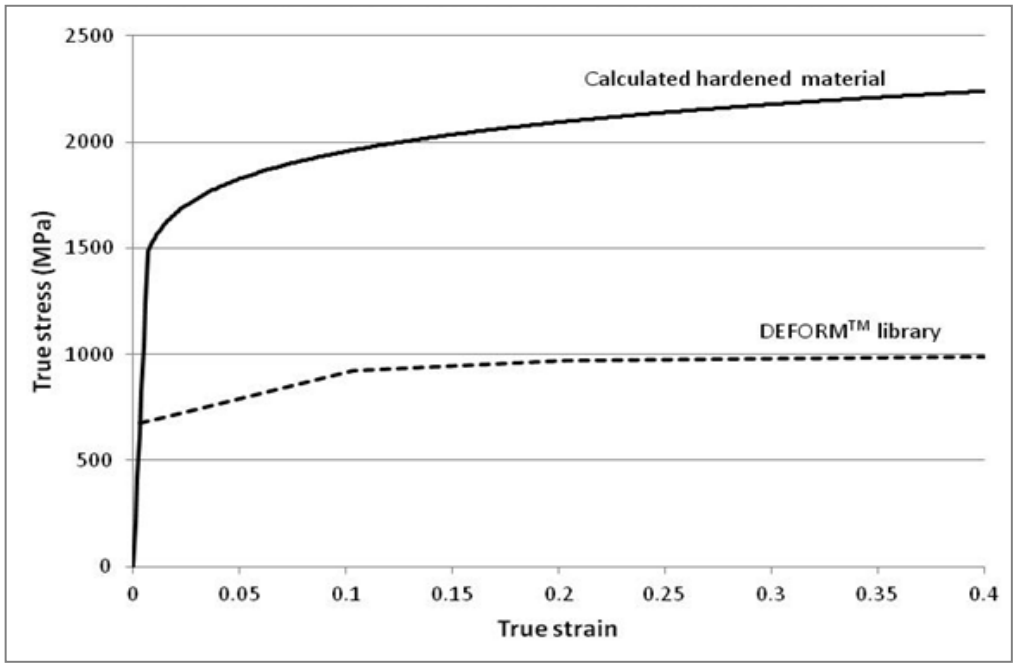

Figure 5.19 – Considered true stress-strain curve of the hardened material to be implemented into FE model, compared to DEFORM™ database for AISI 4140 steel.

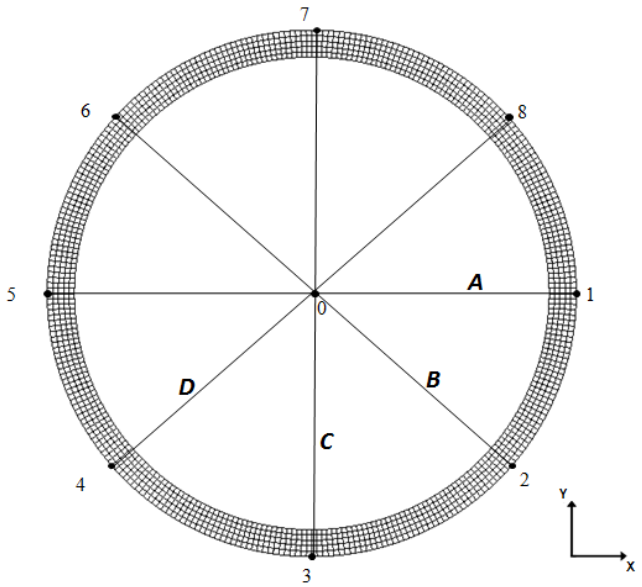

Figure 5.20 – Dimensions to be monitored during simulation, according to ring marks proposed by the methodology.

The ring was positioned to be compressed along the maximum dimension given in Figure 5.13. In this case, *dimension A* is the maximum dimension. The straightening process was performed as shown in Figure 5.21. A first die stroke value of 200mm was

chosen and conducted in the simulation. It is important to mention that the residual stresses in the ring have a drastic drop from the quenched data base to the data base in the beginning of the straightening process. This fact can be verified comparing the residual stresses in Figure 5.21 (a) (beginning of the straightening process) and Figure 5.14 (quenched ring). SFTC has reported it as an interpolation problem, which should be corrected in the next version of the software.

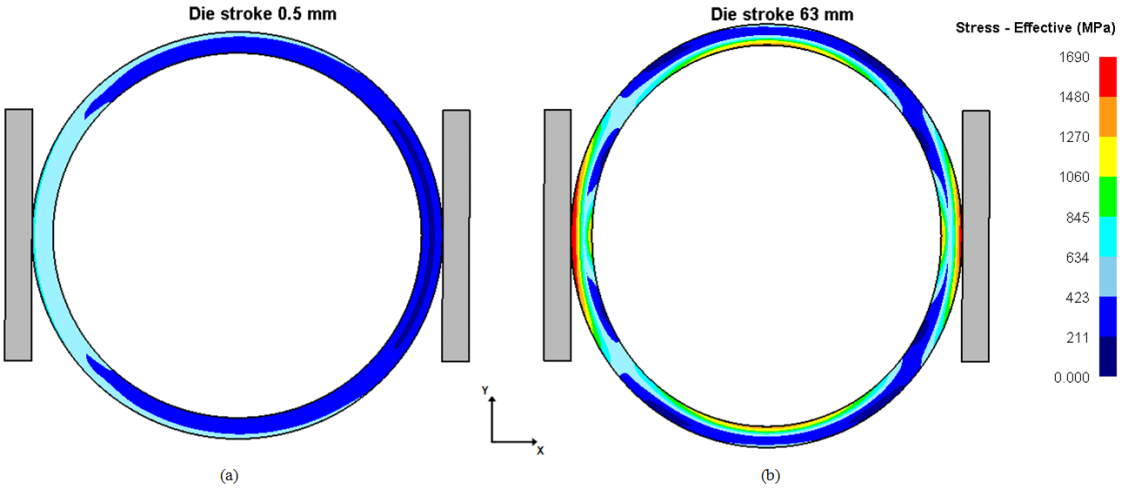

Figure 5.21 – Straightening process: (a) beginning of the compression and (b) after 63 mm stroke.

According to the proposed methodology, the die stroke should be related to the obtained *dimension A* after relaxation of the ring. The optimum die stroke should be defined when the *dimension A* reached the nominal diameter of the ring. Therefore, the simulation of the relaxation of the ring was conducted for the 200 mm stroke, and also for the intermediary strokes: 100, 75, 50 and 25 mm. The final *dimension A* is given in Figure 5.22 (continuous line) as a function of the die stroke. From the graph, the optimum die stroke is 63 mm. The *dimension A* and the die stroke are represented as a relative value to the nominal ring diameter dimension, according to the following equation:

$$Die\,stroke = \frac{\left(A_{\dim} - Diam_{ring}\right)}{Diam_{ring}} x100\% \ , \tag{5.1}$$

where A_{dim} is the *dimension A*, and $Diam_{ring}$ is the nominal ring diameter.

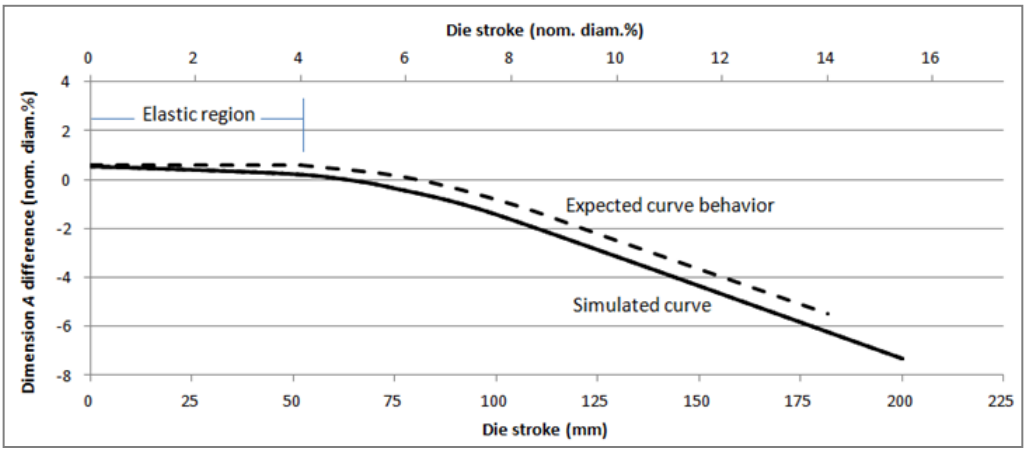

Figure 5.22 – Final *dimension A* as a function of die stroke (first step); ring compressed on *dimension A* direction.

The dashed line in Figure 5.22 shows the expected behavior of the *dimension A* as a function of the die stroke. The *dimension A* should be constant until the effective stress in the ring reaches the Yield Strength of the material, and varying according to the plastic deformation undergone by the ring. It was verified that DEFORM^{TM} was calculating plastic strains in the elements for effective stresses below the Yield Strength. This fact is being investigated by SFTC. However, for the scope of this work, the simulation shows that the methodology can be developed based on simulation tools.

Dimensions A, *B*, *C* and *D* (Figure 5.20) were monitored for the quenching and the straightening process. The difference between the largest and the smallest dimension was defined as the ring ovality. Table 5.3 gives the dimensions and ovality obtained for the quenching and straightening processes. For a 63 mm (4.86%) stroke on the *dimension A* direction, the ovality was already decreased to a value below 2 mm, as specified in the methodology. It means that for this process, including all parameters, only one compression step is enough for the straightening process. The distorted and corrected rings are shown in Figure 5.23. The straightening process also decreases the residual stresses in the part. Despite the interpolation problem for the stresses in the ring (drastic drop) between the quenching and straightening processes, simulation can show the residual stresses decrease, as given in Figure 5.24, comparing the residual stresses in the ring before and after the straightening process.

Table 5.3 – Simulated ring distortion during quenching and straightening processes.

Process stage	Direction	Stroke (%)*	Dimension difference (%)*				Distortion**	
			A	*B*	*C*	*D*	Relative (%)*	Absolute (mm)
Initial	-	-	0.00	0.00	0.00	0.00	0.00	0.00
Austenitized	-	-	1.08	1.08	1.08	1.08	0.00	0.00
Quenched	-	-	0.56	0.08	-0.42	0.06	0.99	12.80
Compressed	*A*	4.86	0.02	0.11	0.01	0.10	0.10	1.32

* (%) is relative to the nominal ring diameter value.

** Distortion represents the difference between largest and smallest dimensions in the ring.

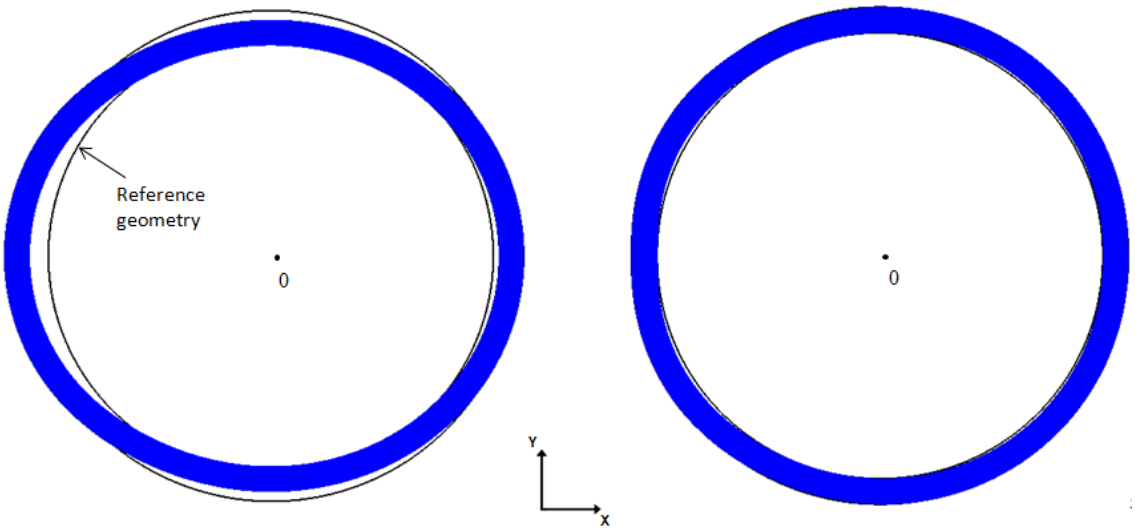

(a) (b)

Figure 5.23 – Ring geometry (a) before and (b) after the straightening process (displacement magnified 10x).

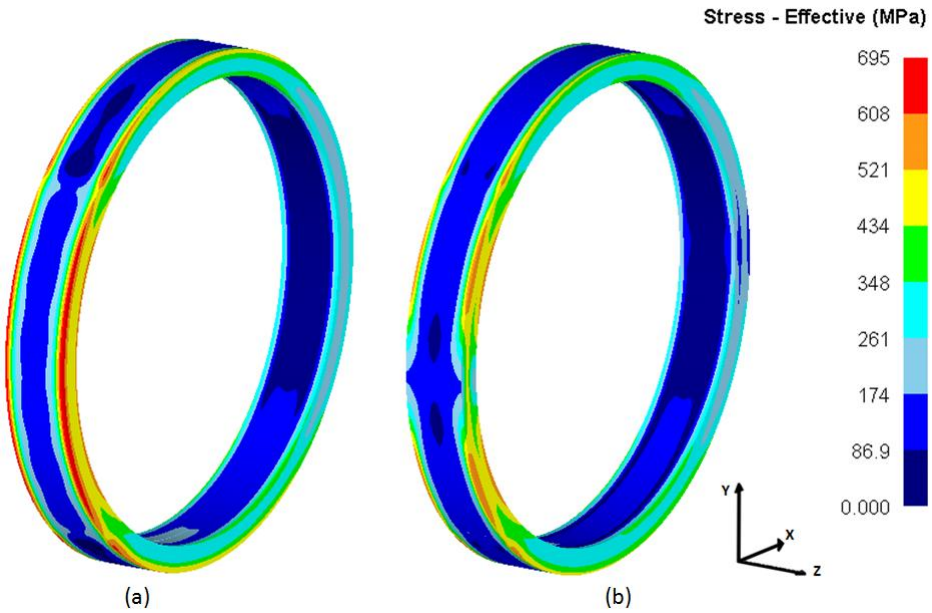

Figure 5.24 – Residual stresses in the ring (a) before and (b) after the straightening process.

6. SUMMARY AND CONCLUSION

In order to define a methodology to predict and correct the ovality (distortion) of hot rolled ring due to heat treatment processes, a project plan was followed, including the tasks:

- validation of the heat treatment simulations using a Navy C-Ring Test;
- prediction of ring ovality during normalizing and quenching processes through simulation;
- and development of the procedure to correct ring ovality supported by computational simulation.

The experimental quenching of the AISI 4140 steel C-rings in oil leads to an increase in both ring gap and outside diameter, as well as to a martensitic microstructure (minimum of 95% martensite) at all points of C-ring, with a hardness of about 55 HRC.

The simulation of quenching, using the DEFORM^{TM} software and material data from JMatPro, led to results very similar to those obtained experimentally, for both geometric distortions and final microstructures and hardness.

A case study considering a large thin-walled ring was used to conduct simulation for predicting ring ovality. For normalizing process, the layout of the rings during the air cooling stage influences in the temperature distribution in the rings. However, for two rings 10 mm distant, the heat exchange by radiation is not a source of distortion (ovality), according to the simulation.

A hypothetical model was developed in order to obtain artificial ring ovality during the simulation of the ring quenching. The non-symmetric martensite formation on the ring's cross section induces non-symmetric circumferential stresses on the ring's cross section, distorting the ring. The results may be considered acceptable since the distortion value falls within the distortion range reported by the industry (between 2 and 18 mm).

A procedure to correct ring ovality in the industry was defined. A complete methodology for predicting and correcting the ring ovality using simulations based on the Finite Elements Method (FEM) was established for a hypothetical case. An optimum die stroke of 63 mm was defined. Only one step for the ring straightening process was necessary to correct the ovality, resulting in a 1.32 mm (0.10%) ovality. The industry has also reported cases in which only one step is necessary. In addition, according to the simulation, the residual stresses in the ring are decreased during the straightening process.

Concluding, a methodology to predict and correct ovality (distortion) of hot rolled and heat treated large rings has been developed. The work is based on numerical simulations using computacional tools. Java-based codes may predict material properties to be used at simulations based on the Finite Element Method. The methodology should be tested at the rolled ring industry. The use of numerical simulations decrease the time and costs of the project. Several rings with different dimensions and materials may be approached.

7. ORIGINAL CONTRIBUTIONS TO KNOWLEDGE

The Navy C-Ring Test was conducted and simulated using two different computational software: DEFORM^{TM}, based on the Finite Element Method, and JMatPro, a java-based materials properties software. The AISI 4140 steel C-ring distortion was experimentally and numerically obtained, presenting a satisfactory agreement. In addition, the hardness and microstructure of the quenched C-ring were experimentally and numerically defined.

The same methodology used to simulate the Navy C-Ring Test was applied to the heat treatment of hot rolled rings. According to the simulation, the radiation heat exchanging between two rings during air cooling is not able to cause ovality. However, the difference between the heat exchange with the surrounding for the inside and outside ring surfaces during the quenching results in non-symmetric formation of martensite on the ring's cross section. This non-symmetric formation of martensite induces non-symmetric circumferential stresses on the ring's cross section, distorting the ring's circumference, characterizing the ovality.

A new procedure has been developed for the industrial straightening process of distorted rings. Despite a hypothetical case study having been used, this process was simulated and established. The same methodology might be applied to real cases.

8. RELEVANCE OF THE RESULTS

This project was sponsored by the rings' industry. The results were obtained according to the interest of academic research and also of industry.

It is now possible to predict ring ovality based on the Finite Element Method. In addition, hardness and microstructure may also be predicted. This first work gives the possibility of continuing this project, optimizing the hypothetical proposed model.

The straightening process is based on trial and error in the industry. The proposed procedure can be used as a knowledge-based methodology for the industrial straightening process of oval rings.

9. FUTURE WORK

Since this thesis has developed the methodology to predict and correct the ring ovality based on a case hypothetical case study, the following work should approach a real case.

Thermocouples should be used to measure the ring temperature next to its surfaces during the quenching process. Based on the temperature, an inverse analysis should be conducted in order to obtain real values for the heat transfer coefficient around the ring. The ring ovality should be predicted based on the calculated heat transfer coefficient.

Another possibility is the use of the same methodology developed in this work, with the hypothetical heat transfer coefficients around the ring. The heat transfer coefficient configuration should be defined as a function of the obtained ovality. Therefore, different ovality magnitudes should be correlated with ring's dimensions and heat transfer coefficient configurations. The same practice could be performed for rings with different materials.

Most of the rings are also tempered after quenched. The tempering process should also be simulated in order to obtain a more realistic distorted ring.

For the simulation of straightening process, tensile tests of quenched and tempered materials should be performed.

The straightening process may be simulated for different rings and ovalities. Therefore, the optimum die stroke could be given as a function of ring's size and material, and ovality magnitude. The simulated results should be compared to industrial results, calibrating and improving the numerical procedure, providing, as a consequence, more realistic simulated results.

The straightening methodology may also be developed based on expander machines.

The described problems in the item should be solved with SFTC’s support.

10. REFERENCES

Altan, T., Ngaile, G., and Shen, G. (2005). *Cold and Hot Forging. Fundamentals and Applications.* Columbus: ASM International. 341p. 1ed.

Altan, T., Oh, S., and Gegel, H. (1983). *Metal Forming. Fundamentals and Applications.* Metal Park: American Society for Metals. 353p. 7ed.

American Society for Metals. (1977). *Atlas of Isothermal Transformation and Cooling Transformation Diagrams.* Materials Park, 422p: American Society for Metals.

Arimoto, K., Yamanaka, S., and Funatani, K. (2008, October 20). Explanation of the Origin of Distortion and Residual Stress in Carburized Ring Using Computer Simulation. *Journal of ASTM International* , p. 9.

ASM International. (1993). *ASM Handbook, Volume 1: Properties and Selection: Irons, Steels, and High-Performance Alloys.* Materials Park: ASM International.

ASM International. (2002). *Atlas of Stress Strain Curves.* Materials Park: ASM International. 816p.

ASM International. (1995). *Heat Treater's Guide. Pratices and Procedures for Irons and Steels.* Materials Park: ASM International.

Atkins, M., and Met, B. F. (1980). *Atlas of continuous cooling transformation diagrams for engineering steels.* Materials Park: American Society for Metals.

Atlas Specialty Metals. (2005). *The Atlas Specialty Metals: Thecnical Handbooks of Bar Products.* Atlas Specialty Metals.

Bamberger, M., and Prinz, B. (1986, April v. 2). Determination of heat transfer coefficients during water cooling of metals. *Materials Science and Technology* , pp. 410-415.

Bates, C. E., Totten, G. E., and Brennan, R. L. (1991). Quenching of Steel. In A. International, *ASM Handbook. Heat Treatment. Volume 4* (pp. 159-290). Materials Park: ASM International.

Bolin, R. (2005). Ring Rolling. In A. International, *ASM Handbook, Volume 14A: Metalworking: Bulk Forming* (pp. 136-155). Materials Park: ASM International.

Brooks, B. E., and Beckermann, C. (2007). Prediction of heat treatment distortion os cast steel c-rings. *Proceedings of the 61st SFSA Technical and Operating Conference*, (p. 30p). Chicago.

Brümmer, M. (2011). Sizes and Production Range. *Advanced Ring Rolling Seminar* (p. 31 s.). Cleveland: SMS Meer.

Buhl, K. (2011). Rolling Defects. *Advanced Ring Rolling Seminar* (p. 31 s.). Cleveland: SMS Meer.

Bullens, D. K., and Battelle. (1948). Steel and Its Heat Treatment. Principles. *Volume I* , 489.

Burchitz, I. A. (2008). *Improvement of Springback Prediction in Sheet Metal Forming.* Rotterdam: PrintPartners. 156p.

Cetlin, P. R., and Helman, R. (2005). *Fundamentos da Conformação Mecânica dos Metais.* São Paulo: Artliber Editora. 263p. 2ed.

Cyril, N., Cyrille, B., Stéphane, L., Mihaela, T., and Régis, B. (2009). Comparison of experimental and simulation distortions of quenched C-ring test parts. *International Journal of Material Forming* , pp. 263-266.

da Silva, A. D. (2009). *Análise de Rota de Fabricação de Fio Retangular de Cobre Eletrolítico, com Seção de 3,5 x 8,8 mm, a partir de Vergalhão Cilíndrico de Diâmetro 8,0 mm.* Belo Horizonte: Escola de Engenharia da UFMG. 192p. (Dissertação, Mestrado em Engenharia Mecânica).

da Silva, A. D., Lizardo, C. F., and Rabelo, F. (2010). Estudo dos Princípios da Simulação de Processos de Conformação Mecânica através de um Ensaio de Tração. Belo Horizonte: 46p.

Dassault Systèmes SolidWorks Corp. (2008). *Understanding Nonlinear Analysis.* Concord: 15p.

Dieter, G. E. (1988). *Mechanical Metallurgy*. 751p.: McGraw-Hill Book Company (UK) Limited.

Ebert, L. J. (1978, November Volume 9A). The Role of Residual Stresses in the Mechanical Performance of Case Carburized Steels. *METALLURGICAL TRANSACTIONS A* , pp. 1537-1551.

Ericsson, T. (1991). Principles of Heat Treating of Steels. In A. International, *ASM Handbook, Volume 4: Heat Treating* (pp. 13-48). Materials Park: ASM International 2172p.

Eshraghi-Kakhk, M., Golozar, M. A., and Kermanpur A. (2011) Application of polymeric quenchant in heat treatment of crack-sensitive steel mechanical parts: modeling and experiments. *Materials & Design*; 32, pp.2870-2877.

Fish, J., and Belytschko, T. (2007). *A First Course in Finite Elements.* West Sussex: JohnWiley and Sons, Ltd.

Freborg, A. M., Li, Z., and Ferguson, B. L. (2007). Assessing Heat Treatment Distortion Sensitivity. *Deformation Control Technology, Inc.*, (p. 11 p.). Cleveland.

Fukuzumi, T., and Yoshimura, T. (1992). Reduction of distortion caused by hea treatment on automobile steel gear. *Proceeding of the First International Conference on Quenching and Control of Distortion*, (pp. 199-203). Chicago.

Furrer, D. U., and Semiatin, S. L. (2010). Introduction to Metals Process Simulation. In A. International, *ASM Handbook, Volume 22B: Metals Process Simulation* (pp. 3-7). Materials Park: ASM International.

Gellhaus, M. (2011). Design Guidelines. *Advanced Ring Rolling Seminar* (p. 22 s.). Cleveland: SMS Meer.

Gonzalez-Mendez, J. L., da Silva, A. D., Jiang, X., and Altan, T. (2012). Distortion in rolled and heat treated rings. *The International Journal of Forging Business & Technology*. February, 2012; pp.12-15.

Grossmann, M. A., and Bain, E. C. (1964). *Principles of Heat Treatment.* Metals Park: American SOciety for Metals, 5 ed.

Grum, J., Bozic, S., and Zupancic, M. (2001). Influency of Quenching Agents on Distortion of Modified Navy C-Rings Made of Heat Treatment Steel 4140. *Proceedings of The 8th Seminar of the Intenational Federation for Heat Treatment and Surface Engineering* (pp. 145-155). dubrovnik: IFHTSE.

Guo, Z., Saunders, N., Miodownik, P., and Schillé, J.-P. (2009). Modelling phase transformations and material properties critical to the prediction of distortion during the heat treatment of steels. *International Journal of Microstructure and Materials Properties* , pp. 187-195.

Gür, C. H., and Tuncer, B. O. (2004). Investigating the Microstructure-Ultrasonic Property Relationships in Steels. *16th World Conference on Nondestructive testing*, (p. 7p). Montreal, Canada.

Hardin, R. A., and Beckermann, C. (2005). Simulation of Heat Treatment Distortion. *Proceedings of the 59th SFSA Technical and Operating Conference* .

Hosford, W. F. and Caddell, R. M. (2007). *Metal Forming. Mechanics and Metalurgy.* Cambridge: : Cambridge University Press, 3ed. 312p.

Houghton. (2011). *Houghton on Quenching.* 75p.

Huyett, G. L. (2004). *Engineering Handbook: Technical Information.* Minneapolis: G. L. Huyett.

Incropera, F. P., DeWitt, D. P., Bergman, T. L., and Lavine, A. S. (2007). *Fundamentals of Heat and Mass Transfer.* Hoboken: John Wiley and Sons, Inc. 6th ed.

Jominy, W. E., and Boegehold, A. L. (1938, Vol. 26). A Hardenability Test for Carburizing Steel. *Trans ASM* , pp. 574-599.

Kalpakjian, S., and Schimd, S. R. (2006). *Manufacturing Engineering and Technology.* Upper Saddle River: Pearson Education, Inc. 1295p.

Kobayashi, S., Oh, S., and Altan, T. (1989). *Metal Forming and The Finite Element Method.* New York: Oxisford University Press, Inc.

Koç, M., Culp, J., and Altan, T. (2006, 174). Prediction of residual stresses in quenched aluminum blocks and their reduction through cold working processes. *Journal of Materials Processing Technology* , pp. 342–354.

Krauss, G. (1980). Principles of Heat Treatment of Steel. 291.

Krauss, G., and Marder, A. R. (1971, September Volume 2). The Morphology of Martensite in Iron Alloys. *METALLURGICAL TRANSACTIONS* , pp. 2343-2357.

Lee, S.-J., and Lee, Y.-K. (56 (2008)). Finite Element Simulation of Quench Distortion in a Low-Alloy Steel Incorporating Transformation Kinetics. *Acta Materialia* , pp. 1482-1490.

Li, Z., Grandhi, R. V., and Srinivasan, R. (2006). Distortion minimization during gas quenching process. *Journal of Materials Processing Technology* , pp. 249-257.

Liscic, B., Luty, W., and Tensi, H. M. (1992). *Theory and Technology of Quenching: a Handbook.* New York: Springer-Verlag, 484p.

Luo, X., and Totten, G. E. (2011) Analysis and prevention of quenching failures and proper selection of quenching media: an overview. *Journal of ASTM International*. v.8, n.4, pp.1-29.

MacKenzie, D. S., and Ferguson, B. L. (2010). Effect of Alloy on the Distortion of Oil Quenched Automotive Pinion Gears. *International Conference on Thermal Process Modeling and Computer Simulation*, (p. 4 p.). Shanghai.

MacKenzie, S., Li, Z., and Ferguson, B. L. (2007). Effect of Quenchant Flow on the Distortion of Carburized Automotive Pinion Gears. *5th International Conference on Quenching and Control of Distortion* (p. 11 p.). Berlin: IFHTSE.

McINNES Rolled Rings. (2011). *Media Gallery.* http://mcinnesrolledrings.com.

Metal Suppliers Online, L. (n.d.). *Properties of 4140*. Retrieved January 15th, 2012, from Metal Supliers Online: www.suppliersonline.com

Milutinivic, M., Vilotic, D., Plancak, M., Trbojevic, I., Skakum, P., Cupkovic, V., and Luzanin, O. (2005). Hot Ring Rolling in Bearing Production. *Journal for Technology of Plasticity*. v.30, n1-2.

Moosbrugger, C. (2002). Representation of Stress-Strain Behavior. In A. International, *Atlas of Stress-Strain Curves* (pp. 1-19). Materials Park: ASM International.

Nallathambi, A. K., Kaymak, Y., Specht, E., and Bertram, A. (210 (2010)). Sensitivity of Material Properties on Distortion and Residual Stresses During Metal Quenching Processes. *Journal of Materials Processing Technology* , pp. 204-211.

Narazaki, M., and Totten, G. E. (2006). Distortion of Heat Treated Components. In G. E. Totten, *Steel Heat Treatment: Metallurgy and Technologies* (pp. 608-648). Boca Raton: CRC Press.

Narazaki, M., Totten, G. E., and Webster, G. M. (2002). Hardening by Reheating and Quenching. In G. E. Totten, M. Howes, and T. Inoue, *Handbook of Residual Stress and Deformation of Steel* (pp. 248-295). Materials Park: AM International.

Ngaile, G., and Altan, T. (2004). Computer Aided Engineering in Forging. *Proceedings of the 3rd JSTP International Seminar on Precision Forging*, (pp. 14-18). Nagoya.

Oh, S.-I., Walters, J., and Wu, W.-T. (2010). Finite Element Method Applications in Bulk Forming. In A. International, *ASM Handbook, Volume 22B: Metals Process Simulation* (pp. 267-289). Materials Park: ASM International.

Pagliettt, A. (2007). Plasticity of Cold Worked Metals. A Deductive Approach. (p. 173). Billerica: WIT Press.

Pascon, F., Blès, G., Bouffliоux, C., Casotto, S., Bruschi, S., and Habraken, A. (2004, v. Supplement Metal Forming 1-3). Prediction of distortion during cooling of steel rolled rings using thermal-mechanical-metallurgical finite element model. *Steel Grips 2* , pp. 457-463.

Pavlina, E. J., and Van Tyne, C. J. (2008). Correlation of Yield Strength and Tensile Strength with Hardness for Steels. *Journal of Materials Engineering and Performance* , pp. 888-893.

Philip, T. V., and McCaffrey, T. J. (1993). Ultrahigh-Strength Steels. In A. International, *ASM Handbook, Volume 1: Properties and Selection: Irons, Steels, and High-Performance Alloys.* Materials Park: ASM Internationl.

Rotek® Rings. (2011). Rotek® Rings Brochure. *ThyssenKrupp* , 2 p.

Schey, J. A. (1970). Metal Deformation Processes. Friction and Lubrication. (p. 807). New York: Marcel Dekker Inc.

Sedighi, M., and McMahom, C. A. (2000). The Influence of Quenchant Agitation on the Heat Transfer Coefficient and Residual Stress Development in the Quenching of Steels. *Proceedings of the Institution of Mechanical Engineers, Part B: Journal of Engineering Manufacture* , pp. 555-567.

Semiatin, S. L. (2005). Introduction to Bulk-Forming Processes. In A. International, *ASM Handbook, Volume 14A: Metalworking: Bulk Forming* (pp. 3-10). Materials Park: ASM International, 888p.

Sente Software Ltd (2011). JMatPro. 6.0, demo version. Surrey, United Kingdom.

Server, N. K., Choi, C., Yang, X., and Altan, T. (2011a, May/June). Determining the flow stress curve with yield and ultimate tensile strengths, Part I. *Stamping Journal* , pp. 14-15.

Server, N. K., Choi, C., Yang, X., and Altan, T. (2011b, July/August). Determining the flow stress curve with yield and ultimate tensile strengths, Part II. *Stamping Journal* , pp. 14-15.

SFTC. (2010). *DEFORMTM 3D Version 10.1.2. User's Manual.* Columbus: Scientific Forming Technologies Corporation.

SFTC. (2005). *DEFORMTM News. Heat Transfer Modeling.* Columbus: Scientific Forming Technologies Corp.

Sharma, R. C. (1996). *Principles of Heat Treatment of Steels.* New Delhi: New Ages Internation (P) Ltd. 335p.

TATA Steel. (2011). *Engineering Steels.* TATA Steel International (Australasia) Ltd.

Tensi, H. M., Stich, A., and Totten, G. E. (1994). Fundamentals About Quenching by Submerging. *Proceedings of International Heat Treating Conference: Equipment and Processes*, (pp. 243-251). Schaumburg.

Thielen, P. N., Fine, M. E., and Fournelle, R. A. (1976). Cyclic Stress Strain Relations and Strain-Controlled Fatigue of 4140 Steel. *Acta Metallurgica* , pp. 1-10.

Tiryakioglu, M. (1996). The Optimization of Heat Treatment of Aluminum Aerospace Castings for Increased Reliability. *Proceedings of the 16th Heat Treating Society Conference and Exposition* (pp. 231-237). Cincinnati: ASM International.

Totten, G. E. (2007). *Steel Heat Treatment: Metallurgy and Technologies.* Boca Raton: Taylor and Francis Group, LLC. 820p.

Totten, G. E., and Howes, M. A. (1997). *Steel Heat Treatment Handbook.* New York: Marcel Dekker, Inc.

Totten, G. E., Bates, C. E., and Clinton, N. A. (1993). *Handbook of Quenchants and Quenching.* ASM International.

Tschaetsch, H. (2005). Metal Forming Practise. Processes Machines Tools. (p. 405). New York: Springer Berlin Heidelberg New York.

Volkov, A. E., Likhachev, V. A., and Nikolaev, P. I. (1984, v.27 n.3). Theory of Transformation Plasticity. *Russian Physics Journal* , pp. 223-225.

Voort, G. F. (1991). *Atlas of Time-Temperature Diagrams for Irons and Steels.* 766: ASM International.

Wallis, R. A. (2010). Modeling of Quenching, Residual-Stress Formation, and Quench Cracking. In A. International, *ASM Handbook, Volume 22B, Metals Process Simulation* (pp. 547-585). Materials Park: ASM International.

Wang, Z. W., Fan, J. P., Hu, D. P. Tang, C. Y., and Tsui, C. P. (2010). Complete Modeling and Parameter Optimization for Virtual Ring Rolling. *International Journal of Mechanical Science*. pp.1325-1333.

Webster, H., and Laird, W. J. (1991). Martempering of Steel. In A. International, *ASM Handbook, Volume 4: Heat Treatment* (pp. 325-368). Materials Park: ASM International.

Xiao, B., Wang, Q., Jadhav, P., and Li, K. (2010). An experimental study of heat transfer in aluminum castings during water quenching. *Journal of Materials Processing Technology* , pp. 2023-2028.

Ye, J., Liu, Y., and Zhou, Y. (2003, v.19, n.4). A Mathematical Model for Forecasting Distortion of Workpieces with Phase Transformation on Cooling Process. *Journal of Material Science and Technology* , pp. 313-316.